Magnetron Output Power Controller Used in the Application of Rooibos Tea Sterilisation

by

Jacobus Pieter van der Merwe

Thesis presented in partial fulfilment of the requirements for the degree of Master of Engineering (Electrical and Electronic) in the Faculty of Engineering at Stellenbosch University

Supervisor: Professor J.B. de Swardt

April 2019

Declaration

By submitting this thesis electronically, I declare that the entirety of the work contained therein is my own, original work, that I am the sole author thereof (save to the extent explicitly otherwise stated), that reproduction and publication thereof by Stellenbosch University will not infringe any third party rights and that I have not previously in its entirety or in part submitted it for obtaining any qualification.

Date: .....April 2019.....

Abstract

The objective of this project was to design a microwave sterilisation system that can be used to sterilise Rooibos tea. Rooibos tea is currently sterilised with a steam treatment, but this affects the tea's colour and flavour. Microwave irradiation was investigated as an alternative form of sterilisation.

Often microwave sterilisation tests are performed without the proper implementation of microwave power control. Accurate microwave output power control was achieved by designing a custom magnetron power supply that uses a TRIAC to switch the mains voltage every half-cycle. A control system, that measures the applied and the reflected microwave power, was implemented to ensure a constant microwave power is delivered to the load. Calibrated measurements were taken of the system input power, microwave output power and applicator temperature. Adjustments were made to the microwave applicator to ensure that the dry tea did not burn.

Microbiological tests were performed on the treated samples for Salmonella, E.Coli/Coliforms and aerobic plate counts (TVC's). The South African standard for microbial safety of Rooibos tea was used as reference. The microwave sterilisation system worked well for Salmonella and TVC's, but E.Coli/Coliforms proved more resilient. A definite batching problem was identified with the sterilisation of raw farm products that contain different concentrations of microorganisms. This study provides a good foundation for any further research on the microwave sterilisation of Rooibos tea, as well as a range of hardware solutions for various other microwave power control applications.

Uittreksel

Die doel van hierdie projek was om `n mikrogolfsterilisasiestelsel vir Rooibostee te ontwerp. Tans word Rooibostee met stoom gesteriliseer, maar dit affekteer die kleur en geur van die produk. Mikrogolfbestraling was ondersoek as `n alternatiewe sterilisasiemetode.

Dit gebeur gereeld dat mikrogolfsterilisasietoetse gedoen word sonder dat behoorlike mikrogolfdrywingsbeheer toegepas word. Akkurate mikrogolfuittreedrywingsbeheer was behaal deur `n gespesialiseerde magnetronkragbron te ontwerp, wat gebruik gemaak het van `n TRIAC om die intreespanning elke halfsiklus te skakel. `n Beheerstelsel, wat die toegepaste en weerkaatste mikrogolfdrywing gemeet het, was ontwerp om te verseker dat die las teen `n konstante mikrogolfdrywing bestraal word. Gekalibreerde metings was gemaak van die stelsel se intreedrywing, mikrogolfuittreedrywing en die temperatuur van die tee. Aanpassings moes gemaak word aan die mikrogolfoond om seker te maak dat die Rooibostee nie brand nie.

Die mikrobiologiese toetse wat gedoen was op die behandelde teemonsters het getoets vir Salmonella, aerobiese plaattellings en E.Coli/Coliforms. Die Suid-Afrikaanse standaard van veiligheid vir mikroorganismes in Rooibostee was gebruik as verwysing. Die mikrogolfsterilisasiestelsel het goed gewerk vir Salmonella en aerobiese plaattellings, maar E.Coli/Coliforms was meer bestand teen die behandeling. `n Definitiewe probleem was geïdentifiseer waar verskillende monsters van `n plaasproduk verskille in mikrobiologiese aktiwiteit getoon het. Hierdie studie bied `n goeie grondslag vir verdere navorsing op die mikrogolfsterilisasie van Rooibos tee, asook `n reeks hardeware-oplossings vir verskeie mikrogolfdrywingsbeheertoepassings.

Acknowledgements

I would like to express my sincere gratitude to the following people and organisations.

EMSS for sponsoring me for the last two years.

Wessel Croukamp for building the tea mixer and providing me with good advice on any other workshop related tasks I had to complete.

Wynand van Eeden for helping me develop the PCB's I needed for the project.

Jenny Martin for ordering all the components I needed and always being friendly and helpful.

Prof. P. Gouws for advising me on the Rooibos tea tests and coordinating any assistance I may have needed.

Jadrie Groenewald for helping me with the Salmonella lab tests.

Elisma Ackermann for helping and assisting with the E.Coli and TVC lab tests.

Stephanus Schoeman for proof reading the thesis and providing me with valuable style and language tips.

Prof. Johann de Swardt for guiding me through this process by having an open door to discuss problems and provide meaningful insight. Teaching me to break a big problem up into smaller segments and tackle them one by one.

Dedications

This thesis is dedicated to both of my parents, who gave me the opportunity to complete this qualification and offered their love and support throughout the duration of my studies.

Contents

List of Figures

List of Tables

Nomenclature

Chapter 2

P	Polarisation Field
P_{max}	Maximum Polarisation Field
P_{ave}	Average Power
E	Electrical Field
E'	Local Electrical Field
E_{max}	Maximum Electrical Field
H	Magnetic Field
D	Electric Displacement Vector
J	Total Current Density
J_c	Conduction Current Density
σ	Conductivity
μ	Dipole Moment
q	Charge
x	Distance Between Charges
α_t	Total Polarisability
α_e	Electrical Polarisability
α_a	Atomic Polarisability
α_d	Dipole Polarisability
α_{sc}	Surface Charge Polarisability
ε_o	Permittivity of Free Space
ε'	Relative Dielectric Constan
χ	Electric Susceptibility
ε_{eff}	Total Loss Factor

ε_e ..... Electric Loss Factor
ε_a ..... Atomic Loss Factor
ε_d ..... Dipole Loss Factor
ε_{sc} ..... Surface Charge Loss Factor
ω ..... Frequency
σ ..... Lag Factor

Chapter 3

TRIAC ..... Triode for Alternating Current
VARIAC ..... Variable Autotransformer
IGBT ..... Insulated Gate Bipolar Transistor
DC ..... Direct Current
AC ..... Alternating Current
V_{RMS} ..... Voltage Root Mean Square
L ..... Inductance
C ..... Capacitance
Q ..... Quality Factor

Chapter 4

$C_{junction}$ ..... Junction Capacitance
$V_{blocking}$ ..... TRIAC Blocking Voltage
P_i ..... Input Power
θ_{oc} ..... Open Circuit Power Factor
θ_{sc} ..... Short Circuit Power Factor
R_s ..... Snubber Resistance
C_s ..... Snubber Capacitance
C_1 ..... Voltage Doubler Capacitance
ζ ..... Damping Ratio
R_t ..... Temperature Dependant Resistance
D_{max} ..... Maximum Voltage Difference
G ..... Voltage Gain

R_g ..... Gain Resistance
ADC ..... Analog to Digital Converter

Chapter 5

VNA ..... Vector Network Analyzer

Chapter 7

PID ..... Proportional Integral Derivative
PI ..... Proportional Integral
A ..... Maximum Plant Output
t_d ..... Delay Time
t_s ..... Sample Time
T_{delay} ..... Total Delay
τ ..... Time Constant
R ..... Reaction Curve Slope
L ..... System Lag
K_p ..... Proportional Parameter
K_i ..... Integral Parameter
K_d ..... Derivative Parameter

Chapter 8

CFU ..... Colony Forming Unit
TVC ..... Total Viable Count
SANS ..... South African National Standards
TMC ..... Too Many to Count
E.Coli ..... Escherchia Coli

Chapter 1

Introduction

1.1 Background

Rooibos tea has a high microbial count, which is mostly accredited to its processing. South Africa and Europe both have standards that specify the maximum microbial count allowed per gram of Rooibos tea [12]. In order achieve these standards, Rooibos tea undergoes a steam treatment. Steam is an effective form of sterilisation, but results in a loss of flavour and quality of the Rooibos tea.

Microwaves are widely used for its heating ability, the most common being the domestic microwave oven. Microwave sterilisation has been proven to work on spices and offers an attractive alternative to steam [13]. The microwave sterilisation process would not add moisture to the tea, possibly resulting in a better quality product. The need is therefore identified to build a small scale microwave sterilisation setup to investigate its viability.

Previous studies have shown cases where microwave sterilisation proved to be more effective than conventional heating methods. This was accredited to the so called "non-thermal" effect of microwave heating. The "non-thermal" effect refers to the frequency and the temperature gradient associated with microwave heating [14]. This project investigated these effects on Rooibos tea.

1.2 Objectives

The main objective of this project was to build a microwave sterilisation system from readily available domestic microwave oven parts. In order to achieve this objective, an accurate magnetron output power control strategy had to be implemented. The second important component was to measure the internal temperature of the microwave applicator. Having accurate power control and temperature measurements allowed for reliable scientific research to be performed using the microwave sterilisation system.

The second objective was to ensure that the microwave sterilisation system is specifically suited for Rooibos tea sterilisation. This required the system to be able to cope with a relatively dry load, which has an effect on microwave power control as well as ensuring that the tea does not burn. The small scale setup had to be capable of sterilising at least 25 g of Rooibos tea at a time.

The final evaluation of the system required testing the sterilisation effect it has on Rooibos tea. This was done by following standard microbial testing procedures to evaluate the aerobic plate count and E.Coli/Coliform counts for a batch of Rooibos tea. These counts were then compared to the maximum allowable values set out in the South African Rooibos standard to evaluate its effectiveness.

1.3 Project Development

Work on this project was completed in the following order:

- The microwave output power of the magnetron in a domestic microwave oven was measured. The diode detectors used in the measurements were then calibrated to ensure the measurement accuracy.
- The first sterilisation tests were done on tea. The initial tea experiments were done to get an idea of the characteristics of tea in a microwave oven and the viability of microwave sterilisation.
- Hardware required to do temperature measurements and input power control was designed and used to build a control system for the temper-

ature of a light bulb. This was done to lay down the necessary control theory under ideal conditions, before implementing and testing it on the actual system.

- Controlling the microwave output power of a magnetron was investigated next. Different methods of power control were tested and a custom solution was found.
- The microwave applicator was modified to be suitable for tea sterilisation. The effects of moisture content as well as the position of the load inside the microwave applicator was investigated. After final modifications the system was evaluated by using thermal imaging to ensure uniform heating.
- A software package was development for the microwave sterilisation system. It serves as a dashboard to monitor and control the microwave output power and temperature of the system and store all data captured during testing.
- The final step was to test the microwave sterilisation system. Rooibos tea was sterilised and microbiological tests were done to evaluate the sterility of the samples.

1.4 Thesis Chapter Breakdown

Chapter 2

The literature review starts off by discussing Rooibos tea and its need for sterilisation. Microwave sterilisation is identified as a possible solution, its advantages and disadvantages are identified and discussed. Microwave heating is discussed to give a more in depth understanding of how it works and the factors that have an influence on its effectiveness. Claims of "non-thermal" effects of microwave heating, as seen in previous studies, are discussed. This poses the question: Does microwaves contribute more than simply the heat generated during irradiation? Finally a set of favorable characteristics for microwave sterilisation systems are identified.

Chapter 3

The focus of this chapter is on the magnetron and customised power supply that was developed to control the microwave output power of the system. The magnetron's structure and how it functions are discussed. Various methods available to control the magnetron's output power are discussed and evaluated. A range of tests performed to compare power supply options are presented and a final design is derived from the results.

Chapter 4

The detailed hardware design of the system is presented in this chapter. Each functional hardware block is covered separately to give more insight into its operation. These blocks include the TRIAC switching circuitry, zero-crossing detection circuit, temperature sensors and the stepper motor control hardware.

Chapter 5

The modifications to the microwave applicator are discussed in this chapter. The implementation of the mode stirrer and the tea mixer is evaluated. The effects of load position and moisture content on the microwave output power of the magnetron are illustrated. The need for accurate microwave power control, especially for the dry loads associated with tea sterilisation, is thus highlighted.

Chapter 6

All of the software developed for this project is explained in this chapter. This includes a master program developed to control the whole system and interface with the various system components. The Arduino code written for the power control and sensor measurements is also explained. This gives an overview of the system and how the components interact.

Chapter 7

This chapter starts by covering the theory required to implement a PID controller. The PI controllers used to control the temperature and microwave output power are explained. All transfer functions and step responses are simulated and compared to the measured results.

Chapter 8

The chapter starts off with basic microbiology theory. The experimental setups and microbiological testing procedures are explained. The results obtained from microwave sterilisation tests are then presented.

Chapter 9

Conclusions are made based on the results obtained during this project. The project objectives stated at the beginning of the project are revisited and evaluated one by one.

Chapter 10

More studies and tests that can be performed now that the system has been developed are suggested. Further possible improvements are presented based on the insights gained during the testing and development of the system.

Appendix A

Illustrates the waveforms obtained from the TRIAC power controller simulation, other waveforms of interest and where improvements can be made in the simulation.

Appendix B

Contains the overall system schematic with all hardware connections.

Appendix C

Shows the raw data for the microbiological test results.

Chapter 2

Literature Study

2.1 Chapter Introduction

The literature review covers the main topics applicable to the scope of the project. The literature review starts with the processing of Rooibos tea, the microbial risk involved with Rooibos tea processing and why microwave heating was investigated as an alternative method of sterilisation. The fundamentals of dielectric heating is covered by looking at polarisation, dielectric constants and the effects of external factors on the dielectric constant. Claims of non-thermal effects seen in previous work is reviewed to identify the criteria on which these claims were either accepted or rejected. The chapter closes off by identifying characteristics of a microwave sterilisation system that allows for research on "non-thermal effects" of microwave heating.

2.2 Rooibos Tea

2.2.1 Processing of Rooibos Tea

The Rooibos plant is harvested annually where the top 30 cm of the shrub is cut off. The lifecycle of an annually harvested plant is between three to five years, after which the plant starts to die and new Rooibos needs to be planted. The newly planted Rooibos will be ready for another annual harvest cycle after approximately two years.

The processing of Rooibos tea involves a calculated set of procedures, which

are closely monitored, to ensure a good quality product that meets microbial standards. Rooibos tea comes in both a red and a green form, each with its own specific processing requirements. The different processing procedures are due to the unique properties of the Rooibos plant. Once the plant is bruised it will turn red during fermentation. Bruising releases the polyphenols and oxidative enzymes necessary to speed up the fermentation process [15].

The work done in this thesis focuses on the well known red Rooibos tea and the processing thereof is described below.

After being harvested the tea is put through a chopping machine that cuts the tea into pieces of about 3 mm in length. Once cut the tea is spread out onto a concrete slab. The tea is then prepared for its fermentation process. For proper fermentation to take place the moisture content of the tea is increased by adding water and a heavy roller is used to bruise the tea. The tea is then collected into heaps and left to ferment over night. The fermentation causes the temperature to rise in the fermentation heap and the colour of the tea to change. The typical temperature in a fermentation heap is about 38 - 40 $^{\circ}C$ [12]. The last outdoors step is to spread the tea out in the sun and allow it to dry.

The tea is sifted after the sun drying process. The sifting removes stems and twigs from the cut tea to improve the quality. The sifted product is then sterilised. The sterilisation is done by steam. Sources state that the steam process exposes the tea to temperatures in the range of 85 - 92 $^{\circ}C$ for about 2.5 minutes [12]. A personal visit to a tea processing plant revealed that sterilisation can also be achieved by exposing the tea to a temperature of about 160 $^{\circ}C$ for a period of 1.5 minutes [16]. After being exposed to the steam the tea is air dried and packed into bags for bulk storage.

2.2.2 Microbial Risk in Rooibos Tea

South Africa and Europe both have standards for the maximum microbial count allowed per gram of Rooibos tea. Microbes are responsible for spoilage

in food and can be classified as a health hazard. These standards are put in place to enforce the importance of minimising the microbial count in Rooibos tea.

The high microbial counts of untreated Rooibos tea are mostly accredited to the nature of the processing of the tea. The processes take place in an open air environment where it is bruised and handled, exposing the tea to many possible sources of contamination. This is in addition to the naturally occurring microorganisms present on the plant before harvesting. The fermentation process requires the addition of water and results in a temperature rise. These high moisture and high temperature conditions provide a very suitable environment for the growth and reproduction of microorganisms [12].

Figure 2.1: The steam sterilisation process at Carmien Tea.

Nonetheless, fermentation is a necessary step in the preparation of Rooibos tea. Therefore sterilisation will always be one of the necessary processing procedures. The need for a possible alternative to the existing steam process is an area that can be investigated. A more delicate method of sterilisation, capable of maintaining the natural flavours and properties of the tea would be of great benefit to the Rooibos industry.

2.3 Microwave Sterilisation

2.3.1 Advantages of Microwave Heating

There are several proven benefits of microwave heating which makes it a very attractive option in food applications.

Microwave heating is known for its steep temperature gradient, which allows for rapid heating. This property allows for shorter processing times. Benefits associated with shorter processing times come down to the preservation of that the product's taste and texture. It has also been shown that better nutrient retention can be achieved with a shorter period of heat exposure [17][18].

Selective heating and volumetric heating can be achieved using microwaves. This is due to the electromagnetic wave's ability to penetrate the irradiated medium. Hence the whole medium can be heated simultaneously, given that the diameter of the load is smaller than the penetration depth. Selective heating refers to the fact that the microwaves will only interact with the water or moisture present in the load [18][19].

The ability to switch the electromagnetic wave on and off at high speeds allows for accurate power control. Therefore better control over temperature profiles and higher product temperatures can be achieved. This level of control allows the freedom to experiment with different radiation strategies for specific applications [17][18][20].

2.3.2 Disadvantages of Microwave Sterilisation

The disadvantages of microwave heating are in actual fact the consequence of some of its benefits.

Uneven or non-heterogeneous heating patters can form due to the electromagnetic waves forming a standing wave inside the microwave cavity. A way of improving the heating pattern can be to continuously move the medium through the standing wave so that no one point gets over exposed. The other approach is to add a mode stirrer.This will cause random reflections inside

the microwave applicator and thus disrupt the standing wave pattern. The assumption can then be made that the electrical field is evenly distributed within the microwave applicator [18].

Edge overheating is due the penetrating capabilities of the electromagnetic waves. This causes objects with sharp edges to be radiated from multiple directions leading to a superposition of microwave energy at the edges of the load [13].

Special precaution must be taken when working with microwave radiation as leakage can be harmful to human beings. This is the main reason for its poor consumer acceptance [17].

2.3.3 Sterilisation of Herbs and Spices using Microwaves

A study looking at the microbiological status of spices in a local market and the sterilisation effects of a domestic microwave oven pointed out that steam is an effective sterilisation method, but has the known side effects of causing discolouration and a loss in volatile oil content in the product. They also recognise the disadvantages associated with microwave heating. The researchers still opted to go for microwave sterilisation as it offers the same benefits as conventional heating but with improved product quality and reduced exposure times. Microwave sterilisation is also known to be effective against a wide range of microorganisms. The conventional microwave oven is identified as a convenient option as it is not hard to find, cheap and easy to use [13].

The experiment consisted of sixteen different herbs and spices, amongst others tea. The tests were done in duplicate at 5 different time intervals over a minute (every 15 seconds). A dry sample test and a wet sample test was also conducted, the wet samples being in a solution.

The samples were tested before sterilisation to identify which microorganisms were present in the samples. Two pathogens were identified namely Salmonella and Staphylococcus aureus. These two microorganisms are responsible for the majority of reported food borne illness cases. Next, aerobic plate counts were done to identify the general microbial activity in the samples. Samples were

also tested for coliforms. Lastly, tests were done for fungi and spore forming bacteria [13]. The spore formers are classified as mesophilic and thermophilic bacteria. Mesophilic means that the bacteria thrive at mid range temperatures around 20 - 40 $^{\circ}C$. Thermophilic bacteria thrive at high temperatures in the range of 40 - 90 $^{\circ}C$ [21].

These tests were then repeated after sterilisation to determine how well the microwaves were able to sterilise the spices. The results indicated that no Salmonella or Staphylococcus aureus were detected after sterilisation, on any of the samples. The specific result of interest is that of the tea test. The tea showed a sharp decline in both fungi and spore forming bacteria for both the wet and dry samples. However, microorganisms in the tea did prove to be more resilient than most of the other spices and only started declining after about 50 seconds at 700 W.

This positive result indicates that microwave sterilisation for the Rooibos industry might be a viable option. Note that no power control was implemented; the spices were simply placed in the microwave oven [13].

2.4 Dielectric Loss

Materials can be divided into two major groups, namely conductors and insulators. The main difference between them being that the electrons in the atomic structure of a conductor are free to move around in the material and not be associated with a specific nucleus. Insulators or dielectrics have electrons bound to specific nuclei that are therefore unable to move freely through the medium [22]. Electromagnetic waves have the ability to heat up non-conductive materials. The generated heat is due to the property of an electromagnetic wave to polarise bound charges in a material and the inability of the polarised charges to follow the rapid oscillations of the electromagnetic field [23].

2.4.1 Polarisation

Polarisation of atoms and molecules in a dielectric medium is essential for high frequency heating to occur. There are different forms of polarisation,

each more prominent at different frequencies. Understanding the types of polarisation and the frequency dependence of each type will provide a good intuitive feeling for what is happening to materials irradiated at the microwave frequency.

The applied electrical field will interact with the electrons around the nuclei of the atoms in a dielectric material. The interaction will cause a displacement of electrons around the nucleus and therefore polarise the atom's electron structure. This displacement is called the dipole moment of the atom. The atom will try and align its polarity to that of the applied field. This is called electronic polarisation [22][23].

Similarly the atomic nuclei of a molecule can also be polarised. This occurs due to uneven charge distributions in the molecular composition, referred to as atomic polarisation. The applied field will therefore cause a dipole moment between unlike atoms in the molecule [1].

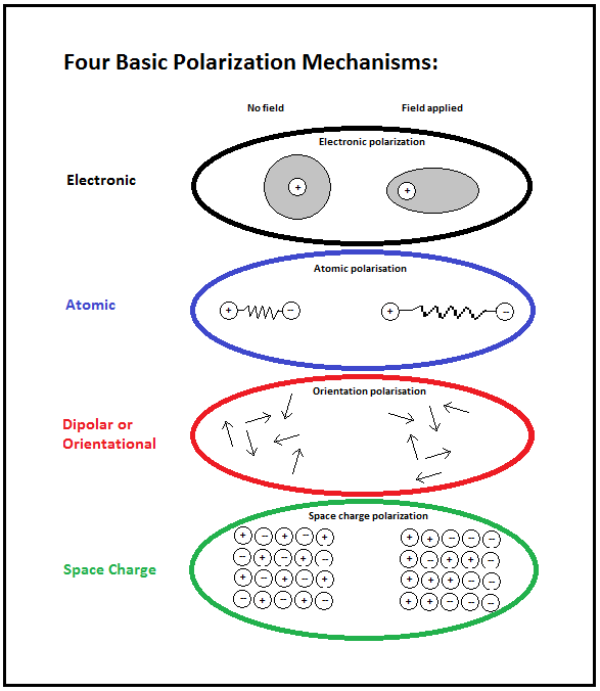

Figure 2.2: The different forms of polarisation [1].

Molecules with a naturally asymmetric charge distribution are referred to as

polar molecules, as one side is more negative or positive than the other, resulting in a permanent dipole moment in the molecule. Applying an electromagnetic field to a polar molecule will result in the reorientation of the molecule to align with the applied field, also called dipolar or reorientation polarisation [22].

Space-charge polarisation is experienced when the applied field causes the built up charges at the surface or interface between two mediums, exposed to the changing electromagnetic field, to be polarised. This is prevalent at low frequencies and usually has a small contribution to the heat generated [23].

2.4.2 The Electric Field at Atomic Level

The polarisability of a medium accompanied by its conductive properties play an important role in high frequency heating [23]. To illustrate the previous statement, the relation between an applied e-field and the e-field at molecular level of the dielectric medium is derived mathematically.

The derivation is started by defining what a dipole moment is: A dipole moment is the product of the charge and the displaced distance between the positive and negative charges. This is expressed mathematically in Equation 2.4.1, where μ is the dipole moment, q the charge and x the distance between the positive and negative charges.

$$\mu = qx \tag{2.4.1}$$

The sum of all these individual dipole moments in the dielectric medium can be described as the polarisation field P. The polarisation field accounts for all the bound charge in the system. This is expressed in Equation 2.4.2, where μ is the dipole moment and N' accounts for the sum of all the individual dipole moments.

$$P = \mu N' \tag{2.4.2}$$

The dipole moment can also be related to the polarisability of the medium and the e-field experienced at molecular level. Therefore the product of the local e-field experienced by a molecule and the polarisability of the medium

gives the resulting dipole moment, this is expressed in Equation 2.4.3. The polarisability accounts for all four types of polarisations discussed above. This is expressed in Equation 2.4.4, where α_t is the total polarisability, α_e is the electronic polarisability, α_a is atomic polarisability, α_d is dipole polarisablitiy and α_{sc} is the surface charge polarisability.

$$\mu = \alpha_t E' \tag{2.4.3}$$

$$\alpha_t = \alpha_e + \alpha_a + \alpha_d + \alpha_{sc} \tag{2.4.4}$$

With the dipole moment defined and its relation to the polarisation field established, the final part of the derivation is to relate the applied e-field to the e-field experienced by a singular atom or molecule.

The total charge in the system can be described by the electric displacement vector D. The total electric displacement field is the sum of the applied e-field in free space and the polarisation field created by the bound molecules. Equation 2.4.5 expresses this mathematically, with P as the polarisation field and $\varepsilon_o E$ as the applied e-field.

$$D = \varepsilon_o E + P \tag{2.4.5}$$

The polarisation field can also be described by some factor relative to the applied e-field and the permeability of free space, so that χ is the factor relating the applied e-field to the polarisation field in Equation 2.4.6.

$$P = \varepsilon_o \chi E \tag{2.4.6}$$

This allows the definition of D to be simplified, redefining it with a relative dielectric constant $\varepsilon^{`}$ in Equation 2.4.7.

$$D = \varepsilon_o E + \varepsilon_o \chi E = (1 + \chi)\varepsilon_o E = \varepsilon_o \varepsilon^{`} E \tag{2.4.7}$$

The derivation is then completed by substituting Equations 2.4.2, 2.4.3 and 2.4.7 into Equation 2.4.5, which results in an expression relating the e-field associated with a specific dipole moment (E') to the applied e-field ($\varepsilon_o E$) as shown

in Equation 2.4.8.

$$\varepsilon_o \varepsilon` E = \varepsilon_o E + (\alpha_t E')N' ==> E'N' = \frac{\varepsilon_o E(\varepsilon` - 1)}{\alpha_t} \tag{2.4.8}$$

This derivation shows that the e-field at the molecular level of the dielectric medium is dependant on the material's polarisability and dielectric constant [23].

2.4.3 Dielectric Constant

The dielectric constant is introduced to represent the loss in a system. A mathematical expression is needed to clarify which factors contribute to the loss experienced in a dielectric medium.

Starting with Maxwell's modified version of Ampere's law in Equation 2.4.9. The line integral of the magnetic field H along a closed path gives the total current enclosed by the path. The total current in the medium is represented by the conduction current density J_c and the displacement current density $\frac{d}{dt}D$ for any surface bound by the closed contour C [24].

$$\oint_C H \cdot dl = \int_S J_c \cdot dS + \int_S \frac{d}{dt} D \cdot dS \tag{2.4.9}$$

The conduction current density in Equation 2.4.10 equals the product of the applied e-field and the conductivity (σ).

$$J_c = \sigma E \tag{2.4.10}$$

The electrical displacement vector D was derived in the polarisation section above.

$$D = \varepsilon_o \varepsilon` E \tag{2.4.11}$$

The e-field in Equation 2.4.12 is a sinusoidally varying field.

$$E = E_{max} e^{j\omega t} \tag{2.4.12}$$

Writing Ampere's law in differential form and substituting Equations 2.4.10 and 2.4.11 produces Equation 2.4.13, where J is the total current density.

$$\nabla \times H = J = J_c + \frac{\partial}{\partial t} D = \sigma E + \frac{\partial}{\partial t} \varepsilon_o \varepsilon^{`} (E_{max} e^{j\omega t}) \tag{2.4.13}$$

Assuming that the e-field is sinusoidal allows the expression to be simplified to the following [23].

$$J = \sigma E + j\omega \varepsilon_o \varepsilon^{`} E = j\omega \varepsilon_o (\varepsilon^{`} - j\frac{\sigma}{\omega \varepsilon_o}) \tag{2.4.14}$$

It is known that the loss is represented by the imaginary part of the dielectric constant [25], but it is difficult to isolate and measure the effect of each type of polarisation on the loss of the dielectric medium. Therefore, to make Equation 2.4.14 hold for all frequencies, the losses in the dielectric material can all be added together to form a total loss factor ε_{eff} in the dielectrc constant.

$$\varepsilon_{eff} = \varepsilon_e + \varepsilon_a + \varepsilon_d + \varepsilon_{sc} + \frac{\sigma}{\omega \varepsilon_o} \tag{2.4.15}$$

$$J = j\omega \varepsilon_o (\varepsilon' - j\varepsilon_{eff}) E \tag{2.4.16}$$

Equation 2.4.16 shows that the loss factor is dependent on both the polarisability and the conductivity of the dielectric medium. Therefore any losses experienced when irradiating a dielectric material can be accredited to these two factors [23].

2.4.4 Qualitative Description of Microwave Heating

The sections above are brought together to provide a good description of microwave heating and why it occurs at the frequency that it does. The Debey equation (Equation 2.4.17) is used to describe the average power dissipated in a dielectric medium per unit volume. It makes use of the maximum electrical field (E_{max}), maximum polarisation field (P_{max}), frequency (ω) and a lag factor (ϕ). The lag factor indicates how far the polarisation field is out of phase with the applied electrical field. The emergence of a lag factor is due to the polar molecules having a time constant associated with its polarisation. This refers back to the polarisability of the dielectric medium.

$$P_{ave} = \frac{1}{2} E_{max} P_{max} \omega \sin \phi \tag{2.4.17}$$

With this knowledge in mind the following can be concluded: At low frequencies the variation in the electromagnetic field is slow and the dipoles have

enough time to change orientation with the field. This means that most of the energy applied to the system is being used to change the orientation of the molecule and is therefore absorbed. As the frequency increases and the variations in the electromagnetic field become faster, the molecules have more difficulty changing orientation and therefore the applied field starts to lag. The lag in orientation brings about the loss in the system which contributes to the heat generated. Very high frequencies decrease the polarisation of the molecules. The ability to generate phase lag between the applied field and the polarisation field is lost as the molecule no longer oscillates. Therefore no more power is dissipated in the load and no more heat is generated in the medium [23].

2.4.5 Factors Influencing Dielectric Constant Value

2.4.5.1 Effect of Moisture on Dielectric Constant

Generally, the dielectric constant increases with moisture content. It is important to note that a critical moisture content value exists for each dielectric medium. The critical point occurs at the transition between free moisture and bound moisture within the material. The increase of free water in a medium brings about a steep increase in the dielectric loss factor, whereas the dielectric constant remains relatively constant once the free moisture is removed [23].

2.4.5.2 Effect of Temperature on Dielectric Constant

For materials with a low moisture content the dielectric constant initially increases with temperature. The increase in temperature reduces the amount of physical bindings in the material which allows more dipoles to orientate themselves with the applied field. High moisture content has the opposite effect on the dielectric constant. Increased temperature decreases the dielectric constant and is balanced out by an increase in conductivity [26][23].

2.4.5.3 Effect of Frequency on Dielectric Constant

At low frequencies the conductivity of the dielectric medium dominates its dielectric constant. As the frequency increases the conductivity contributes less and the polarisation takes over.

For the purposes of this project the microwave operating frequency remains constant. At the microwave frequencies allocated to industrial microwave heating the dipole polarisation has the greatest contribution to the value of the dielectric constant [26][23].

2.5 Non-Thermal Effect

There is a considerable amount of literature concerning microwave sterilisation. A number of research groups have pointed out that their recorded results cannot be explained merely by the thermal effect of microwave radiation.This section is based on a literature summary that tries to address the question of the "non-thermal" effect of microwave irradiation.

The traditional temperature model that was commonly accepted is the same as that which is explained in the dielectric heating section above. The proteins and molecules interact directly with the electrical field,resulting in rapid oscillation. The resistance to rotation causes a rise in temperature. The second contributor to the heating property is the conductivity of the medium. However, the results could not be recreated when the tests were repeated under similar temperature profiles with conventional heating. The conclusion was made that an acceleration of chemical transformations were observed in the presence of microwave irradiation, which was then called the "non-thermal" effect of microwave sterilisation. The term "non-termal" is misleading since the phenomenon is in actual fact still thermal in nature.

Attempts to explain this so called "non-thermal" effect gave rise to the following suggestions: Since the temperature gradient of microwave heating is much higher than that of conventional heating, the measurement techniques used are inadequate to accurately measure the rapid temperature increase of the dielectric medium. Therefore an un-measurable thermal force exists which causes a rapid temperature increase. The microwave effect is then pinned on the rate of change of temperature in the medium. The medium's microwave absorbing ability increases with temperature, therefore the microwave energy pronounces the material properties of the medium under heated conditions. This explains the "non-thermal" effects recorded in the test results.

A revisited temperature model is proposed to account for the results obtained by various research groups. In conventional heating the heat is supplied by a source until temperature equilibrium is reached between the source and the medium. This temperature measured during conventional heating is referred to as the bulk temperature. Microwave heating, on the other hand, is capable of delivering a large amount of energy at rapid rates, directly to the molecules in the heated medium, creating a temperature non-equilibrium. The non- equilibrium results in high instantaneous temperatures that cannot be measured due to its short period of existence and the fact that it happens at molecular level.

The model is thus based on having both an instantaneous and a bulk temperature. The bulk temperature is measured with conventional instrumentation, whereas the instantaneous temperature is not measurable. This distinction allows the argument that higher microwave power results in more high instantaneous temperature instances to occur, which leads to a faster increase in the bulk temperature. It can then be said that high instantaneous temperatures may interact with molecules and proteins to account for the so called "non-thermal" effect.

The authors conclude the paper by stating that all microwave sterilisation is thermal in nature and the "non-thermal" effect should rather be termed "micro-effects", specific to microwave radiation. This highlights the need for proper microwave power control and temperature measurement in a microwave environment when investigating any microwave application [14][27][28][29].

2.6 Desirable Characteristics of a Microwave Sterilisation System

This section identifies a set of desirable characteristics that a microwave sterilisation system must adhere to in order to perform scientific research. These characteristics are specifically required if the "non-thermal" effects of microwave sterilisation will be investigated. The microwave output power control, bulk temperature measurement and distribution of the e-field are all critical in mi-

crowave sterilisation system. If these characteristics are not considered in the design of a microwave sterilisation system it could compromise the outcome of the research performed using the system.

The microwave output power of the sterilisation system is the most important parameter to be controlled. The magnetron's microwave output power is what determines the instantaneous temperature in the dielectric medium. The microwave power can either be pulsed or continuous.

The bulk temperature of a medium must be closely monitored and controlled as it is the main figure of merit used to relate microwave sterilisation to conventional heating methods. The measuring technique must be closely considered to ensure that no extra unknowns are added to the system through measurement. For example, a metal temperature probe will introduce a local e-field in the medium it is measuring.

The distribution of the e-field inside the microwave cavity must be closely analysed. Whether it is controlled in a wave guide setup or a multimode cavity with a mode stirrer, the field distribution must be evaluated. Ideally the researcher must be able to make the assumption that the e-field is uniform throughout the microwave cavity [14][29].

2.7 Chapter Conclusion

The chapter started by introducing the steps followed when sterilising Rooibos tea. The microbial risk associated with Rooibis tea and the need for an alternative sterilisation technique was raised. The successful sterilisation of herbs and spices were then reviewed to illustrate that microwave sterilisation might be a viable alternative. The nature of dielectric heating was then covered in detail, in order to let the research tie in with the claims of the so called "non-thermal" effect. The desirable traits identified for microwave heating research is what the chapter built up to. These traits determined the decision making in the hardware design and the validity of the results obtained from the final tests.

Chapter 3

The Magnetron Power Controller

3.1 Chapter Introduction

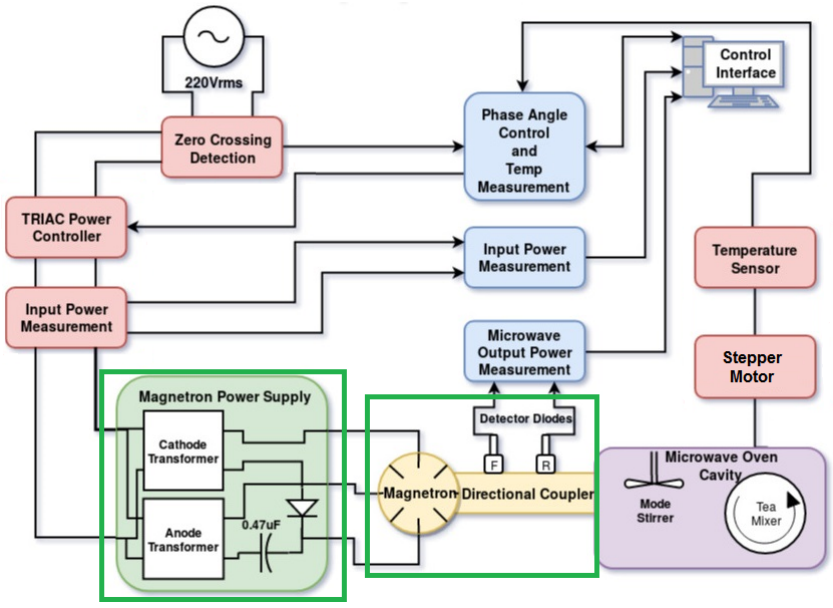

Figure 3.1: Complete system overview.

The chapter starts off by looking at the the magnetron. A theoretical overview of the magnetron's functionality gives a better understanding of the parameters that can be adjusted to change its microwave output power. The different power control methods are discussed and tested. The strengths and weaknesses

of each of the tested systems are identified. Based on the findings, in the analysis of the magnetron power supply strategies, the TRIAC controller was chosen as the preferred method to control the magnetron's output power.

3.2 Magnetron Operations

3.2.1 The Magnetron

The magnetron generates microwaves at a fixed frequency of 2.45 GHz. The mechanical structure of the magnetron has four main components, namely the anode, cathode or filament, antenna and a magnet [30].

The anode is a hollow cylindrical structure with quarter wavelength fins protruding inward. This makes it a resonant structure, causing the magnetron to oscillate at its rated output frequency [31].

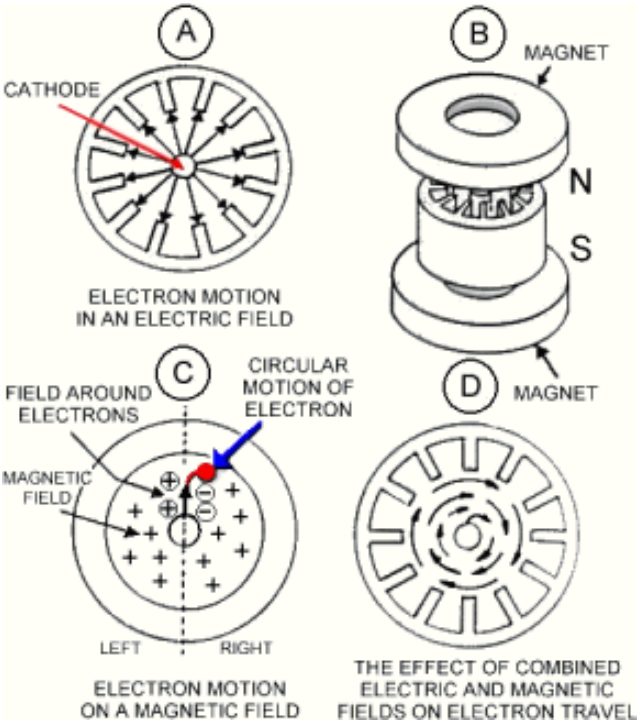

Figure 3.2: Different components of the magnetron structure [2].

The cathode generates the electrons in the magnetron. This happens when a high supply current heats up the cathode and it starts expelling electrons. The large DC potential between the cathode and anode allows the electrons to accelerate radially toward the anode [2]. The applied magnetic field is perpendicular to the electron motion and therefore has a curl effect on the motion of the electrons. The electrons spin around the cathode in an electron cloud until it escapes the magnetic field and reaches the anode. Current starts to flow when the electrons reach the anode [31].

The magnetron is described as a diode-type electron tube [19]. This is because it has two main modes of operation, namely oscillating mode and non-oscillating mode. A specific DC potential is required for the electrons swirling around the cathode to escape the force of the magnetic field. Consequently the magnetron switches on and starts to oscillate above a specific DC potential between the anode and cathode. This characteristic is illustrated in Figure 3.3, showing that very little current flows until the potential between the anode and cathode reaches 3.5 kV, after which a sharp increase in anode current is experienced. This voltage is called the π-mode voltage as it allows for the π-mode to dominate [3][30][31].

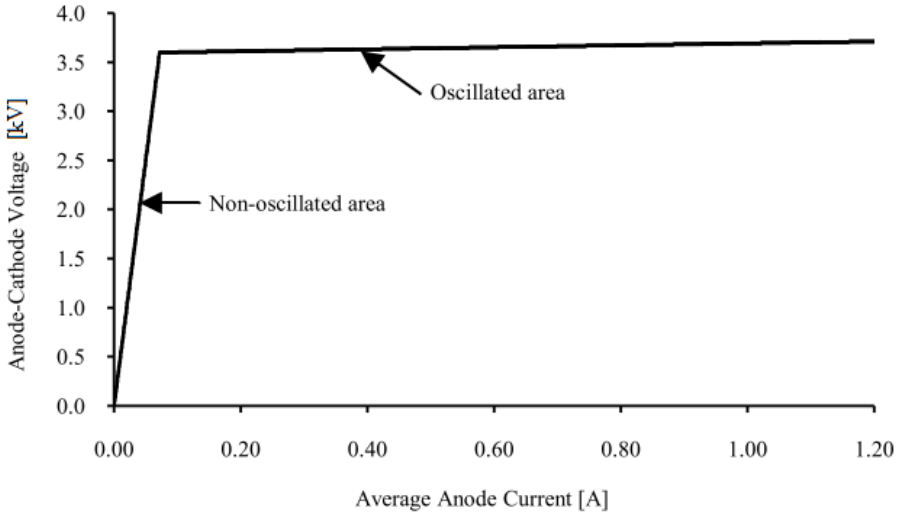

Figure 3.3: Magnetron anode voltage vs anode current plot [3].

The π-mode refers to the mode where the magnetic field on each consecutive anode fin has an opposite polarity. Therefore there is a 180 degree phase shift between anode fins. The cavities between the anode fins act as high Q parallel LC circuits [2]. When current starts to flow in the fins of the anode, it induces a fringing magnetic field between adjacent anode fins. This fringing field couples the fins and causes the polarity on each consecutive fin to be opposite. Other modes also exist, but to ensure that the π-mode dominates, the magnetron design is changed to connect every second anode fin with metal straps to ensure that they will have the same polarity. The microwaves are coupled to the waveguide via a coil in one of these resonant chambers of the magnetron [2][32].

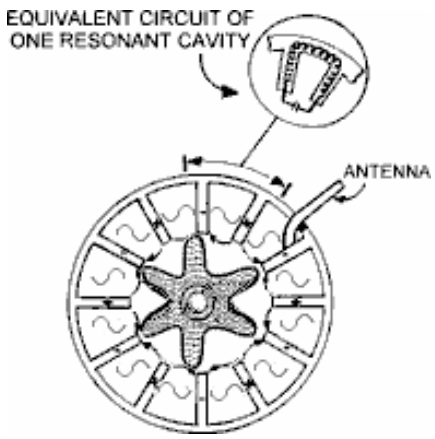

Figure 3.4: Swirling electron cloud inside the magnetron [2].

Conceptual operation of the magnetron can therefore be seen as a swirling cloud of electrons attracted to the positively charged fins on the anode. The polarity of the fins also moves on one fin at a time, causing the electron cloud to move with the polarity of the fins. When the potential between the anode and cathode is increased, the electrons start to spin faster around the cathode. This speed is limited by the induced magnetic field which slows down the electron spin by forcing it to follow the changing polarities on the anode fins, resulting in a constant frequency with increased power. It is important to note that the electrical path around the anode is $2n\pi$ [2][31][33].

The magnetron's performance can be affected by its load. The reactive component of the load impedance can add an inductive or capacitive effect to the resonant structure of the anode causing variations in its output frequency. Similarly, the real part of the load can have an effect on the microwave output power delivered. Variation in frequency and output power is to be expected since a wide variety of materials are placed inside a microwave oven.

The Rieke diagram is a way to show the constant power and frequency circles of a magnetron on a Smith diagram. Each point on the circle shows a load impedance value that delivers the same frequency and output power from the magnetron. One way to avoid the effect of varying load impedance is to place a circulator between the magnetron and the load [31][33].

3.2.2 Magnetron Power Control

The magnetron's output power is related to the interaction between the electrons and the magnetic field. Increasing the applied DC potential between anode and cathode attracts more electrons to the anode at a time. Similarly a change in the magnetic field produces an identical anode voltage vs anode current graph, but increases or decreases the π-mode voltage or turn-on voltage. The π-mode voltage is directly proportional to the magnetic field, because the magnetic field determines how much energy is required for electrons to escape and flow through the anode [31][33]. Furthermore, the cathode supply current determines how long the cathode takes to heat up and start emitting electrons. Increasing or decreasing the cathode supply current determines the amount of electrons expelled by the cathode. Hence, the cathode supply current has an effect on the output power and turn-on time of a magnetron [31].

The power control theory covered in this section will be used to evaluate different magnetron power supplies later in this chapter.

3.3 Microwave Output Power Measurement and Calibration

A calibration setup was used to measure the magnetron output power under ideal conditions. The calibration setup was also used to evaluate and compare properties of different magnetron output power control methods. The intention was to determine the range and resolution of the magnetron output power control methods, without actually implementing controller feedback.

A magnetron output power controller would be used to compensate for the varying impedance of the load. Using water as the load reduces these variations. The high moisture content absorbed most of the radiated microwave output power. However, to be safe and completely eliminate all microwave output power reflections from the load, a circulator was inserted between the magnetron and the load.

The circulator is a standard microwave component that allows microwave power through in one direction, but diverts all of the reflected microwave power into an ideal water load. Since no reflected microwave power reached the magnetron, it eliminated the need for a controller and power levels could simply be set by adjusting the input power to the system [4].

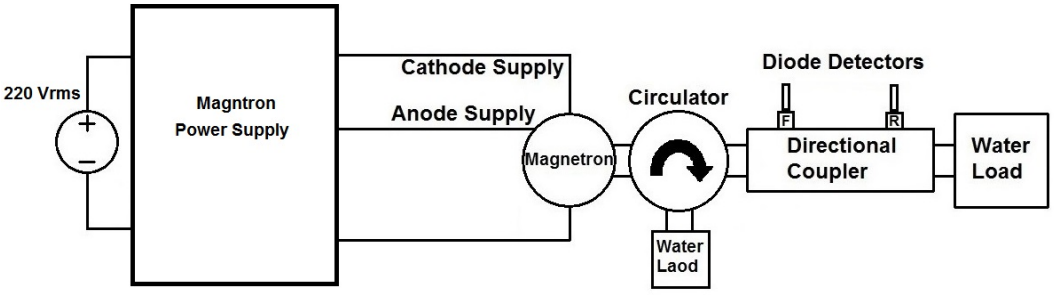

Figure 3.5: Overview of the calibration setup [4].

The complete magnetron calibration setup can be seen in Figure 3.5. This setup was used to measure the microwave output power of a standard domestic

microwave oven. All other magnetron output power control methods were compared with the standard domestic microwave oven power supply using this setup. The microwave output power was measured using detector diodes and a directional coupler.

3.4 Power Measurements

3.4.1 Power Detector Diodes

Detector diodes were used to measure the microwave output power of high frequency 2.45 GHz signals transmitted by the magnetron. The envelope of the pulses transmitted by the magnetron could then be related to a proportional output voltage pulse from the detector diodes. An example of a typical magnetron output pulse can be seen in Figure 3.6. The output voltage vs. input power curve derived from the detector diodes is a non-linear curve that had to be calibrated to ensure accurate output power measurements for both the forward and reflected microwave output power measurements.

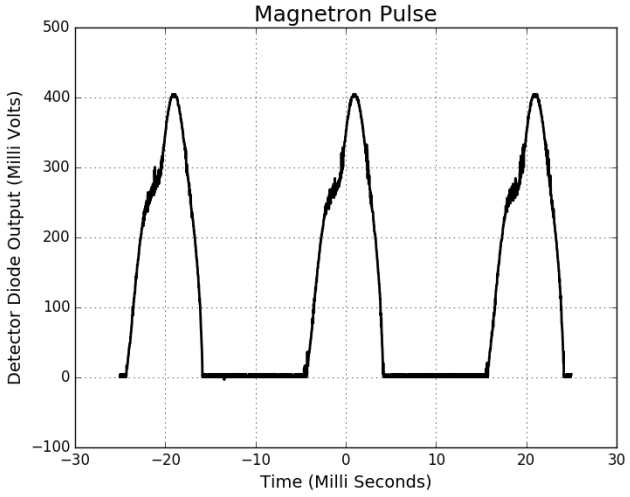

Figure 3.6: Power detector diode output waveform.

3.4.2 Power Detector Diode Calibration

Calibration of the detector diode was done using a signal generator and an oscilloscope. The output power of the signal generator was varied and the

respective output voltage at the desired 2.45 GHz was measured on the oscilloscope. The power delivered to the diodes was verified with a power meter.

The calibration values for the various input power values of both diode 1 (D1) and diode 2 (D2) can be seen in Table 3.1.

Table 3.1: Diode calibration values.

Signal Generator Input Power (dBm)	Power Meter D1 (dBm)	D1 Output Voltage (mV)	Power Meter D2 (dBm)	D2 Output Voltage (mV)
5	5.01	416.00	4.96	458.00
4	4.02	374.00	3.98	401.00
3	3.11	341.00	2.96	356.00
2	2.13	304.00	1.97	309.00
1	1.12	270.00	0.96	266.00
0	0.12	240.00	-0.04	229.00
-1	-0.9	211.00	-1.07	193.00
-2	-1.92	192.00	-2.01	172.00
-3	-2.92	167.00	-3.01	144.00
-4	-3.92	147.00	-4.01	121.00
-5	-4.93	126.00	-5.03	99.90
-6	-5.94	107.00	-6.04	81.80
-7	-6.92	92.30	-7.05	66.10
-8	-7.92	78.40	-8.06	53.10
-9	-8.91	64.50	-9.06	41.80
-10	-9.91	53.10	-10.06	32.60
-11	-10.92	43.60	-11.09	25.30
-12	-11.94	35.80	-12.12	19.50
-13	-12.94	28.90	-13.12	14.60
-14	-13.94	22.70	-14.14	10.80
-15	-14.95	18.40	-15.16	8.00
-16	-15.92	14.30	-16.1	5.92
-17	-16.94	11.00	-17.12	4.32
-18	-17.94	8.48	-18.12	3.12
-19	-18.94	6.48	-19.11	2.18
-20	-19.94	4.96	-20.12	1.44
-21	-20.94	3.68	-21.13	1.04

3.4.3 Microwave Output Power Measurements

The magnetron calibration measurements were done using an oscilloscope connected to a computer to store the pulse profiles of both the forward and reflected channels of the directional coupler. The sampled data was then evaluated using the calibration curves for the respective detector diodes. The result was integrated over the sample period to obtain the average output power.

3.5 Magnetron Power Supplies

There are a variety of available magnetron power supplies each employing a different strategy to control the magnetron's output power. The discussion in this section will look at how each power supply controls the magnetron's output power, the response time of the power supply, when its power setting is changed, and its microwave output power resolution.

3.5.1 Domestic Microwave Oven Power Supply

The schematic in Figure 3.8 is a simplified version of the typical magnetron power supply in a domestic microwave oven. This schematic was adapted from the schematic available on the back of the microwave oven.

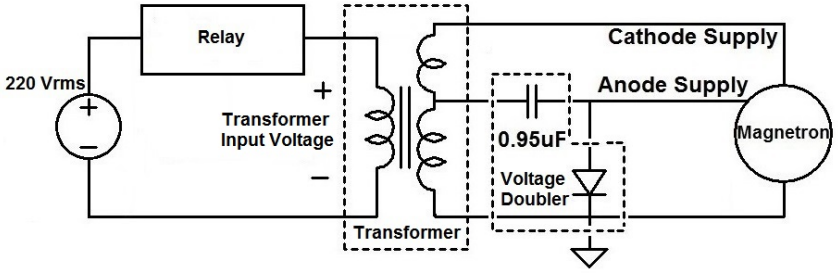

Figure 3.7: Domestic microwave oven power supply schematic [4].

The circuit works as follows: Assume the relay is conducting, thus allowing the 220 V_{RMS} mains voltage to flow to the high voltage transformer. The transformer has two coils, the cathode supply with the smaller coil receives a low voltage with a high current to heat up the magnetron filament. The second coil supplies the voltage doubler circuit, this voltage is stepped up to

2000 V_{RMS} with a low current. The stepped up voltage has a frequency of 50 Hz, meaning it has a 20 ms period, where the first 10 ms is the positive half cycle of the sine wave and the last 10 ms is the negative half cycle. During the positive half cycle the capacitor charges up and the anode voltage remains low. During the second half cycle the polarity on the transformer changes, allowing the diode to conduct and the capacitor to discharge at the same time.

Consequently the voltage from the capacitor and the negative voltage from the transformer superimposes on each other and supplies the magnetron's anode with -4000 V_{DC} for the duration of the second half cycle. The anode voltage exceeds the π-mode voltage during the second half cycle and the magnetron transmits microwave power.

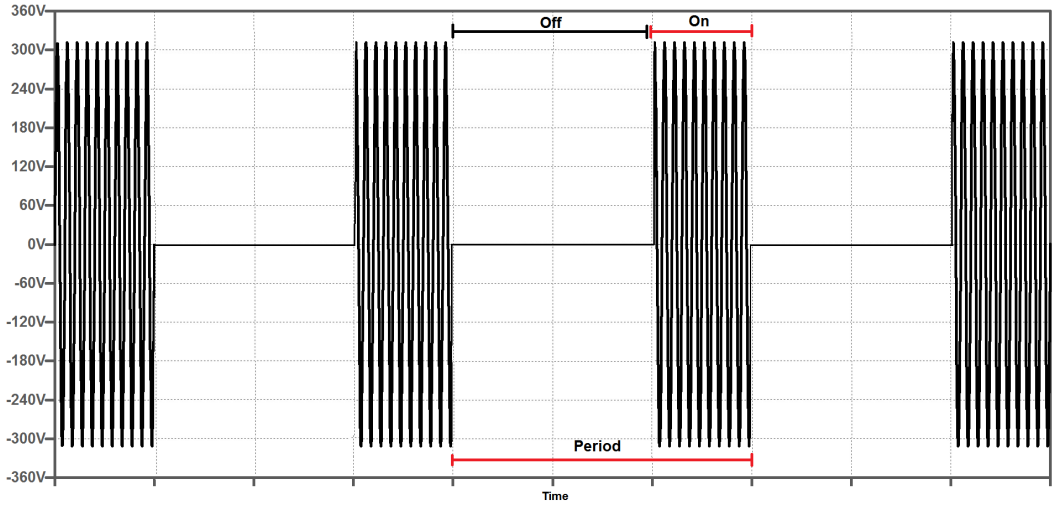

Figure 3.8: Input voltage waveform for duty cycle control of microwave output power.

The magnetron output power control strategy implemented with this power supply is to use the relay to switch the magnetron on and off for longer and shorter durations over a set period, therefore using duty-cycle control to vary the average magnetron output power. Figure 3.8 shows the typical duty-cycle of the input power to the magnetron power supply and Table 3.2 shows the typical power setting for a domestic microwave oven that can be achieved by setting the duty cycle [34].

Table 3.2: Typical microwave output power settings on microwave oven [11].

	Power Output	Description
1	100%	HIGH
2	85%	M.HIGH
3	66%	MEDIUM
4	48%	M.LOW
5	40%	DEFROST
6	17%	LOW

This power supply is simple to implement and sufficient for use in domestic microwave ovens. However, it is important to note that whenever the relay is conducting the magnetron transmits 100% of its rated microwave output power. The average microwave output power is only lower when integrated over the entire period. This means that the response time of the microwave output power controller can only be as fast as the period of the duty cycle allows, which can be in the range of seconds.

3.5.2 Variable Transformer Power Supply

The variable transformer replaces the relay in Figure 3.8. Therefore the mains voltage amplitude can be linearly reduced from 220 V_{RMS}. This means that linear microwave output power control can be achieved for the transformer input voltage range that still allows the magnetron to reach its π-mode voltage. The transformer input voltage waveform will be a pure sine wave with varying amplitudes. For this method to be implemented in a feedback control setup it would make use of a motorised mechanism to mechanically adjust the turn ratio on the transformer. The mechanical solution would have drawbacks in controller response time as well as mechanical wear and tear on the setup [4][31].

3.5.3 TRIAC Control Power Supply

The TRIAC circuit accompanied by a zero-crossing detection circuit would replace the relay in Figure 3.8. The TRIAC has a fast switching capability, with the limitation that it can only switch off once the current flowing through

it returns to zero. The switching of the TRIAC is syncronised with zero-crossing detection of the 50 Hz input voltage. This allows for the transformer input voltage to be switched on at any time during the 10 ms half-cycle and switched off on the next zero crossing. The TRIAC can also be seen as two back to back thyristors, allowing it to conduct in both directions. This property enables the TRIAC to achieve full-wave power control [35][36]. The mains voltage can therefore be "chopped" in both the positive and negative 10 ms half-cycles of its 20 ms period. The resulting transformer input waveform is a "chopped" sine wave as shown in Figure 3.9 below.

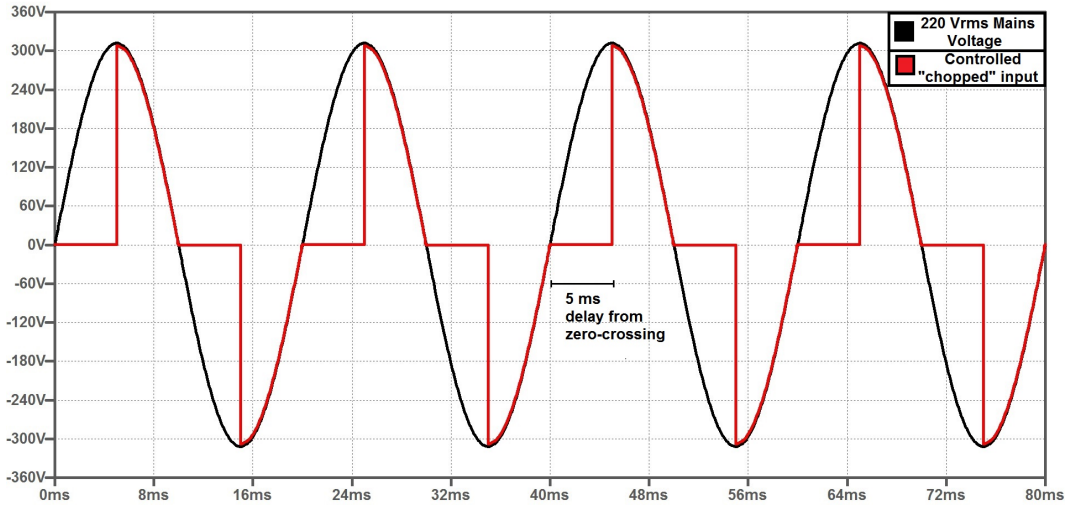

Figure 3.9: Ideal TRIAC power controlled transformer input voltage waveform.

This offers a fast responding controller option, since the power can be changed every 10 ms. The transformer input power is controlled by determining the delay time between zero-crossing and switching on the TRIAC. The delay can therefore be anything in the range of 0 to 10 ms, also sometimes expressed as a phase angle. Equation 3.5.1 shows the phase angle for a TRIAC switching on 5 ms after zero-crossing [37][38][4].

$$PhaseAngle = \frac{DelayTime}{Period} * 360° = \frac{5ms}{20ms} * 360° = 90° \qquad (3.5.1)$$

3.5.4 Variable magnetic field control

The magnetic field of the magnetron can be controlled by using an electromagnet with a variable source. This method is usually more attractive for high power industrial use as it does not affect the power factor, current waveform or the efficiency. The setup can either have an electromagnet directly coupled to the magnetron or a separate electromagnet that opposes the magnetic field of the magnetron's fixed magnets. The drawback for this method is that a separate controllable power source, capable of delivering high current, is required for the electromagnet to be strong enough to have any effect on the magnetron's output power [31][4]. For this project the standard domestic microwave oven power supply would have had to be switched on at 100%, with the controller being on the electromagnet power supply.

3.5.5 Inverter Power Supply

Inverter type power supplies exploit the fast switching properties of the Insulated Gate Bipolar Transistor (IGBT) to work at higher frequencies. The benefits of these topologies are that the power supply reduces in physical size and weight. The input power to the magnetron can be accurately controlled by adjusting the duty cycle of the control signal supplied to the IGBT drive circuitry [39][4]. This method requires a whole new power supply with different transformers and power electronics, which is not particularly suited for this project as we aim to make use of standard domestic microwave oven parts.

3.5.6 Saturable reactor control

This discussion pertains to the high voltage transformer and voltage doubler circuit in Figure 3.8. The high voltage transformer acts as a reactor. Once the core is saturated, the impedance of the output coil drops. The high voltage capacitor in the voltage doubler circuit is series resonant with the inductance of the high voltage transformer. This means that the impedance cancels out and is at a minimum at the resonant frequency. The standard microwave oven circuitry is designed to be resonant at about 15% above the 50 Hz input power frequency. Changing the capacitor value will either move the resonant point closer or further away from the 50 Hz frequency. The result is that the impedance at 50 Hz can be adjusted, changing the output power of the system.

Increasing the capacitance results in an increased output power and decreasing the capacitance limits the output power [31][4]. This is not a feedback control option, but rather a fixed hardware power limit that can be adjusted by changing the voltage doubler capacitor value.

3.6 Comparing Two Possible Control Strategies

The variable ratio transformer and TRIAC control methods were chosen for further investigation. The variable ratio transformer offers a pure sine wave transformer input voltage that can be linearly varied. This is appealing as it offers good microwave output power resolution. However, the trade off is that the controller will have a slow response time due to the mechanical adjustments that are required to compensate for microwave output power control.

The TRIAC, on the other hand, has a very fast response time. The factors that were taken into account with TRIAC control was the power resolution and the range over which the phase angle setting would have an effect on the microwave output power. The effects of the different transformer input voltage waveforms was also taken into account. In other words, how the pure sine wave transformer input voltage compare to the "chopped" TRIAC waveform.

3.6.1 Variable Ratio Transformer Controller Setup

The variable ratio transformer setup required little modifications. The VARIAC was connected directly to the low voltage side of the high voltage transformer. The VARIAC was not motorised, so the power settings were done manually by turning the knob and verifying the transformer input voltage with a connected multimeter.

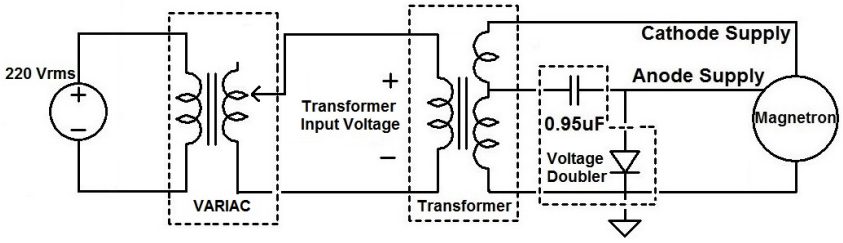

Figure 3.10: The variable ratio transformer setup schematic [4].

3.6.2 TRIAC Controller Setup

The TRIAC controller hardware required a few modifications before it could be compared to the variable ratio transformer setup. The initial setup made use of the standard domestic microwave oven power supply, but replaced the relay with a TRIAC switching circuit and a zero-crossing detection circuit, as seen in Figure 3.11 below.

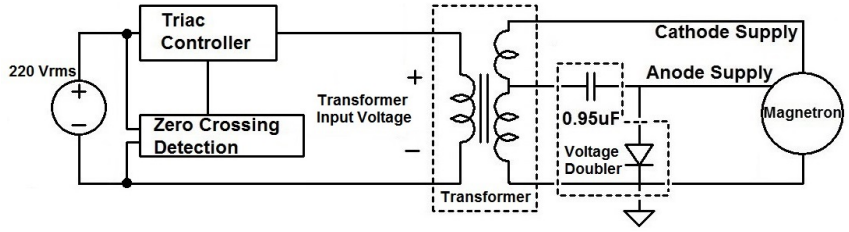

Figure 3.11: Initial TRIAC controller setup schematic [4]

The first problem identified with this setup was that the magnetron was taking longer to switch on as the phase angle increased. This was because the "chopped" sine wave was applied to both the anode and the cathode of the magnetron. Therefore, not only did the input power to the magnetron's anode decrease, but also to the cathode. This meant that the cathode or filament took longer to heat up at the lower input power levels. This affected both the response time of the TRIAC controller and the range over which the magnetron output power could be controlled.

A possible solution wad to connect a second transformer to the cathode, giving

a constant supply of 220 V_{RMS} regardless of the input power setting to the anode. This solution would keep the cathode hot and improve the magnetron's response time [3]. Figure 3.12 shows the modified setup with two separate transformers for both the anode and cathode of the magnetron. A photo of the actual power supply can be seen in Figure 3.13.

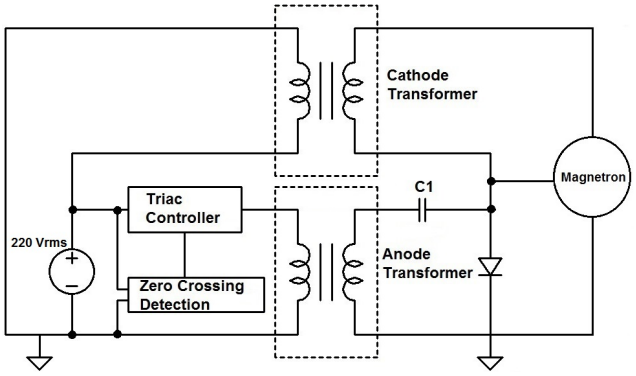

Figure 3.12: Anode and cathode transformer setup schematic [4].

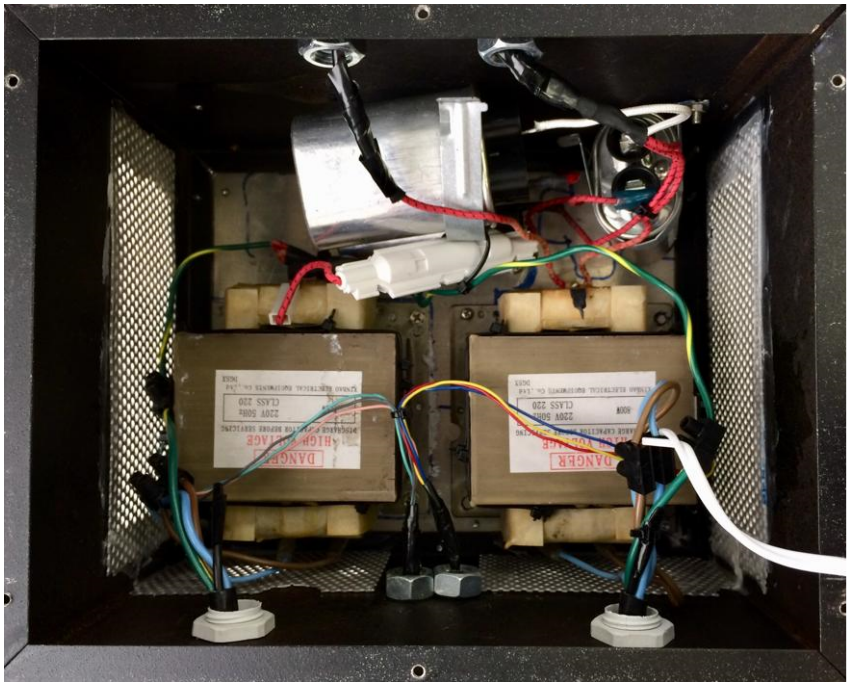

Figure 3.13: Photo of the anode and cathode transformer power supply.

Testing the setup with two transformers proved that the response time of the TRIAC controller did indeed improve. Comparing the microwave output power curves of the single transformer with that of the multiple transformer setup, can be seen in Figure 3.14, revealed that the controllable range of the microwave output power has also increased. From the graph in Figure 3.14 it can be seen that the range over which the microwave output power can be controlled has improved from about 30% of the available range to about 55%.

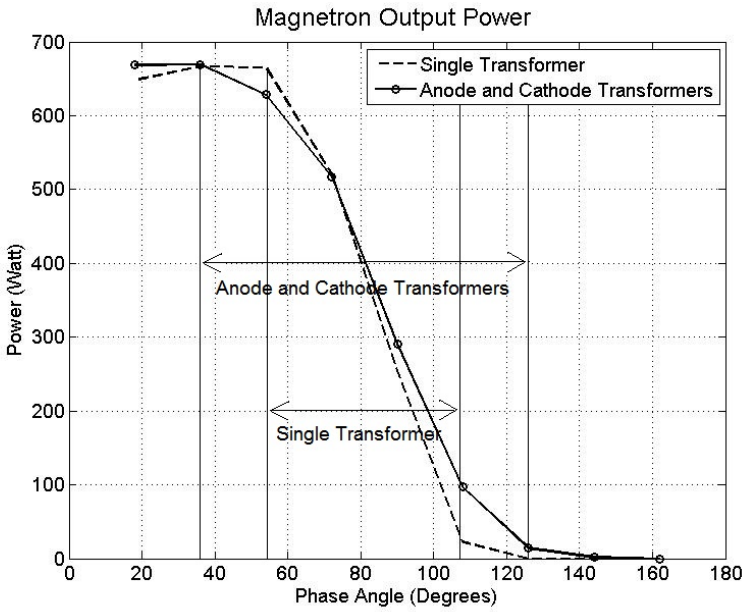

Figure 3.14: Testing single vs multiple transformer setup [4].

Another problem was identified during the testing of the multiple transformer setup. It was found that the anode transformer, as named in Figure 3.12, was heating up rapidly. This was concerning, because the high temperatures would lead to fatigue and insulation failure of the high voltage transformer [40].

Transformers are designed to function at a rated frequency and works best with sinusoidal loads. When supplying a transformer with a non-sinusoidal load the losses increase, resulting in the high temperatures observed in the core [40][41]. The solution to the overheating of the transformer is to either increase the transformer rating or reduce the input power and essentially derate the existing transformer.

Saturable reactor control (explained in section 3.5.6) offers a way to limit the magnetron's input power, which in turn allows the transformer to better cope with the non-sinusoidal load applied to it. A set of tests were performed on the multiple transformer TRIAC control setup, where the high voltage capacitor of the voltage doubler circuit (C1 in Figure 3.12) was decreased in value. The temperature of the anode transformer (Figure 3.17) and the input and microwave output power curves (Figure 3.15 and Figure 3.16) were recorded for each capacitor value to determine the effects of these changes.

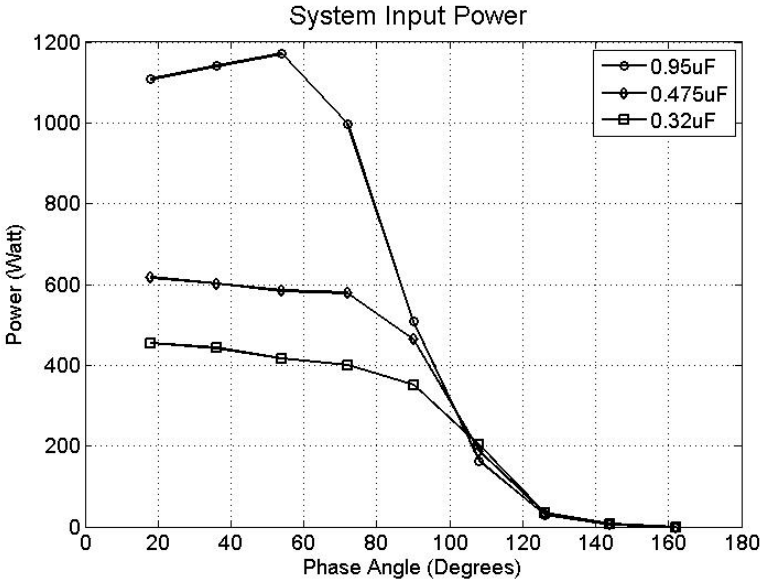

Figure 3.15: Input power for various capacitor values of C 1 [4].

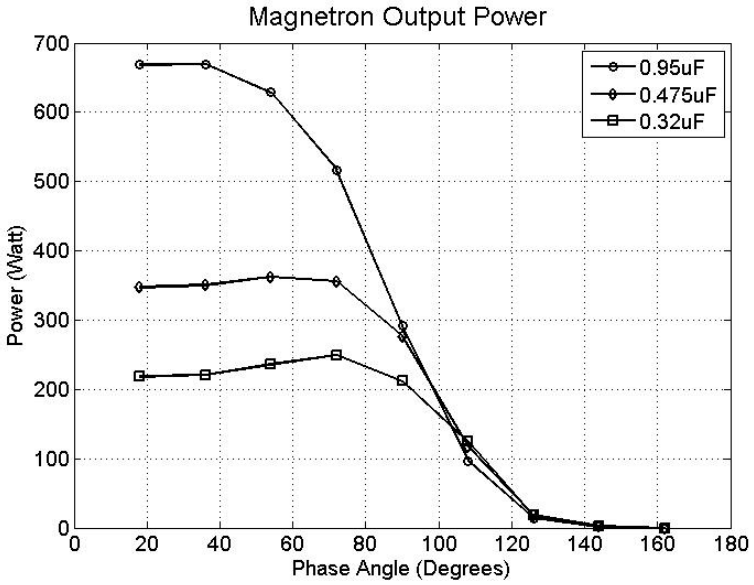

Figure 3.16: Microwave output power for various capacitor values of C 1 [4].

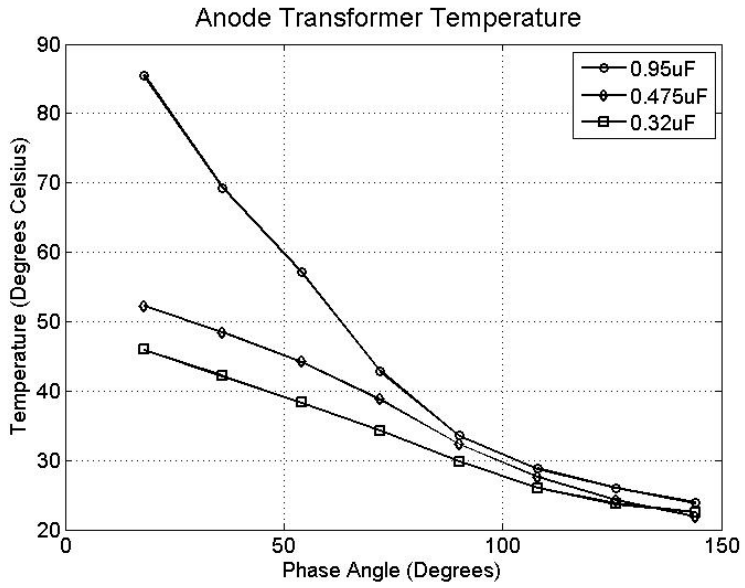

Figure 3.17: Anode transformer temperature for various capacitor values [4].

The results show that the anode transformer temperature is directly proportional to the power it delivers. These anode transformer temperatures are more manageable and suitable for use over extended periods of time with the

0.32 μF capacitor. The gradient of the linear region of the microwave output power, in Figure 3.16, has decreased. The microwave output power resolution is therefore slightly improved. Thus by limiting the microwave output power range, the anode transformer temperature was improved, as well as the resolution of the microwave output power control. Should the original microwave output power range want to be kept, a larger transformer would have to be used in order to be able to cope with the transformer losses.

3.6.3 Controller Comparison Results

Before the results are compared it is important to note that the TRIAC controller setup was as indicated in Figure 3.12, where the voltage doubler capacitor (C1) had a value of 0.95 μF. This allowed the power levels of the two controllers to be in the same range. Since the two input power setting parameters for the respective systems were not the same, they could not directly be related to one another. The results were plotted over the entire microwave output power range of both setups to compare the shape and gradient of the curves. The variable ratio transformer was stepped from 220 V_{RMS} to 150 V_{RMS}. The delay time between zero-crossing and switching on the TRIAC controller was stepped from 1 ms to 8 ms.

3.6.3.1 Comparing Input Power and Microwave Output Power Curves

The plots for the input power curves, microwave output power curves and efficiency of the system is given in Figures 3.18 to 3.21. It is good to note that the shapes of the input power and microwave output power plots look the same. This shows that the measurements were accurate as the input power was calculated with current and voltage measurements and the microwave output power was calculated with the diode detector measurements.

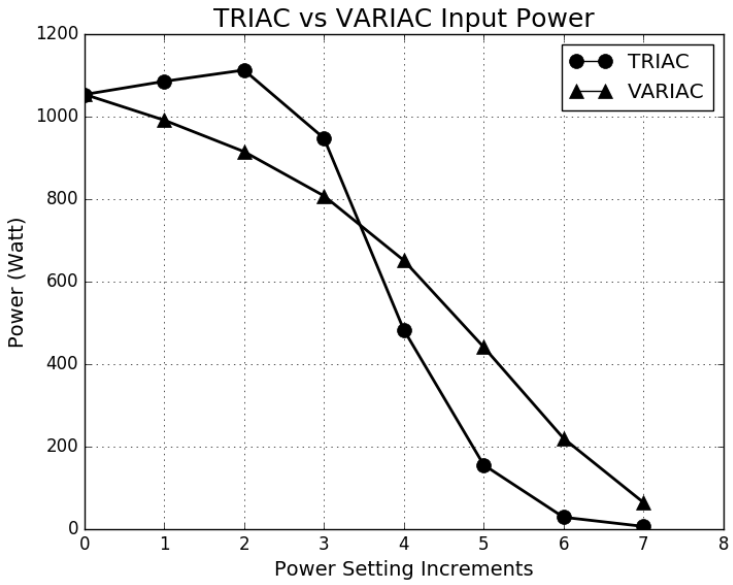

Figure 3.18: Variable transformer vs TRIAC input power curves [4].

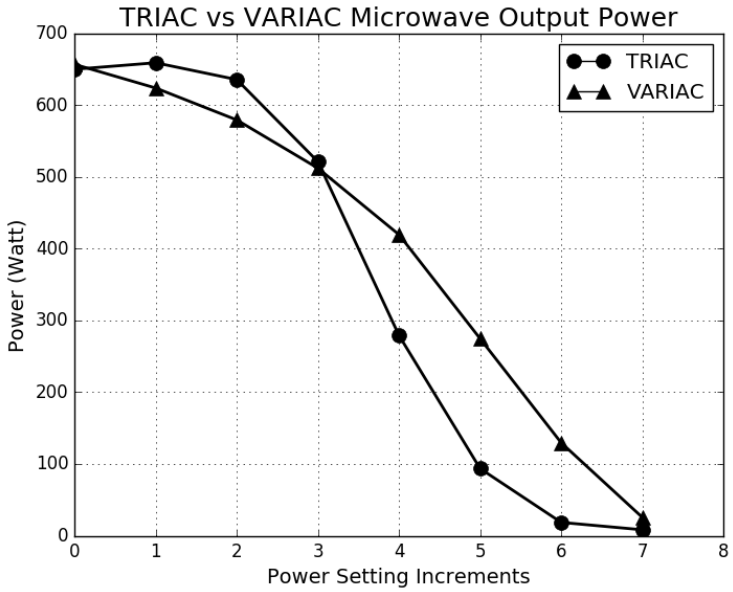

Figure 3.19: Variable transformer vs TRIAC microwave output power curves [4].

The results show that the variable ratio transformer method produced a linear microwave output power curve over the entire range of its power settings. The TRIAC reached the same microwave output power range, but was linear over

a shorter span of input power setting range. however, this does not necessarily mean that the microwave output power resolution of the one was better than the other. The TRIAC controller's power resolution would depend on the timer implemented in software to trigger the switching time (8 bit or 16 bit timer). The variable ratio transformer would depend on the stepper motor and the number of steps available on the variable ratio transformer.

The reason for the output power curve of the TRIAC power controller is due to the bell shape of the half-wave sine curve. Most of the power is contained in the middle of the bell and becomes almost negligible as it tapers off towards the sides. The highlighted area in Figure 3.20 is the area that affects the power setting.

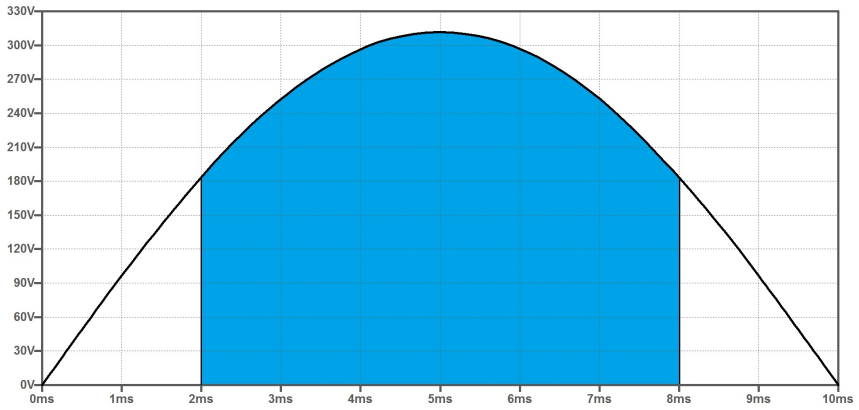

Figure 3.20: Power concentration in half sine wave.

The efficiency of the magnetron is roughly 60% [31]. The variable ratio transformer setup had a fairly constant efficiency. The TRIAC deviates somewhat more, but it was still within a reasonable margin. The efficiency would not be a problem when choosing between the two control strategies.

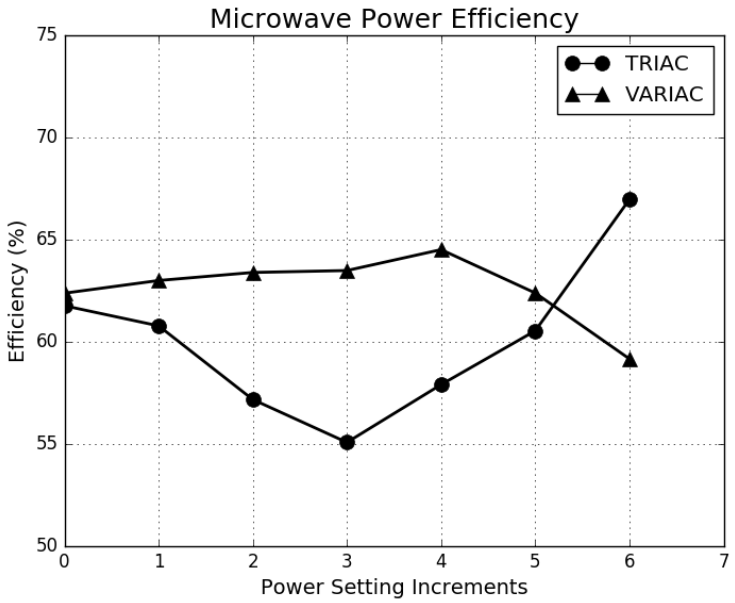

Figure 3.21: Magnetron efficiency for variable transformer and TRIAC.

3.6.3.2 Comparing Sinusoidal and Non-Sinusoidal Transformer Input Voltages

The effects of the different transformer input voltage waveforms were evaluated by looking at the losses in the system. The temperatures of the magnetron and transformers were recorded to determine the extent of the effect that the sinusoidal and non-sinusoidal transformer input voltage waveforms would have. The variable ratio transformer was expected to be the ideal case and the TRIAC the worst case. The losses were already observed during the development of the TRIAC controller. This section serves as a comparison to illustrate how much the TRIAC controller differs from the ideal variable ratio transformer setup.

The temperatures are the average temperatures of the components measured over a five minute period. The components were allowed to cool down to room temperature before the next test was run. Also note that the magnetron and transformers were fan cooled during these temperature tests. The power increments from 0 - 7 started with the highest power setting at 0 and ends with the lowest power setting at 7.

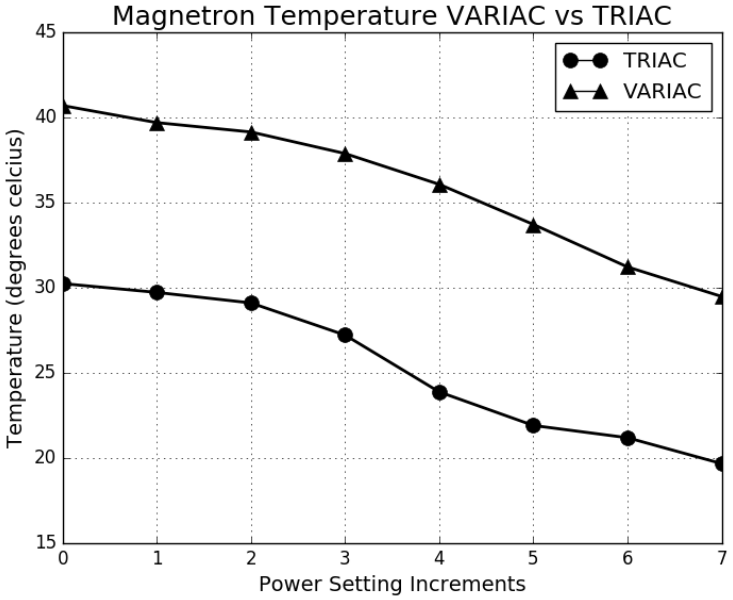

Figure 3.22: Magnetron temperatures for TRIAC and variable ratio transformer.

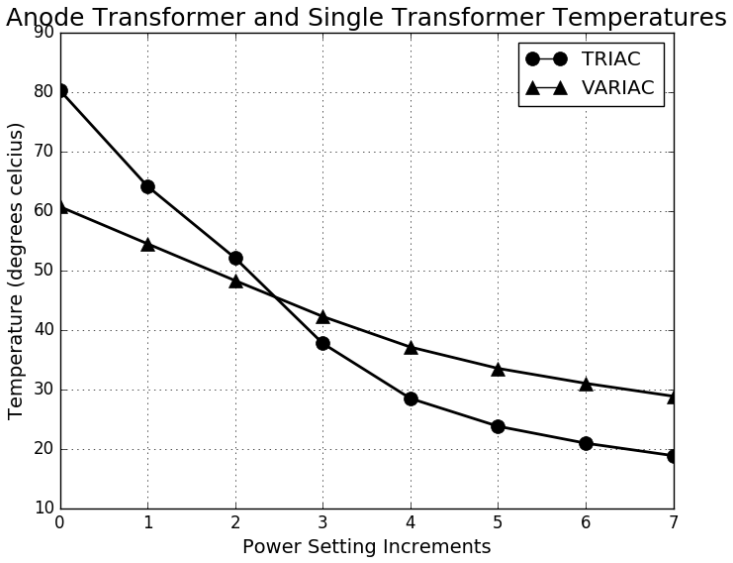

Figure 3.23: Anode transformer temperature vs single transformer temperature.

The temperatures of the magnetron, in Figure 3.22, followed the same shape as the respective power curve of the two controller setups. This was to be expected as more electrons collide with the magnetron as the power increases,

giving off more heat. No significant impact could be seen by the different input waveforms on the losses in the magnetron.

The transformer temperatures refer to the single transformer in the variable ratio transformer setup and the anode transformer in the modified TRIAC controller setup, refer to Figure 3.12.

The temperature measurements, in Figure 3.23, show that the transformer does copes better with a pure sine wave input voltage. The higher order harmonics introduced by "chopping" the sine wave, to produce the same power level in both setups, resulted in a 20 $°C$ temperature difference. It is also clear that higher power levels would increase the losses in the transformer for both cases.

The TRIAC controller temperature readings dropped below that of the variable ratio transformer due to the difference in power resolution. The variable ratio transformer power levels were higher for longer whereas the TRIAC controller's power levels drop much faster. Refer to Figure 3.19 to see what the microwave output power was for each power setting.

3.7 Chapter Conclusion

There are various ways to control the magnetron. The variable ratio transformer method is the most straight forward method when it comes to implementation and quality. The one big disadvantage is that it will always be slow compared to the TRIAC. The TRIAC control on the other hand has its own set of complications, as was pointed out in the chapter. With a good knowledge of the magnetron operation and power control strategies, a combination of these strategies was used to properly implement TRIAC control. Depending on the application, a custom TRIAC controller could be designed to meet microwave output power specifications with a fast time response. After careful consideration the decision was made to continue with the TRIAC controller option for the rest of the project. There was no compromise for the response time that the TRIAC controller offers.

Chapter 4

System Hardware Design

4.1 Chapter Introduction

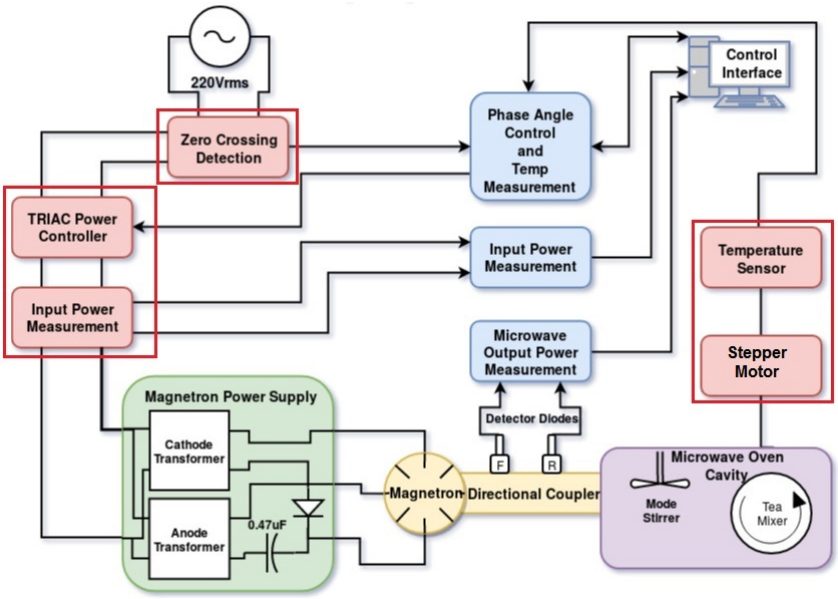

Figure 4.1: Complete system overview

This chapter covers all of the hardware designed in the microwave sterilisation system, as indicated by the red squares in Figure 4.1. After doing the controller comparison in Chapter 3, the TRIAC controller was chosen for its fast response time. The TRIAC was used in conjunction with a zero-crossing

detection circuit. The zero-crossing signal was used to trigger the delay for the phase angle setting of the TRIAC. This produced a "chopped" sine wave. The controller would vary the delay times to control the input power to the magnetron power supply.

The magnetron power supply consisted of separate anode and cathode transformers with a voltage doubler capacitor value of 0.32 μF, shown by the schematic in Figure 3.12. The TRIAC was implemented in a modified light dimmer circuit, which required the design of a snubber circuit [42]. A snubber circuit allowed the TRIAC to reliably switch an inductive load like the high voltage transformer. Other hardware designs that are discussed includes the temperature measurement hardware and stepper motor driver circuit. A stepper motor was used to move the temperature probe around inside the microwave applicator. Lastly, the hardware required to measure the input power to the magnetron power supply will also be discussed.

4.2 TRIAC Controller Design

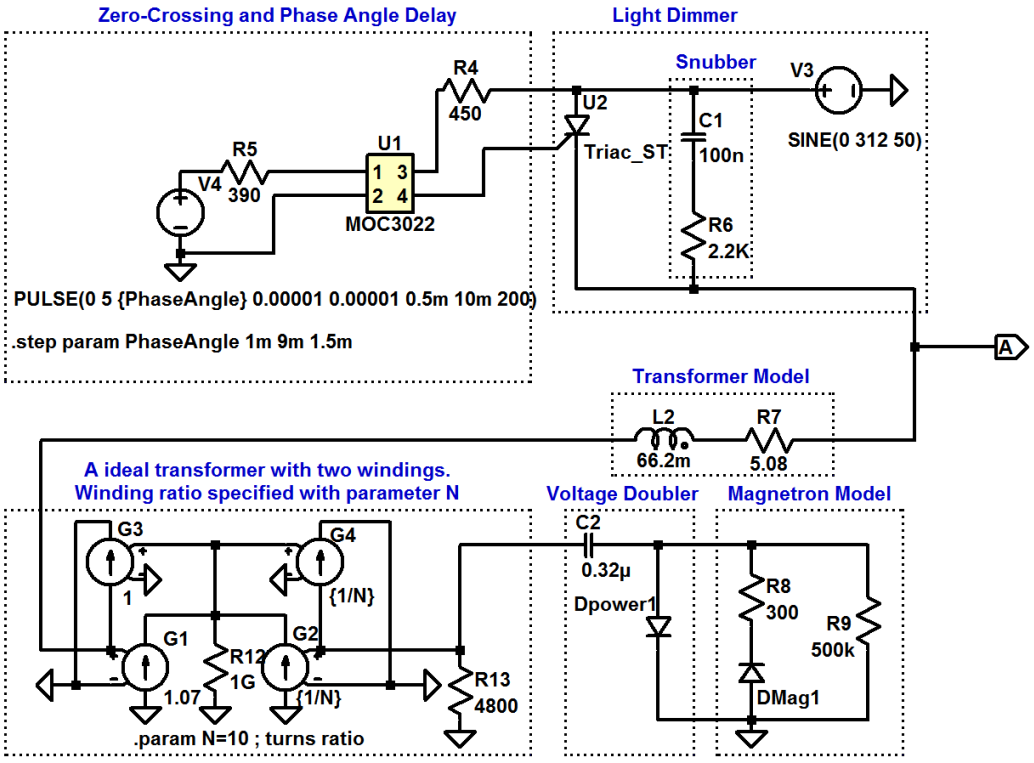

Figure 4.2: LT-Spice model for the TRIAC controller.

Figure 4.2 shows the schematic of the LT-Spice simulation used in the design and analysis of the TRIAC controller. A basic explanation of each block in the schematic is given to establish a top level understanding of their specific functions. Specific design details of the components are discussed later in the chapter.

The TRIAC blocks the mains voltage when it is off. An appropriate signal to the gate terminal of the TRIAC would switch it on and allow it to conduct. A microcontroller was used to rapidly switch the TRIAC on and off. The microcontroller knew that the mains voltage has passed through zero when its hardware interrupt pin was triggered by the zero-crossing signal. The hardware interrupt triggered a timer in software that is used to determine the delay

time. Once the delay time has passed, the TRIAC was switched on and started to conduct the mains voltage. The gate signal from the microcontroller was passed through an optically isolated DIAC package (MOC3022) to protect it from the high voltage on the TRIAC side. This process repeated for both the negative and positive half cycle of the mains voltage, producing a "chopped" sine wave at point "A" in Figure 4.2.

The snubber circuit was used to ensure that the TRIAC does not switch on without an appropriate gate signal from the microcontroller. This was specifically necessary when switching an inductive load like a transformer. The simplified transformer model was derived to simulate the effects that the anode transformer, in the magnetron power supply, would have on the TRIAC's switching ability. The ideal transformer was used to step the voltage up instead of using two coupled inductors. This was done to avoid adding more inductance to the transformer model.

The magnetron model has two modes of operation as was shown in Figure 3.3. The 500 $k\Omega$ resistor draws very little current and represent the non-oscillated part of the graph where the magnetron is off. The diode "DMag1" has a breakthrough voltage equal to the π-mode voltage of the magnetron. Therefore, when the voltage is high enough the magnetron switches on and starts to draw current.

4.2.1 The TRIAC

The TRIAC is a switching device capable of blocking high voltages. Once the TRIAC is triggered through its gate terminal it has the ability to conduct in both directions. The TRIAC can be switched on during any time in the half-cycle, but has the condition that it will only switch off again when the current flowing through it returns to zero or lower than its holding current [43].

When designing a TRIAC switching circuit, the type of load it would be switching has to be taken into account. Resistive loads would mean that the voltage and current waveforms are in phase. Inductive loads introduce a phase shift between the current and voltage waveforms. The phase shift would causes the current to lag the voltage, resulting in a reapplied blocking voltage across the

TRIAC by the time the current passes through zero. The TRIAC has a maximum rate of reapplied voltage that it can handle, before switching on again without an appropriate gate signal. The reason why the rate of change of the reapplied voltage can switch the TRIAC on is due to a junction capacitance introduced by the PN-junction of the semiconductor arrangement. This would mean that $i = C_{junction}\frac{dV_{blocking}}{dt}$ and if the current value exceeds the gate current the TRIAC would switch on without a gate signal being applied [43]. A snubber circuit was used to limit the rate of increasing blocking voltage to prevent the TRIAC from switching on without a proper gate signal being applied [44][45].

4.2.2 Transformer Model

The snubber circuit was placed in parallel with the TRIAC to prevent it from switching on unintentionally. Therefore, when the TRIAC is off, it becomes an open circuit and the snubber circuit is in series with the load. With an inductive load this becomes an RLC circuit that must satisfy the TRIAC's switching conditions [44]. The assumption was made that the inductive effect of the high voltage transformer, in the magnetron power supply, would dominate the TRIAC's load characteristic. A transformer model was derived to simulate the effect of a snubber circuit when switching the inductive load of the high voltage transformer.

The standard transformer model is given in Figure 4.3. Its parameters was determined by performing an open circuit and short circuit test on the transformer.

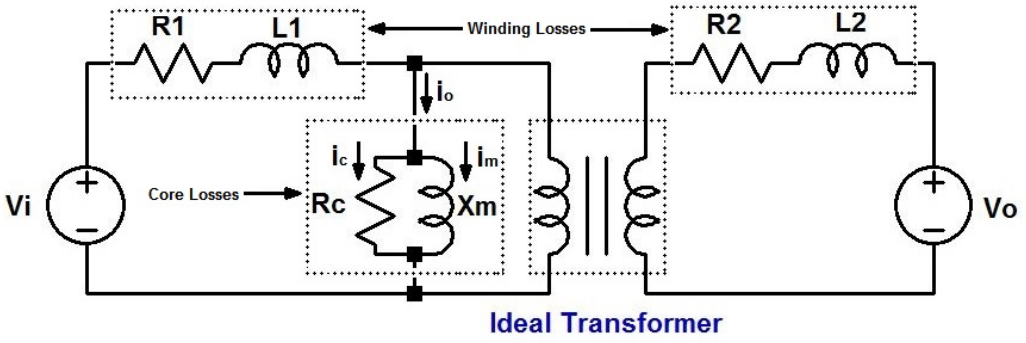

Figure 4.3: Transformer model [5].

Open Circuit Test

Performing the open circuit test consisted of applying 220 V_{RMS} to the primary winding of the transformer while measuring the resulting input power and no-load current. A power meter was inserted between the variable ratio transformer and the high voltage transformer, with two multimeters to measure the voltage (V_i) and current (i_o), as shown in Figure 4.4 [5].

The open circuit test was used to determine the values of the core losses in Figure 4.3. This is because, under no-load conditions, any current drawn by the secondary winding of the transformer was considered to be coming from losses in the core [46]. The winding losses were ignored in this test since the no load current was so small [47].

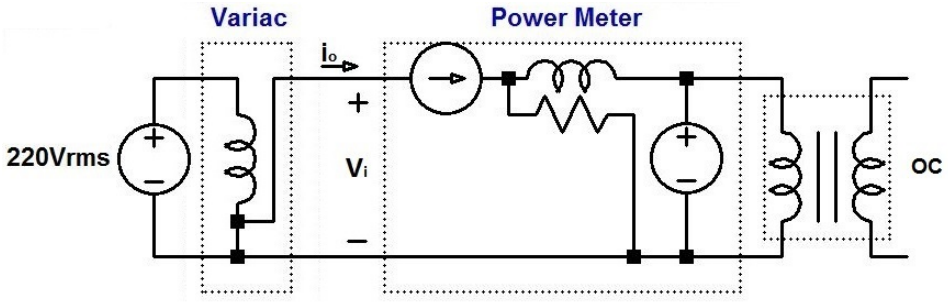

Figure 4.4: Open circuit or no load test setup.

The measurements made with the experimental setup in Figure 4.4 are shown in Table 4.1, where P_i is the input power, V_i is the input voltage and i_o is the loss current flowing in the core.

Table 4.1: Measurements made during the transformer open circuit test.

Measurement	Value
P_i	80 $Watt$
V_i	220 V_{RMS}
i_o	270 mA

The measured values were used to calculate the no load power factor (θ_{oc}) of the transformer with Equation 4.2.1.

$$cos(\theta_{oc}) = \frac{P_i}{V_i i_o} \tag{4.2.1}$$

The loss current (i_o) composed of core (i_c) and magnetizing (i_m) loss current components as shown in Equation 4.2.2.

$$i_o = i_c + i_m = i_o cos(\theta_{oc}) + i_o sin(\theta_{oc}) \tag{4.2.2}$$

The no load power factor is used to find the magnetizing and core loss current components of the transformer. Equations 4.2.3 and 4.2.4 are used to find the resistive (R_c) and reactive (X_m) components of the transformer model in Figure 4.3.

$$R_c = \frac{V_i}{i_c} \tag{4.2.3}$$

$$X_m = \frac{V_i}{i_m} \tag{4.2.4}$$

The calculated parameters for the open circuit test is shown in Table 4.2.

Table 4.2: Calculated values for the open circuit test.

Calculated Parameter	Value
θ_{oc}	17.76°
i_c	257.13 mA
i_m	82.36 mA
R_c	605 Ω
X_m	$j81.94$

Short Circuit Test

The short circuit test was performed by shorting the secondary winding and applying a small percentage of the rated voltage to the primary winding. The variable ratio transformer was set to zero and the voltage was gradually increased until the rated current flows in the windings. Once the rated current was reached, the input power and voltage was measured as shown in the test setup of Figure 4.5.

The short circuit test was used to determine the losses in the windings of the transformer, as shown in Figure 4.3. Since the applied voltage was relatively small, it made the core losses negligible and all other loss was assumed to be in the form of heat in the windings [5].

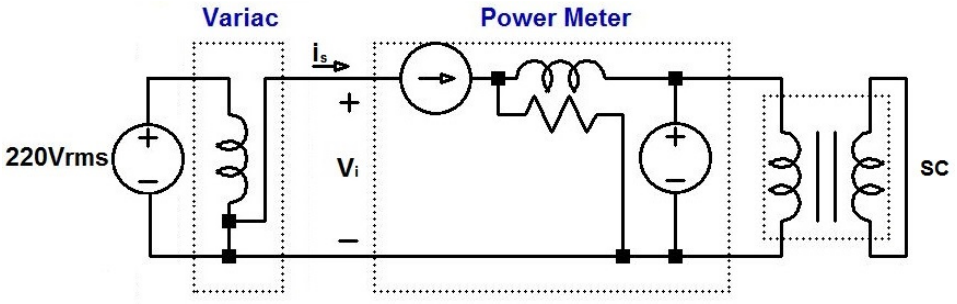

Figure 4.5: Short circuit test setup.

The measurements made with the experimental setup in Figure 4.5 are shown in Table 4.3, where P_i is the input power, V_i is the input voltage and i_s is the input current flowing in the windings of the transformer.

Table 4.3: Measurements made during the transformer open circuit test.

Measurement	Value
P_i	67 $Watt$
V_i	55 V_{RMS}
i_s	3.63 A

The impedance (Z_{sc}) of the combined effect of the primary and secondary winding was calculated using the recorded input voltage (V_i) and current (i_s), as shown in Equation 4.2.5.

$$Z_{sc} = \frac{V_i}{i_s} \tag{4.2.5}$$

The short circuit power factor (θ_{sc}), calculated with Equation 4.2.6, was used to break the impedance value up into resistance ($R_1 + R_2'$) and reactance ($X_1 + X_2'$) components, using Equations 4.2.7 and 4.2.8.

$$cos(\theta_{sc}) = \frac{P_i}{V_i i_s} \tag{4.2.6}$$

$$(R_1 + R_2') = Z_{sc} cos(\theta_{sc}) \tag{4.2.7}$$

$$(X_1 + X_2') = Z_{sc} sin(\theta_{sc}) \tag{4.2.8}$$

The calculated parameters for the short circuit test is shown in Table 4.4.

Table 4.4: Calculated values for the short circuit test.

Calculated Parameter	Value
θ_{sc}	76.27°
Z_{sc}	21.42
$R_1 + R_2'$	5.08 Ω
$X_1 + X_2'$	j20.8

Combining Short Circuit and Open Circuit Test Results

The values obtained for the open circuit and short circuit tests were substituted into the approximate transformer model in Figure 4.6. The shunt branch values were obtained from the open circuit test and the values for the combined winding losses were obtained from the short circuit test. The observation was made that core losses are dependent on voltage, while the winding losses are dependent on current [46].

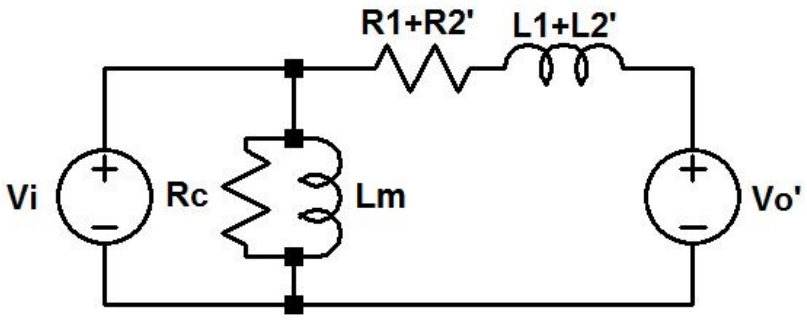

Figure 4.6: Approximate transformer model [5].

The values of the circuit components in Figure 4.6 are listed in Table 4.5.

Table 4.5: Component values for the transformer model.

Component	Value
R_c	1200 Ω
L_m	258 mH
$R_1 + R_2'$	5.08 Ω
$L_1 + L_2'$	66.2 mH

4.2.3 Calculating Snubber Values

The snubber circuit is an important component that allows the TRIAC to successfully control the input power to the magnetron power supply. The TRIAC controls the input power by rapidly switching on and off every half cycle of the mains voltage. The fast switching of an inductive load was achieved by limiting the rate of increasing blocking voltage across the TRIAC with a snubber circuit [44].

The theoretical values of the derived transformer model was used in an LT-Spice simulation. Since the shunt branch or core losses of the transformer model was so low it was omitted from the simulation. Only the winding losses were taken into account,as can be seen in Figure 4.2.

Figure 4.7 shows the equivalent transformer model in series with the snubber circuit, where $R_t = R_1 + R_2' = 5.08\ \Omega$ and $L_t = L_1 + L_2' = 66.2\ mH$. When the TRIAC is off it was considered to be an open circuit. The load and the snubber circuit were therefore in series when the TRIAC was switched off. The simplified model of the load left a second order differential equation with regards to the voltage variation across the snubber capacitor (C_s) and the TRIAC to be solved. The calculations of C_s and R_s are not trivial; the manufacturer of the TRIAC released an application note with a solution of the differential equation and design suggestions [44].

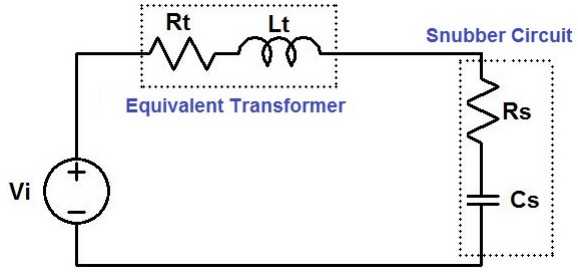

Figure 4.7: Equivalent circuit with TRIAC "off" and snubber circuit in series with load.

The snubber circuit values used by [48] in a microwave power control circuit was used in this setup as well, where $R_s = 2.2K\Omega$ and $C_s = 100nF$. The snubber circuit values were evaluated using the LT-Spice simulation.

The simplified transformer model could be used to calculate a theoretical damping ratio of the reapplied blocking voltage. Equation 4.2.9 was derived from Figure 4.7 [44].

$$\zeta = \frac{R_s + R_t}{2}\sqrt{\frac{C_s}{L_t}} \tag{4.2.9}$$

The theoretical damping ratio of the reapplied blocking voltage with the given transformer model was $\zeta = 1.36$. Specific snubber circuit values were simulated to illustrate the effect of the damping ratio on the blocking voltage of the TRIAC. The results of the tests are shown in Table 4.6. The "No snubber

circuit" row in Table 4.6 shows that the TRIAC controller does not block the voltage properly without the snubber circuit.

Table 4.6: Illustrating the effect of the different snubber circuit damping rations.

Effect of snubber circuit values on TRIAC output voltage	
Component Values	Simulated Result
Damping ζ =0.027, Snubber Values $R_s = 40\ \Omega$, $C_s = 100$ nF	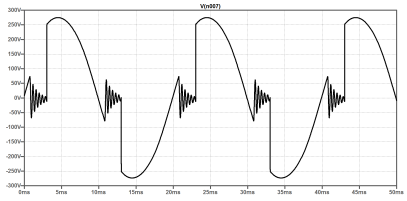
Damping ζ = 0.6, Snubber Values $R_s = 1$ KΩ , $C_s = 100$ nF	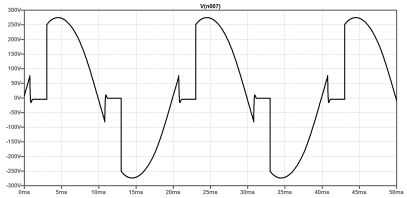
Damping ζ =1.36, Snubber Values $R_s = 2.2$ KΩ , $C_s = 100$ nF	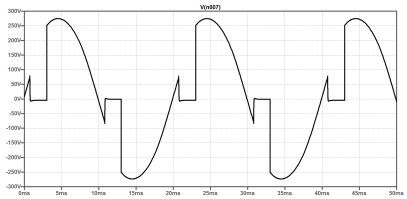
No snubber circuit	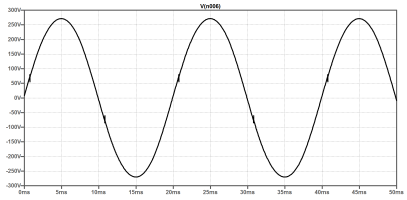

The results in Table 4.6 show that the simulated snubber circuit values are not that sensitive and that any R_s value between 1 kΩ and 2.2 kΩ would have worked with this load. The capacitor value was kept constant at $C_s = 100$ nF. The snubber circuit values were obtained from another source, but the snubber circuit application note also suggested using a capacitor value between 10 nF and 100 nF [44]. The LT-Spice simulation worked well to test these effects.

The LT-Spice simulation is compared to the actual measured waveforms of

the system in Table 4.7. The "chopped" waveform at point "A" in Figure 4.2 was measured for a range of input power settings. The phase angle was incremented over the TRIAC's controllable range. The resulting measured and simulated "chopped" waveforms were compared to show that the LT-Spice simulation did indeed produce an accurate representation of the voltage waveforms in the system.

There are still areas of the model that can be improved. The current waveforms, magnetron pulses and high voltage waveforms can be improved. This would be due to the nature of the transformer model, which did not take into account any transformer saturation effect or interactions with the voltage doubler circuit. The waveforms for these values are included in Appendix B, where all the measured and simulated waveforms of the LT-Spice model are included as reference for further improvements in later work.

Table 4.7: Comparing simulated and measured input voltage waveforms.

Measured vs Simulated Voltage Waveforms for a Range of Phase Angle Settings		
Phase Angle	Measured Waveforms	Simulated Waveforms
18°	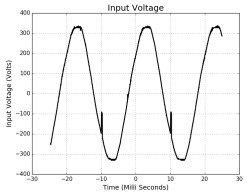	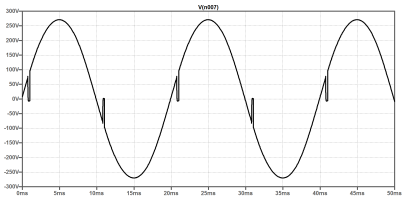
36°	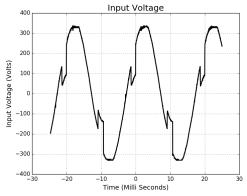	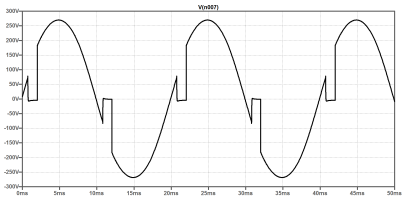
54°	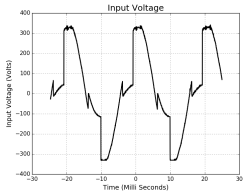	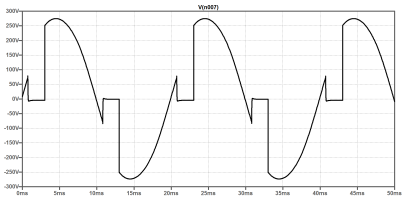
72°	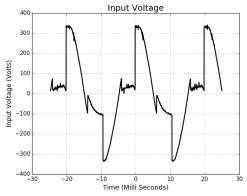	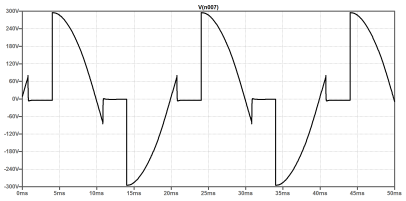
90°	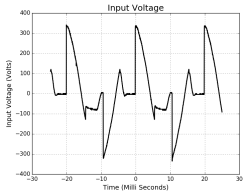	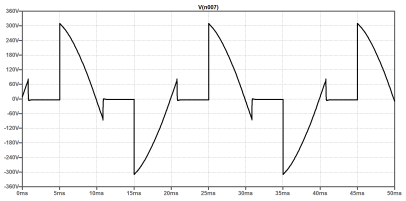
108°	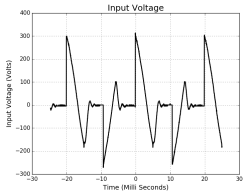	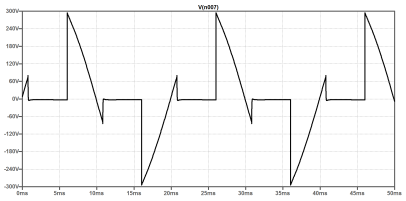
126°	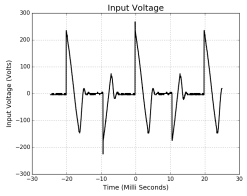	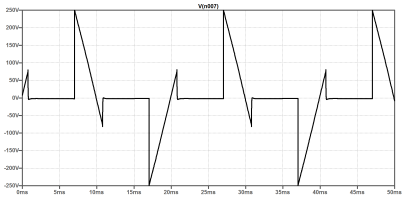

4.2.4 Zero-Crossing

The zero-crossing signal had two purposes in the system. First, to trigger the phase angle delay of the TRIAC controller and secondly, to synchronize all the microcontrollers in the system.

Zero-crossing refers to the instant where the mains voltage passes through the x-axis and its polarity in the y-axis changes. The mains voltage was a 220 V_{RMS}, 50 Hz sine wave. Theoretically the ideal zero-crossing detection circuit should then see a crossing event every 10 ms, since the period of the sine wave was 20 ms long [49].

The circuitry designed to detect the crossing event made use of the MOC8050 optically isolated package with a darlington transistor output, as seen in Figure 4.8. The opto-coupler has fast switching capabilities with an isolation rating of 5300 V_{RMS} which made it ideal for the given application [50]. This would protect the microcontroller should anything happen on the high voltage side. It would also switch fast enough to do the power control.

A series resistor was used to limit the current at the input terminal to 10 mA. The darlington output transistor pair was biased to saturate and give a square wave output. The transistor output has switching delays as enough current had to flow at the input for the transistor to switch on. The switching delays were compensated for by passing the transistor output through a rail-to-rail operational amplifier. The high gain of the operational amplifier gave out a square wave with improved switching delays. Any further delays could be compensated for in software. The actual delay was measured to be 250 μs and the output square wave had a maximum amplitude of 5 V.

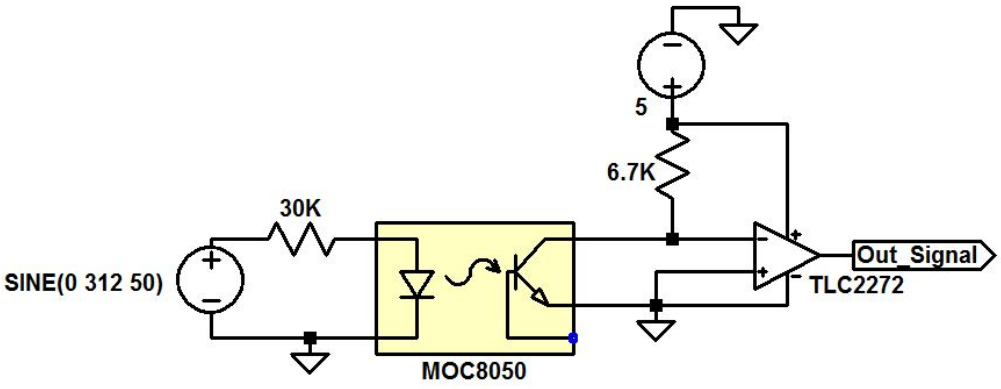

Figure 4.8: Schematic for zero-crossing detection circuit.

4.3 Temperature Measurement

The PT100 was chosen as the temperature sensor. The sensor works as a temperature-dependent resistor. The PT100 temperature table indicates that the resistance will be 100 Ω at 0 $°C$ and 175 Ω at 200 $°C$ [51]. There are various ways to measure the changing resistance value. The method chosen in this project was to implement it in a Wheatstone bridge configuration, as shown in Figure 4.9 [52].

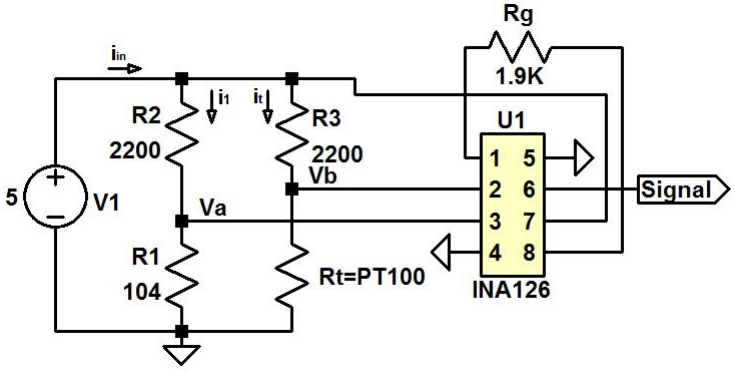

Figure 4.9: Wheatstone bridge schematic.

The INA126 is a low noise difference amplifier with an adjustable gain between 5 and 10000. The gain could be adjusted by changing the value of Rg in Figure 4.9 [53]. The difference between V_a and V_b was amplified to give an output between 0 V and 5 V.

The expected temperature swing was between 10 $°C$ and 145 $°C$. The resulting swing in resistance would be between 104 Ω and 156 Ω. The current through the sensor had to be kept at a minimum to avoid self-heating. The resistors were chosen to keep the current at 2 mA. By choosing the same resistors in each branch the current split equally between the two branches.

The current calculation for the Wheatstone bridge in Figure 4.9 is shown here:

$$R_x = R_1 + R_2 = R_3 + R_t \tag{4.3.1}$$

$$R_{eq} = R_x//R_x = \frac{R_x}{2} \tag{4.3.2}$$

$$i_{in} = i_1 + i_t = \frac{V}{R_{eq}} = \frac{10}{R_x} \tag{4.3.3}$$

Designing the Wheatstone bridge to have a maximum current of $i_t = 2$ mA, the theoretical $R_x = R_3 + R_t = 2500\ \Omega$. The resistance of the PT100 at the minimum expected temperature was 104 Ω . The value for $R_3 = R_x - 104\ \Omega$ was therefore chosen as 2.2 $k\Omega$. The value of $R_1 = 104\ \Omega$ and $R_2 = 2.2\ k\Omega$ were chosen to have a voltage difference of 0 V between the two branches of the bridge when the temperature is at the lower end of its range. The appropriate gain setting depended on the difference between V_a and V_b at the upper limit of the temperature range.

Using node voltage analysis to determine the values of V_a and V_b resulted in :

$$V_a = \frac{5R_1}{R_1 + R2} \tag{4.3.4}$$

and

$$V_b = \frac{5R_t}{R_t + R3} \tag{4.3.5}$$

Substituting $R_1 = 104\ \Omega$, $R_2 = 2200\ \Omega$, $R_3 = 2200\ \Omega$ and $R_t = 156\ \Omega$ to find $V_a = 225.7\ mV$ and $V_b = 331.1\ mV$. The maximum voltage swing between V_a

and V_b was found with Equation 4.3.6 and used to determine the needed gain in Equation 4.3.7.

$$D_{max} = V_b - V_a = 105.36mV \tag{4.3.6}$$

$$G = \frac{5}{0.10536} = 47.5 \tag{4.3.7}$$

The Appropriate resistor value for R_g is determined by Equation 4.3.8, resulting in $R_g = 1.9\ k\Omega$.

$$G = 5 + \frac{80k\Omega}{R_g} \tag{4.3.8}$$

A decision was made to use the already calibrated temperature vs resistance table of the PT100 as the calibration reference. This decision was made due to the errors made in the calibration process when using ice water (0 ° C) or boiling water (100 $°C$) for temperature references. The resistance of the sensor was related to a temperature in software with an approximated linear relationship between the change in resistance from 0 $°C$. Therefore the resistance increases linearly with a gradient of 2.56 from 0 $°C$

$$Temperature = (R_t - 100) * 2.56 \tag{4.3.9}$$

For this approach to work, accurate measurements had to be taken of the actual values in the system to reliably convert the ADC value back to a resistance. These values are shown in Table 4.8. The temperature readings were verified using ice water and boiling water to ensure that the calibration was indeed correct. A laser pointer thermometer was used as a third confirmation that the temperatures were measured accurately.

The parameters in Table 4.8 are shown in Figure 4.9.

Table 4.8: Theoretical vs. actual values in temperature measurement circuit.

Parameters	Theoretical	Measured
V_a	0.2257 V	0.228 V
R_3	2200 Ω	2150 Ω
G	47	46.7

The measured values were used in Equations 4.3.10 to 4.3.12 to relate the ADC value to the actual resistance of the sensor:

$$Signal = (ADC * 5)/1024 \tag{4.3.10}$$

$$V_b = (Signal/G) + V_a \tag{4.3.11}$$

$$R_t = (V_b * R_3)/(5 - V_b) \tag{4.3.12}$$

4.4 Stepper Motor Driver Circuit

A stepper motor was used to move the temperature probe around inside the tea mixer. Initial tests on the system showed that tea in the immediate proximity of the tip of the metal probe was burning. This was due to a higher electric field at the tip of the probe. The solution was to move the probe around. This allowed for temperature readings in different positions of the tea sample as well as avoiding an induced hot spot. The tea mixer moved in a circular motion while the temperature probe moved up and down along its length.

The stepper motor functioned completely independently from the rest of the system. Once the power was switched on, the motor would automatically start moving the probe back and forth inside the microwave applicator. The movement of the stepper motor was controlled by an Arduino Leonardo connected to an L293D. The L293D is a push-pull four channel driver integrated circuit meant for driving inductive loads [54]. The existing "Stepper" function provided by Arduino was used [55]. This allowed for the control of the motor speed as well as the amount of steps taken by the motor. The interrupt on the Arduino allowed the direction of the motor to be changed and the motor to reverse with the same amount of steps. The timing of the interrupt was determined experimentally. The schematic of the stepper motor drive circuitry is shown in Figure 4.10.

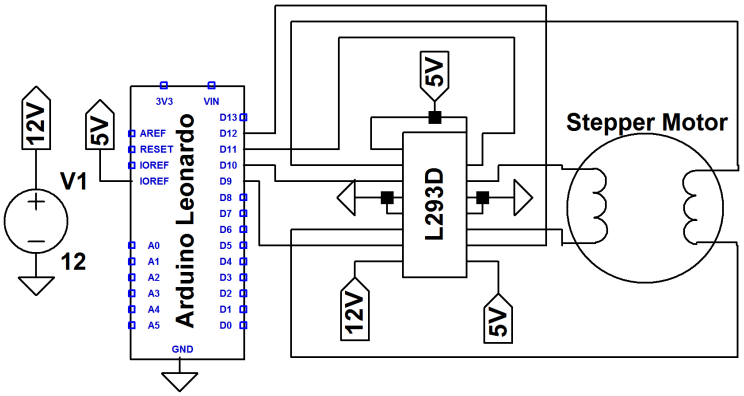

Figure 4.10: Stepper motor driver schematic.

4.5 Measuring Controlled Power to Magnetron Power Supply

To measure the system input power a current and voltage waveform was required. Both waveforms were interfaced with the ADC of an Arduino UNO.

The voltage was measured by stepping down the TRIAC output voltage using a transformer and doing further voltage division to ensure the output did not exceed the Arduino's maximum input voltage. Connecting the output voltage to ground would result in only the positive half cycle of the AC signal to be sampled by the ADC. Therefore 0 to 220 V_{RMS} was represented in a 0 to 5 V signal and an appropriate calibration was performed to recreate the values in software.

The current sensor used was a hall effect sensor. The input power wire was fed through the sensor once and the output current was configured to swing around 2.5 V. The calibration of the current sensor was done by building a current source capable of delivering 1 A. The input current was confirmed with a multimeter and the calibration was done by recording the resulting output voltage. The calibrated value indicated that 1 A input current would give a 110 mV output voltage. Knowing that the input current peaked at 8 A, the output voltage was passed through a non-inverting amplifier to maximize the

ADC resolution over the expected current range.

4.6 Chapter Conclusion

The TRIAC controller was designed and simulated in LT-Spice. A transformer model was derived and used in the LT-Spice simulation to represent the load that the TRIAC would be switching. The simulations were used to verify the snubber circuit values and pointed out the necessity of a snubber circuit. Zero-crossing detection was used to control the timing of the phase angle delay as well as synchronising the microcontrollers in the system. The hardware to detect zero-crossing was designed and explained. The temperature measurement hardware was also designed and explained. Finally the stepper motor drive circuitry and input power measurement hardware were discussed. The chapter covered all the hardware in the system. The schematics and PCB layouts can be found in Appendix A.

Chapter 5

Microwave Applicator

5.1 Chapter Introduction

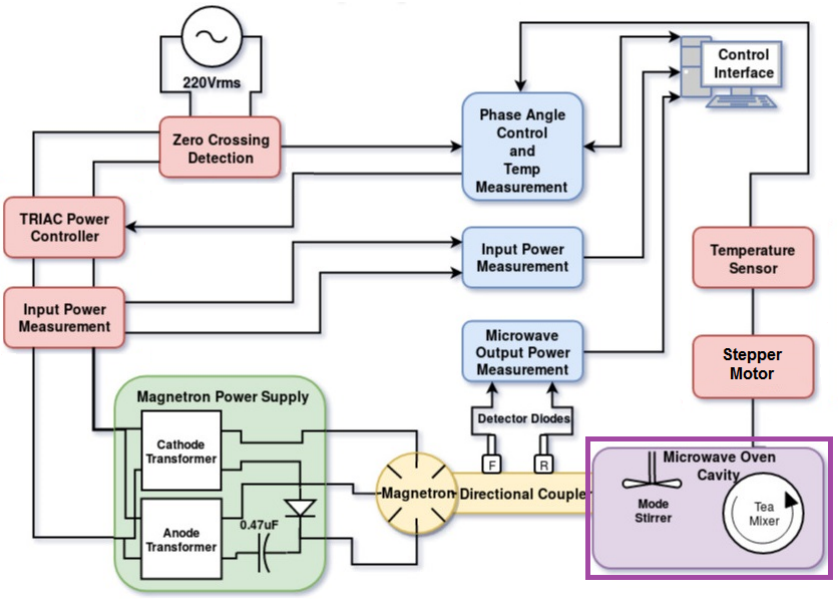

Figure 5.1: Complete system overview.

The microwave applicator needed modification to be suited for the specific function of sterilising Rooibos tea. Each modification had an effect on the load that the magnetron would see. These effects could influence the magnetron's microwave output power and frequency.

Another critical component of the system was the mode stirrer. The mode stirrer would ensure the even distribution of heat throughout the medium. Tea being a dry medium made it a difficult medium to work with. This chapter therefore aims to test the extent of the effects that moisture content, mode stirrers and load location had on the microwave power delivered to the applicator.

Finally, after modifications, it is shown that an even heat distribution was achieved and that the applicator was indeed suited for Rooibos tea sterilisation. Most importantly this chapter points out the necessity of implementing a microwave power controller that would ensure the irradiation of the load was done at a constant microwave power.

5.2 Applicator Modifications

The final modified microwave applicator can be seen in Figure 5.2. The motivation behind each of the modifications is discussed in this subsection.

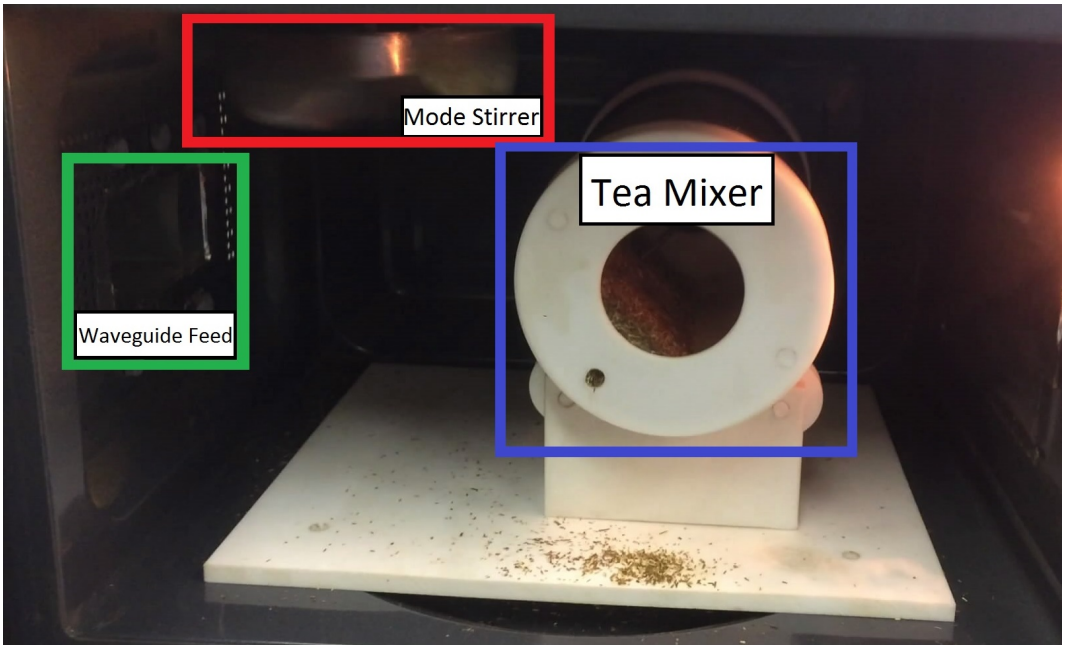

Figure 5.2: Final microwave oven modifications.

5.2.1 Mode Stirrer Theory

Mode stirrers are moving metallic devices inserted inside a multi-mode microwave cavity to ensure uniform heating patterns. Metallic fans work well for this as it continuously deflects the electromagnetic waves inside the cavity. Microwaves are fed to the microwave applicator with a waveguide leading from the magnetron. The effect of the mode stirrer can therefore be maximised by installing it close to the feed of the waveguide inside the microwave applicator. Due to the complexity of the analysis of mode stirrers on electromagnetic level, it is best to evaluate the effectiveness of an installed mode stirrer by empirical measurements [56].

5.2.2 Achieving Uniform Heating

Figure 5.3 shows the comparison of a microwave applicator with and without a mode stirrer. The effectiveness of the mode stirrer is illustrated by the amount of neon lights that lit up. The setup on the left in Figure 5.3 did not have a mode stirrer, resulting in only some of the lights lighting up.

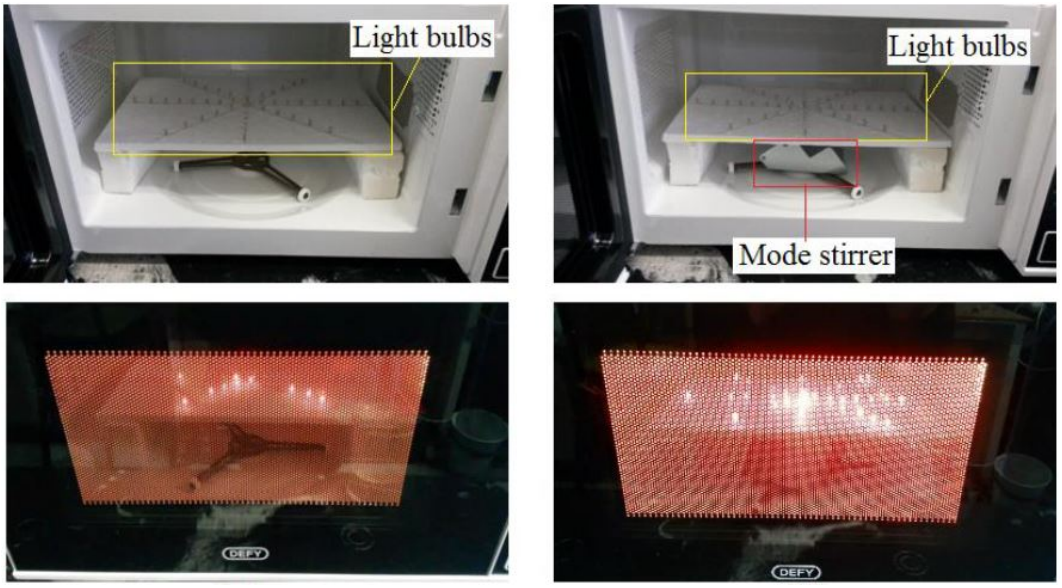

Figure 5.3: Neon lights used to indicate effects of mode stirrer [6].

This is because of the standing wave that forms inside the microwave applicator. The setup on the right in Figure 5.3 had a mode stirrer and the effect can be seen by the number of lights that lit up. The mode stirrer reflected the electromagnetic waves, preventing a standing wave from forming inside the microwave applicator. The result was a more random electrical field distribution, leading to a more uniform heating pattern.

The setup in Figure 5.3 was used by [6] to achieve uniform heating in a continuous flow sterilisation system. The same mode stirrer implementation was tested on Rooibos tea. The tea was placed in a microwave safe plastic container and the magnetron output power was set to 700 Watt. The tea got burnt and the container melted after two minutes, as seen in Figure 5.4. This indicated that further modifications were necessary to ensure that the microwave applicator would be suitable for Rooibos tea sterilisation.

Figure 5.4: Slow mode stirrer microwave applicator environment.

The mode stirrer speed had to be fast relative to the process, to ensure that the temporary hot spots did not burn the medium [56]. The mode stirrer mounted on the microwave oven turntable motor was rotating at 6 revolutions

per minute. The new mode stirrer, consisting of a metallic fan, was installed in front of the waveguide feed into the microwave cavity as in Figure 5.2.

Figure 5.5: Burnt tea after 2 min at 700 W with slow mode stirrer.

A 50 Hz 220 V_{RMS} fan was used for the mode stirrer, giving out a theoretical 3000 revolutions per minute; significantly faster than the previous mode stirrer implementation. The faster rotation and specific placement was chosen to try and achieve a better average microwave energy distribution. The motor of the fan was mounted on the outside of the microwave oven, with a Teflon axle connecting the fan to the motor drive. This was done to ensure that the fan is far enough from the sides of the applicator, to avoid sparks, and isolated from the motor.

A tea mixer, shown in Figure 5.6 had to be designed to ensure that the tea did not burn during the sterilization process. The materials used was a microwave safe glass tube and Teflon. The tea mixer was driven by a microwave turntable motor, rotating at 6 revolutions per minute. The mixer would rotate and slowly turn the tea over inside the glass tube.

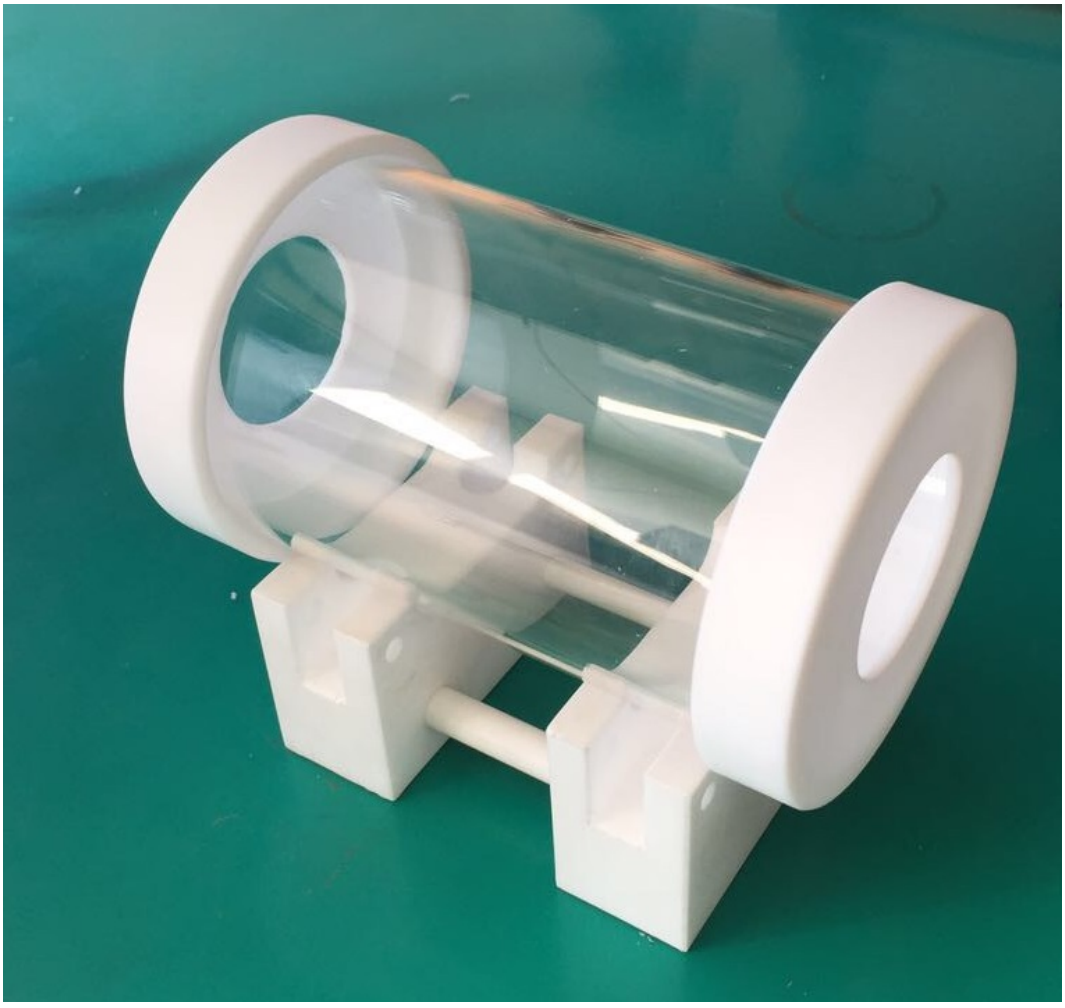

Figure 5.6: Tea mixer used inside the microwave applicator.

Introducing new materials into a microwave applicator created the possibility for some of microwave power to be absorbed by the new material. Ideally all the microwave power in the applicator had to be applied to the medium being sterilised and not any of the other material introduced into the applicator. This would provide more certainty when discussing power dosage, temperature gradients and microwave effects in the research results.

One of the materials introduced into the microwave applicator was a glass plate to provide a level surface for the tea mixer to stand on. The glass plate was noticeably warmer to the touch after testing. Thermal images were used to

test the difference between a Teflon plate and a glass plate. Figures 5.7 and 5.8 show the difference in heat between the glass and Teflon plates, illustrating the power absorbed by each material. Figure 5.7 shows that the glass plate absorbed almost all of the microwave power. Contradictory Figure 5.8 shows the hotspot inside the tea mixer rather than on the Teflon plate supporting the tea mixer.

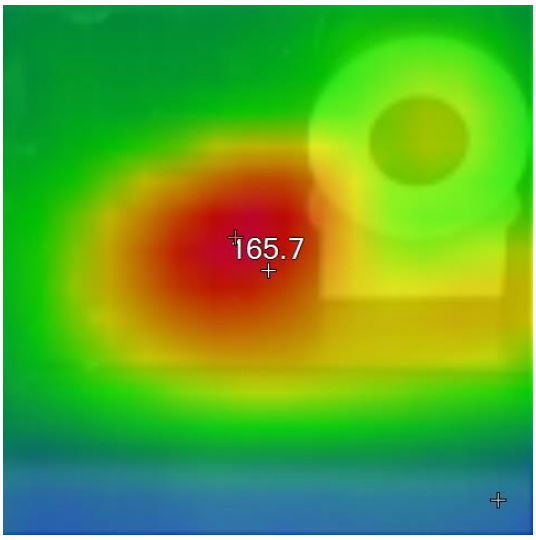

Figure 5.7: Glass plate in microwave oven.

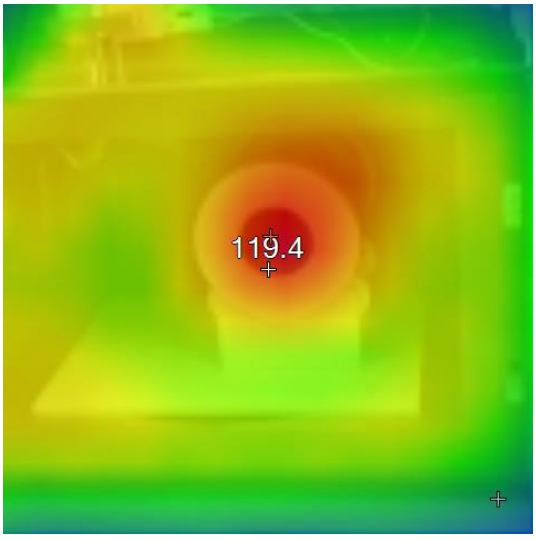

Figure 5.8: Teflon plate in microwave oven.

The tea mixer was placed on a Teflon plate since it was the material that absorbed the least microwave power. The final interior setup of the microwave applicator is shown in Figure 5.2 and the even heat distribution achieved is shown in Figure 5.9.

The tea mixer was tested by irradiating Rooibos tea at 700 Watt. After 10 min the Rooibos tea did not burn. Lower power levels were also tested where the Rooibos tea could be irradiated for up to 30 min without burning. The modification to the microwave applicator were accepted as suitable for tea sterilisation. The newly modified microwave applicatror was used in all further tea sterilisation tests.

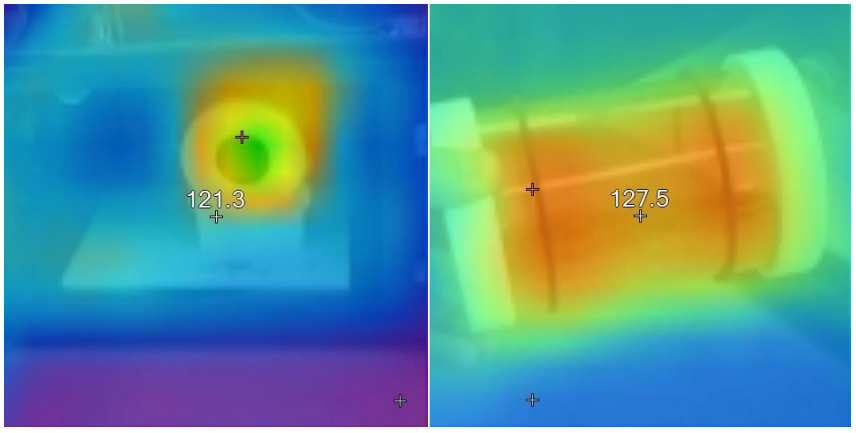

Figure 5.9: Heating pattern achieved through tea sample.

5.3 Reflection Coefficient of Microwave Applicator

The reflection coefficient is defined as the amplitude of the reflected voltage wave normalised to the amplitude of the incident voltage waveform [57]. With microwave ovens a variety of materials can be placed in the applicator cavity, affecting the reflection coefficient. The position, moisture content and frequency all has an effect on how well the load absorbs the microwave power. This section investigates the effects that variations in load and modifications

to the microwave applicator had on the reflection coefficient of the applied microwave power.

5.3.1 Effect of Mode Stirrer

A vector network analyser (VNA) was used to try and gauge the effect a mode stirrer would have on the reflection coefficient seen by the magnetron. The input port of the VNA was connected to a waveguide which fed into the microwave applicator. The load inside the microwave applicator was 500 ml of water in a glass container. Water was chosen as the load because of its good absorbing properties at the microwave frequency.

The mode stirrer was switched on and a repetitive pattern could be seen for the S_{11} measurement on the display screen of the VNA. Figures 5.10 to 5.12 are samples taken to show the extent of the change in the reflection coefficient pattern due to the mode stirrer. The frequency was varied to determine if slight changes in the output frequency would have an effect on the reflection coefficient. The tests were performed at 2 440 MHz, 2 450 MHz and 2 460 MHz.

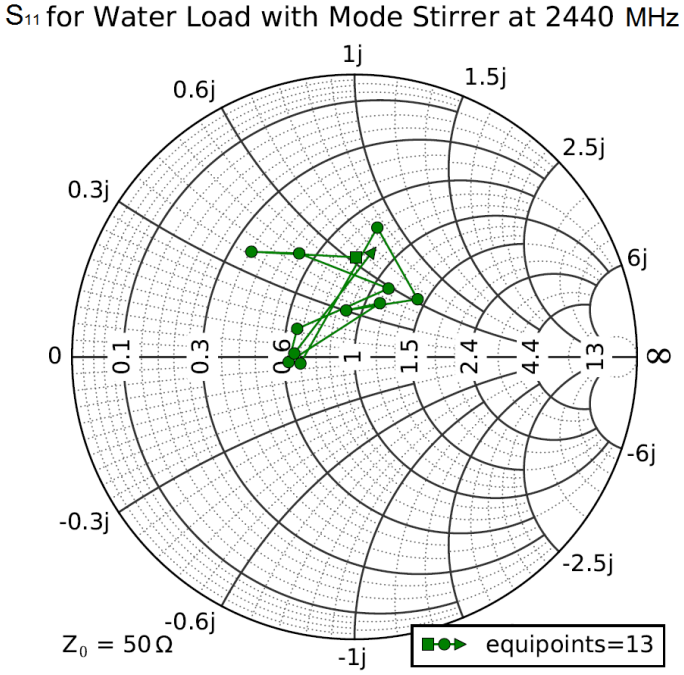

Figure 5.10: Smith chart showing mode stirrer pattern at 2440 MHz.

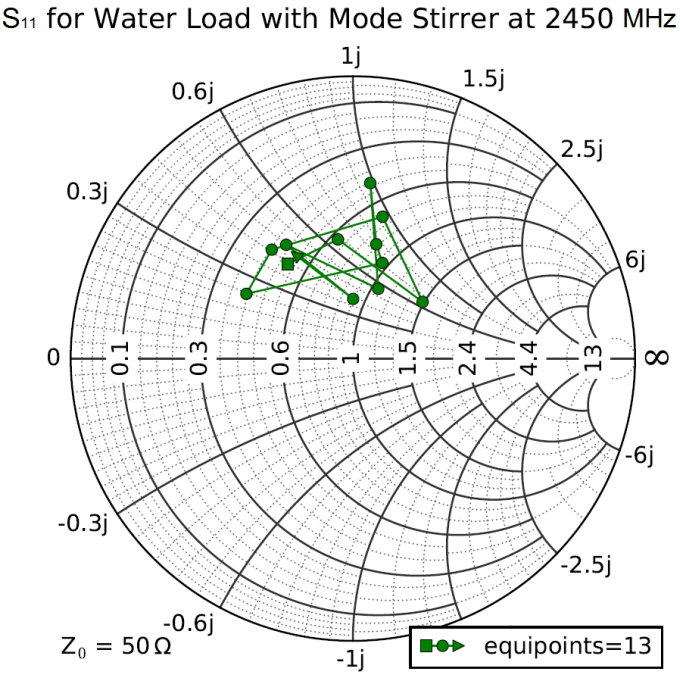

Figure 5.11: Smith chart showing mode stirrer pattern at 2450 MHz.

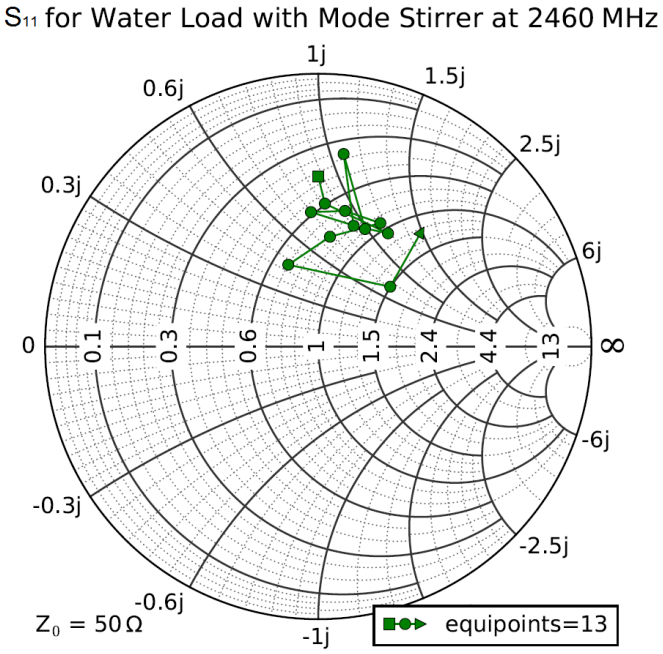

Figure 5.12: Smith chart showing mode stirrer pattern at 2460 MHz.

The results showed that, as the frequency increased, the load appeared to become slightly more inductive. However, the reflection coefficient was still within the same concentrated area of the smith chart and the effect of the changing frequency would not make a very big difference. The fact that the reflection coefficient follows a repetitive pattern proved that the mode stirrer was working. This means that the same reflection happened every time the mode stirrer was in the same position and that a standing wave did not form.

A glass of water is considered a good load and the reflection coefficient was expected to be close to the center of the Smith chart, where it would be perfectly matched. The result indicated that the load was not perfectly matched, as expected. The reflection coefficient was still reasonably well matched despite the mode stirrer. The result was therefore seen as positive since the addition of the mode stirrer did not result in a reflection coefficient close to the periphery of the Smith chart. The reflection coefficient approaches unity as it gets closer to the periphery of the Smith chart. This would mean that all microwave power was being reflected, possibly damaging the magnetron.

5.3.2 Effects of Load Position in Microwave Applicator

Microwaves form a standing wave inside the multi-mode cavity of the microwave applicator. The effect of moving a fixed load around to different positions would give a similar result to that of a mode stirrer. This is essentially what the turntable of a microwave oven achieves. This test was performed by placing the same 500 ml water load in nine different positions in the applicator cavity. The reflection coefficient for each position is indicated in Figure 5.13 as well a map of the load placement positions.

No mode stirrer was used, so the reflection coefficient was a constant value measured from the VNA. Moving the load around inside the applicator cavity resulted in different reflection coefficients. This is because the load absorbed microwave power better in certain spots corresponding with hot spots in the applicator cavity. These hot spots occur due to the standing wave that forms in the applicator cavity. The load was better matched in this case than it was in that of the mode stirrer, where the metal fan caused random reflections in the applicator cavity. However, it must be observed that the two different

methods achieved the same result. Thus, the same outcome can be achieved by either moving the load around, or by introducing a moving metal object in the microwave applicator.

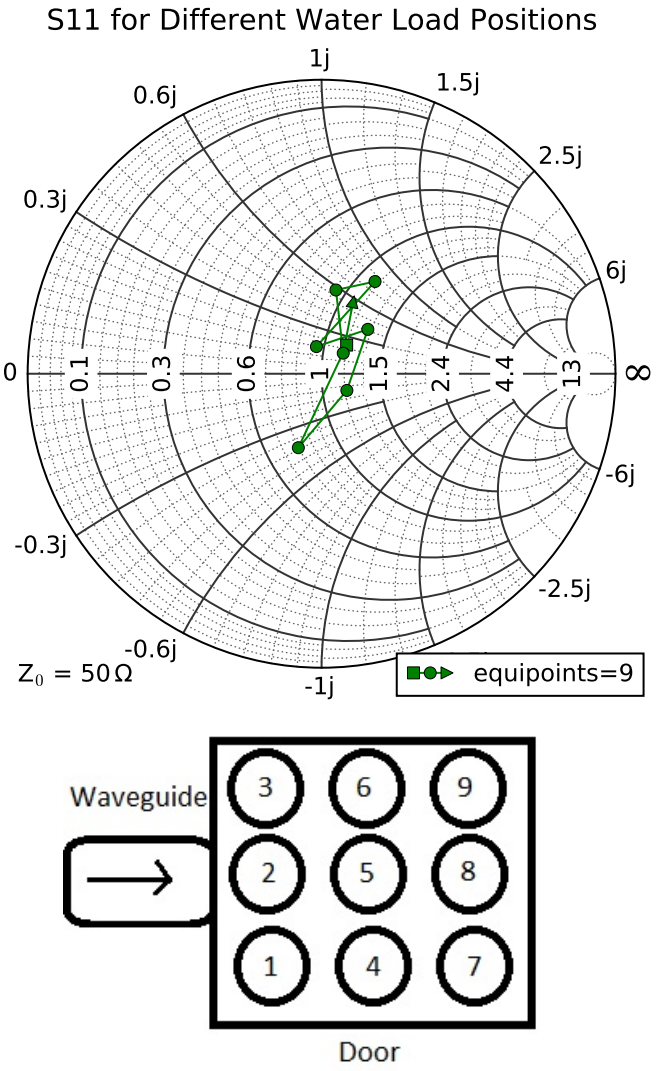

Figure 5.13: Effect of load position on reflection coefficient.

5.3.3 Load Moisture Content Test

Rooibos tea sterilisation would typically involve working with low moisture content loads. Test were performed to evaluate what would happen to the reflection coefficient when the moisture content of the load is reduced.

There was no mode stirrer in the applicator cavity and a 500 ml water load was used for the test. Each point on the Smith chart is the reflection coefficient after 100 ml of water was removed. Therefore starting at 500 ml and ending on 0 ml for the last measurement. The results show that the reflection coefficient tended to a complete reflection or open circuit as the moisture content was reduced. This result confirmed that high moisture content loads are better matched, because they absorb more microwave power.

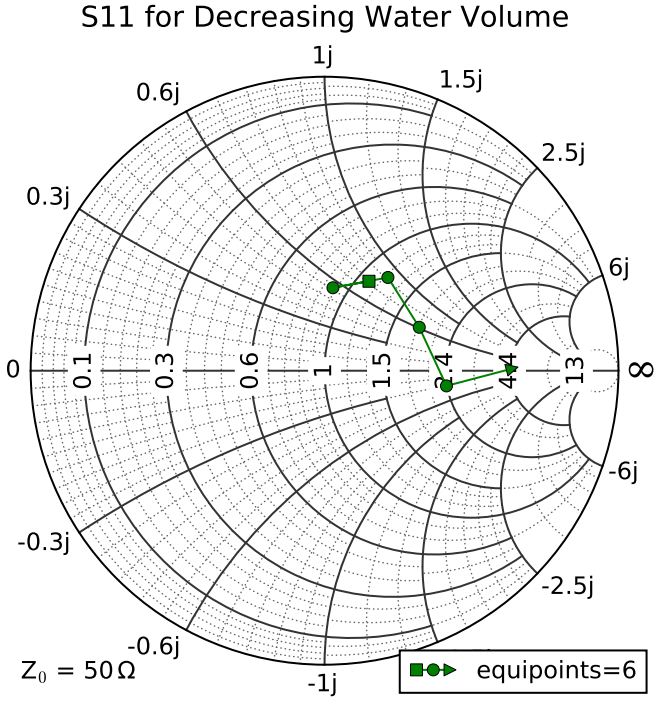

Figure 5.14: Smith chart showing S_{11} as load moisture content is decreased.

5.4 Power Measurements

The effects seen on the VNA can also be seen by looking at the actual microwave power measurements. Diode detectors and a directional coupler were used to measure the applied forward and reflected microwave power waveforms. The actual microwave power delivered to the load was the applied forward microwave power minus the reflected microwave power. The reflection coefficient could also be found by dividing the reflected microwave power by the applied forward microwave power [57]. Therefore, a better matched load would have had a small amount of reflected microwave power and the forward minus the reflected waveform would have been similar to the applied forward microwave power.

The first test performed was to place a 500 ml glass container of water in the middle of the microwave oven on the turntable. The resulting microwave power measurements can be seen in Figure 5.15. The resulting output power shows that most of the microwave power was absorbed and that the load was well matched. The periodicity of the rotating turntable can be seen as specific reflections occurring six times per minute.

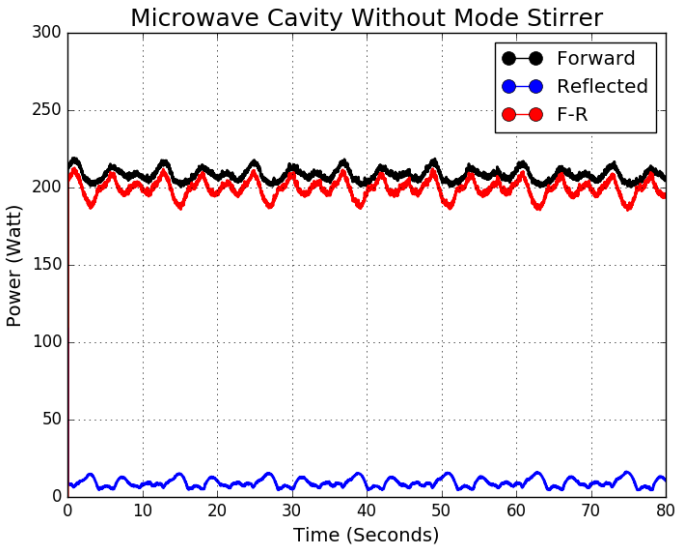

Figure 5.15: Applicator with cup of water and no mode stirrer.

The second test was to put a glass container with dry tea on a metal plate,

which served as a slow mode stirrer, moving at the same speed as the turntable. Large reflections of microwave power can be seen in Figure 5.16 due to the low moisture content of the tea. The mode stirrer's speed is also clearly visible in the periodicity of the reflected waveforms in Figure 5.16.

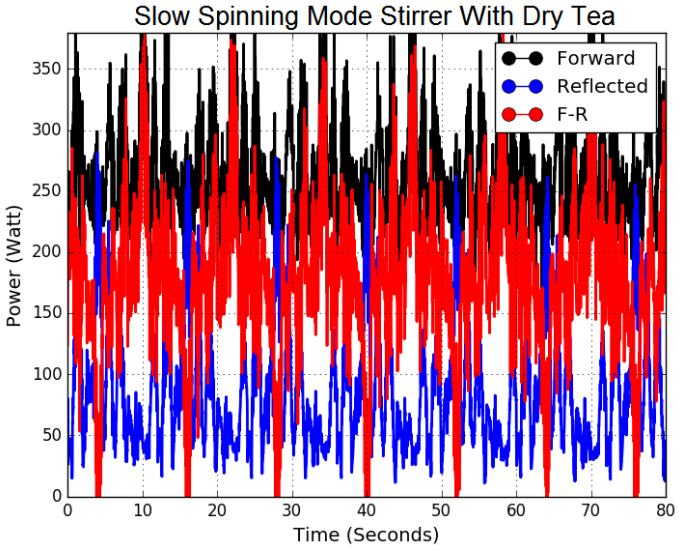

Figure 5.16: Applicator with dry tea and slow spinning mode stirrer.

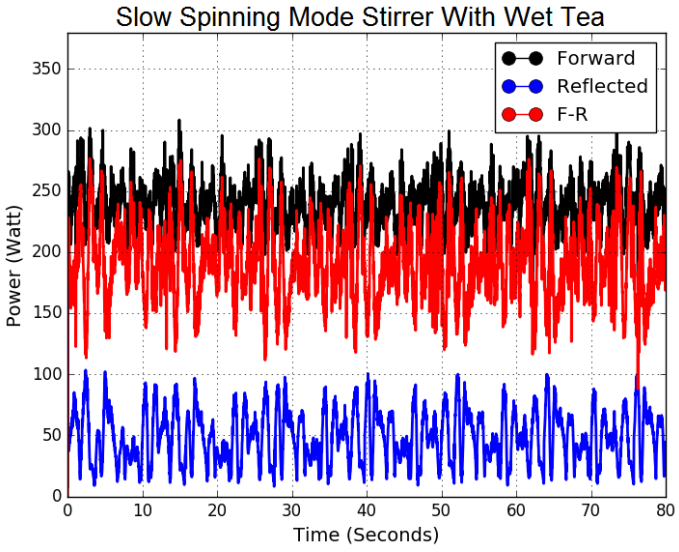

Figure 5.17: Applicator with wet tea and slow spinning mode stirrer.

The third test was to add moisture to the tea, confirming that wetting the tea would improve the matching of the load. Water was added to the tea until it formed a wet paste. Figure 5.17 shows that less microwave power was reflected as the moisture content was increased.

The first tests were repeated with a fast spinning mode stirrer (rotating at 3000 rpm) to determine how the increased speed would affect the power measurements. The results in Figure 5.18 is for a 500 ml water load in the center of the microwave applicator cavity with a fast spinning metal fan as a mode stirrer.

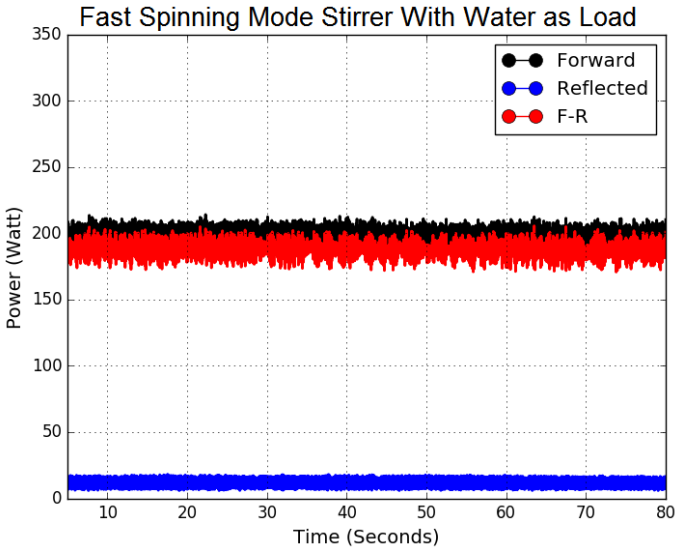

Figure 5.18: Applicator with cup of water and a fast spinning mode stirrer.

The fast spinning mode stirrer produced the same power measurement values as in Figure 5.15, but with a much faster varying set of power measurements. This shows that the heating time constant has been improved and that a good even heat distribution would be achieved with the faster mode stirrer.

Combining the fast mode stirrer and placing a glass of water on the turntable produced a result where both the effect of a mode stirrer and the location of the load in the applicator had an effect on the reflection coefficient. The result in Figure 5.19 shows how the mode stirrer caused the fast varying power

waveform, as well as the effect of the slower turntable moving the load around inside the microwave applicator.

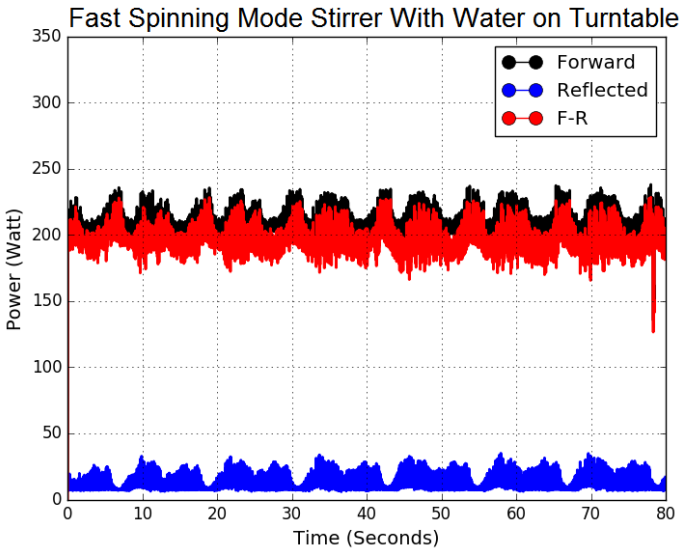

Figure 5.19: Applicator with cup of water on turntable and fast spinning mode stirrer.

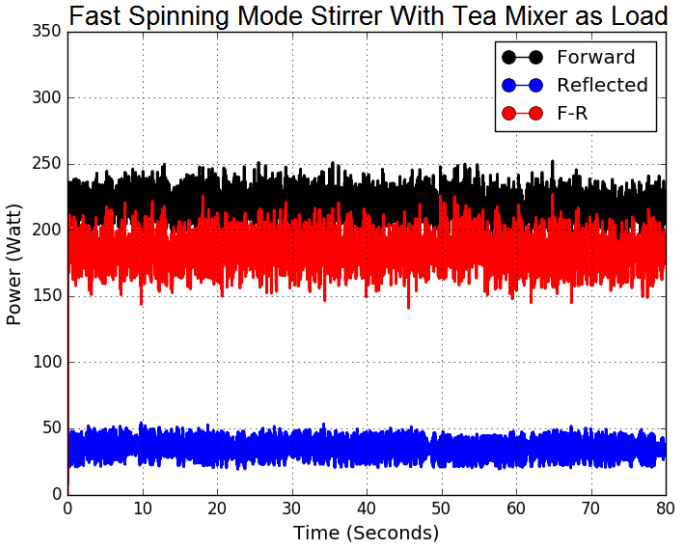

Figure 5.20: Applicator with tea mixer and fast spinning mode stirrer.

The final test was to look at the microwave power measurements of the modified system in Figure 5.2. This setup had a fast spinning mode stirrer, a tea mixer filled with Rooibos tea and a Teflon plate supporting the mixer. Therefore the load comprises of Teflon, microwave safe glass and rooibos tea.

The power measurements for the final modified microwave applicator, seen in Figure 5.20, produced a much better result than that of the dry tea with a slow mode stirrer in Figure 5.16. This could have been due to the location and the shape of the mode stirrer used. The slow mode stirrer was in the middle of the microwave applicator cavity whereas the fast spinning mode stirrer was close to the waveguide feed with blades at about 45°. The glass and Teflon used to build the tea mixer could also have contribute by absorbing some of the microwave energy.

5.5 Chapter Conclusion

The chapter identified that the magnetron was sensitive to changes in its load. The different materials introduced into the microwave applicator cavity were evaluated to ensure the microwave power was applied only to the load. The reflection coefficient of the microwave applicator was investigated for varying frequencies, load positions and moisture content using the VNA. These findings were then confirmed by looking at the actual microwave power measurements for the same load variations.

It was clearly seen that the moisture content of the load affected the amount of microwave power absorbed and reflected . Therefore the reflection coefficient decreased with increasing moisture content. It could also be concluded that a faster mode stirrer would produce a faster varying electrical field which will produce better heat distribution and a shorter heating time constant. The shorter heating time constant is important, as it would help to not burn the Rooibos tea. The tests helped to create a suitable environment to proceed with the tea sterilisation tests. Equally important is that the results make it clear that a fast responding microwave output power controller had to be designed to ensure that the correct microwave output power was applied to the load while irradiating Rooibos tea.

Chapter 6

Software

6.1 Chapter Introduction

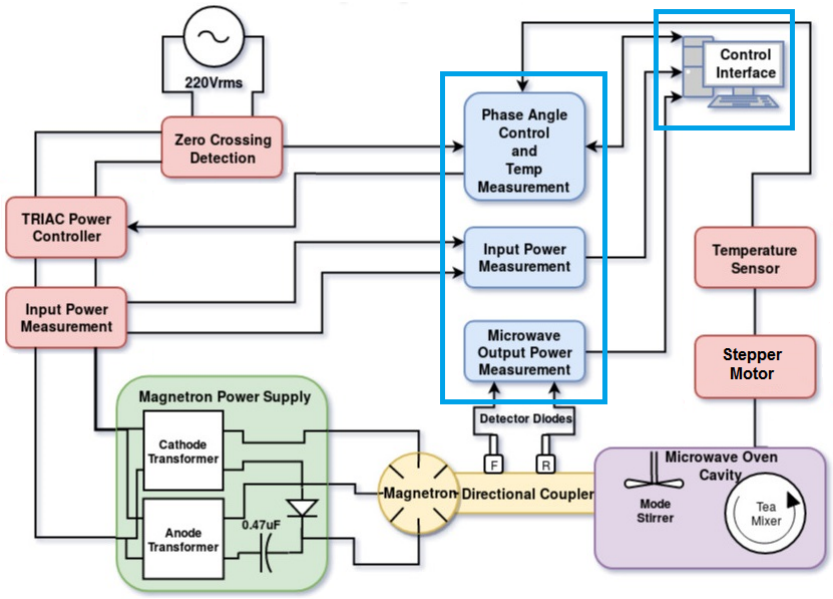

Figure 6.1: Complete system overview.

This chapter covers all of the software developed during this project. Looking at Figure 6.1, the control interface is discussed and the functionality of the developed software package is highlighted.

The microwave output power, system input power and phase angle control was done with three separate Arduino Unos. The specific sampling and timing strategies between the different controllers is discussed, as well as the interaction between the three microprocessors and the master control interface. Finally the complete system is discussed and the compromises made for timing and resolution are highlighted.

6.2 Functionality of Microwave Monitoring Dashboard

The "Microwave Monitoring Dashboard" was developed to give a user friendly graphical aid in setting up microwave experiments. The software offers a platform to set up tests that can easily be repeated. Apart from offering visual representations of all the important waveforms in the system, it also enables the user to control the power of the magnetron. The functionality of the system is discussed below.

Upon startup all options in the main window, as seen in Figure 6.2, are blanked out and unavailable to the user. Only the "COM Setup" frame is active. Clicking the "Check" button checks the serial connection between each Arduino and the monitoring program. Only once each unique identifying character has been received, will the connect button work and allow the user to proceed with the setup of the session. Once the connection is established, the user can select the directory in which to store the data acquired from the session.

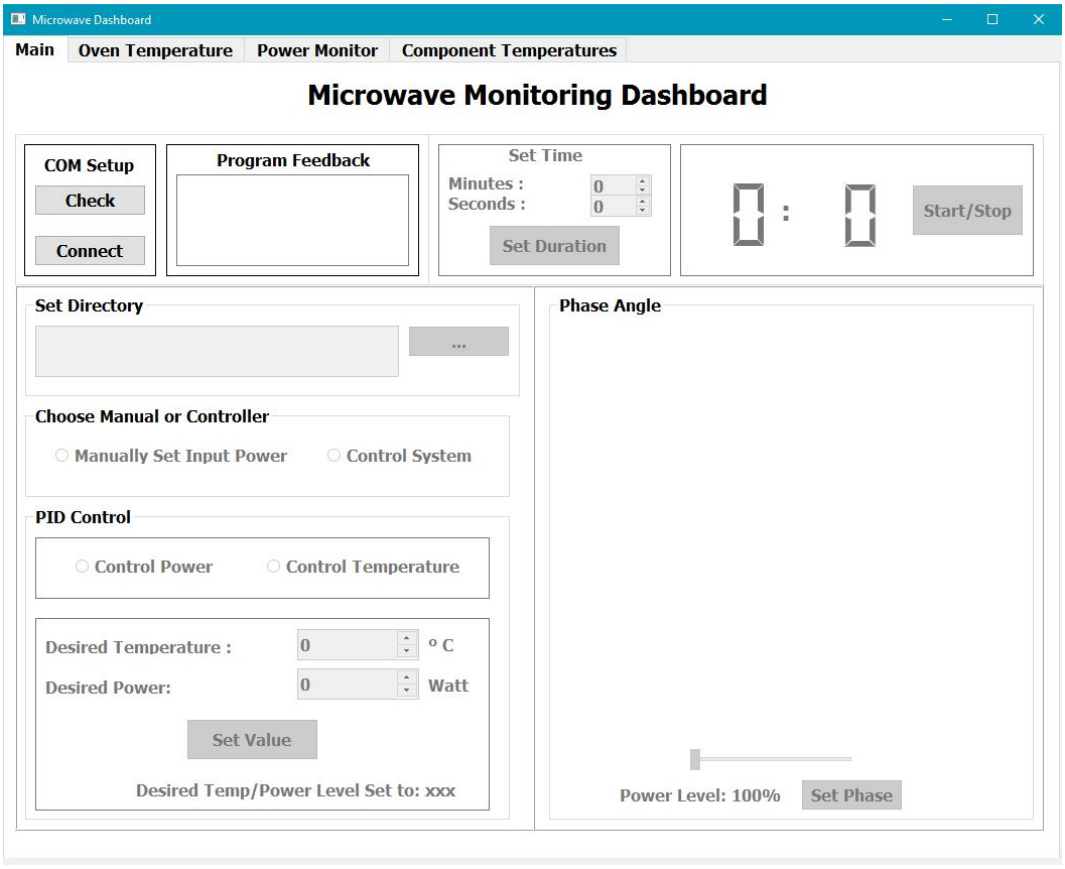

Figure 6.2: Main window of microwave dashboard.

The user chooses if the magnetron must operate at a set input power setting or have the microwave output power controller take over. Choosing to manually set the input power activates the "Phase Angle" block, allowing the user to choose a fixed phase angle by sliding the slider bar to the desired percentage of input power. If the "Control System" option is chosen instead, the "PID Control" block will activate. Either temperature control or power control can be selected, depending on the nature of the test being run. The correct edit box will activate to set either the temperature or power set points. Finally the "Set Time" block will activate once either the "Set Value" or "Set Phase" button is clicked. Once the time is set, the "Start/Stop" button activates, allowing the test to be started.

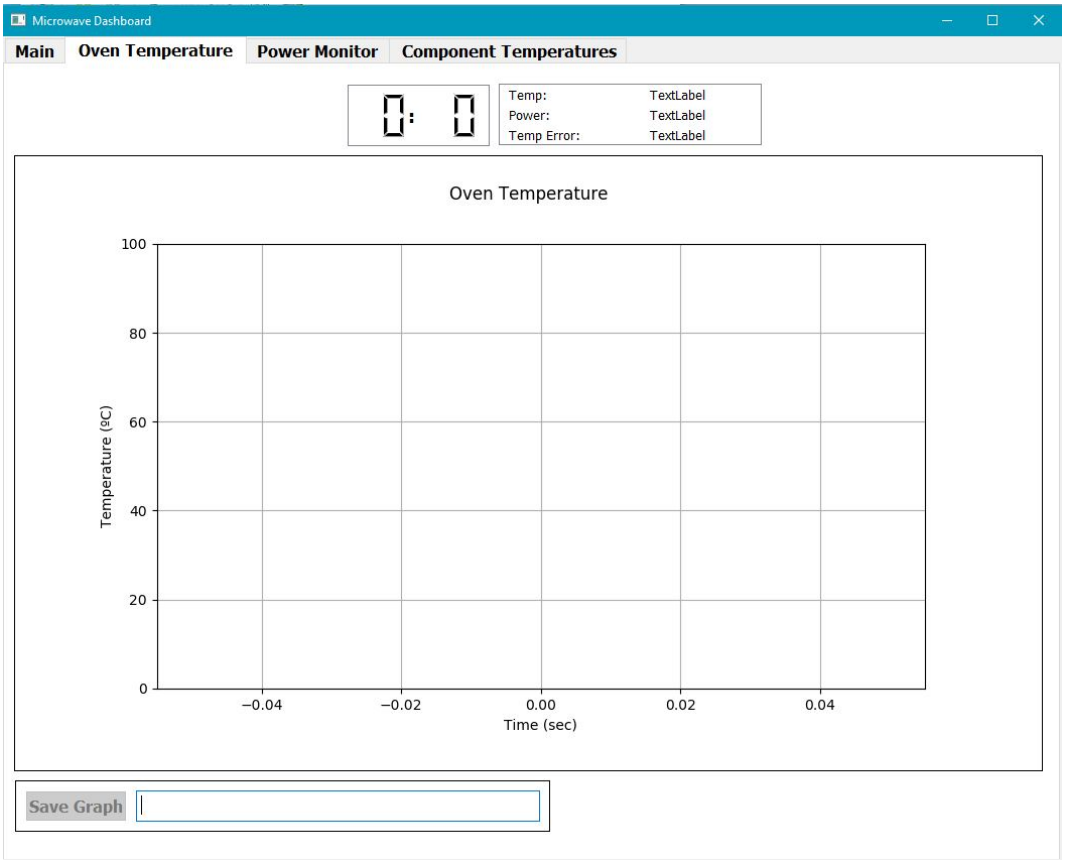

Figure 6.3: Oven temperature window of microwave dashboard.

Clicking the "Start/Stop" button starts the magnetron and the data from the Arduinos are then processed in separate threads. Moving through the tabs activates specific plotting canvases and produces a live update of the received data. Specifically looking at the "Oven Temperature" tab, seen in Figure 6.3, the temperature reading of the tea in the mixer is plotted. The temperature, microwave output power and the set point error is displayed accompanied by the countdown timer. These values are updated every second, as well as the temperature plot. The "Save Graph" button can be clicked once the time runs out. This saves an image of the plot as well as a data file with the plot points.

Figure 6.4: Power monitoring window of microwave dashboard.

The exact same routine holds for the "Power Monitor" and "Component Temperature" tabs. The graphs of the system input power, total microwave output power, input current and voltage waveforms, forward and reflected microwave pulses, average forward and reflected microwave power and power efficiency can be monitored in the "Power Monitor" tab, as shown in Figure 6.4. Similarly the temperatures of the magnetron, anode transformer and cathode transformer can be monitored in the "Component Temperatures", as shown in Figure 6.5.

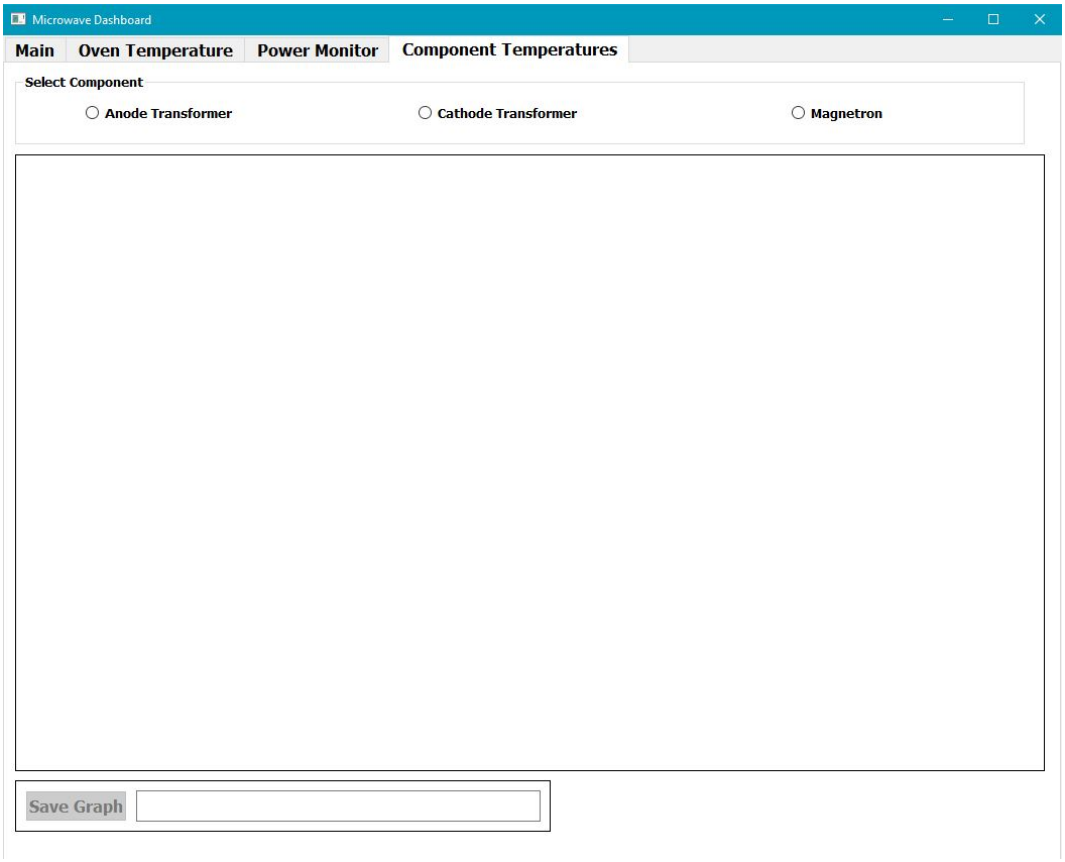

Figure 6.5: Component temperature window of microwave dashboard.

6.3 System Interactions

6.3.1 Overview

Three Arduinos were used to interact with the master control program. Two of the Arduinos were used to sample the input power and the microwave output power respectively. The reason why two separate Arduinos were used was because the two power readings had to happen at the same time. The sampling was synchronized using the zero crossing signal, which triggered a hardware interrupt on each Arduino. The third Arduino was used to control the magnetron power and measure the temperature in the microwave applicator. Therefore every 10 ms all three microcontrollers would be synchronized and specific events would be triggered. The Arduinos would act as slaves to

the master control program. The overview is given in Figure 6.6.

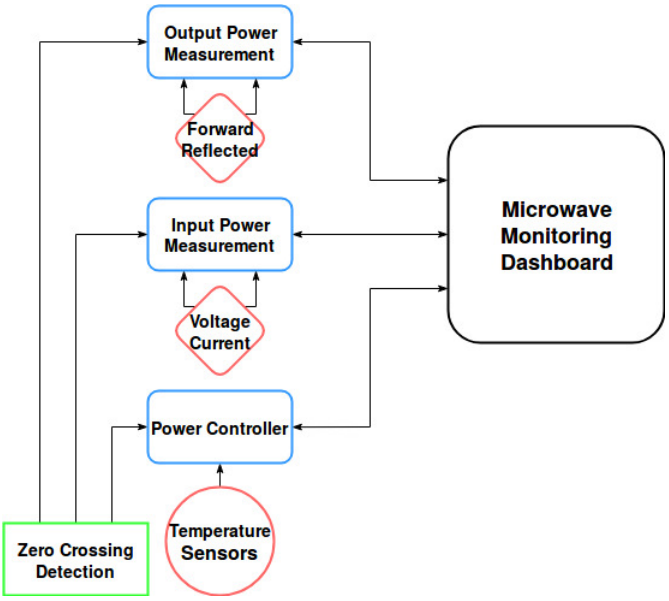

Figure 6.6: Overview of master slave interaction with Arduinos and control program.

6.3.2 Arduino Code

The sampling scripts for the input power and microwave output power measurements were exactly the same. The input power measurement required a current and a voltage waveform to calculate the input power. The samples from each channel were then multiplied together to find the instantaneous power. The instantaneous power was integrated over the 10 ms sample period to find the average input power.

Similarly the microwave output power was calculated by sampling the forward and the reflected microwave power channels on the directional coupler. Both the forward and reflected channels were then integrated over the 10 ms sampling period to find the average microwave power for each channel. The microwave output power was calculated by subtracting the reflected power from the forward power.

Both the input power and microwave output power scripts would sample two waveforms every 40 ms, generating 50 samples per channel/waveform over a 10 ms period. Therefore 200 samples were generated every 40 ms and sent back to the control program where the integration and power calculations occurred. The flow diagram in Figure 6.7 shows the structure of the sampling script used for both the input power and microwave output power.

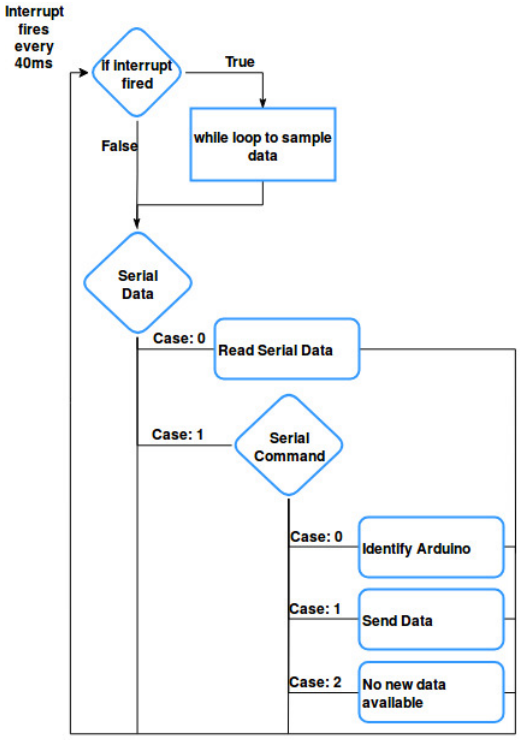

Figure 6.7: Flow diagrams of the Arduino data sampling scripts.

The sampling only happened over a single half-cycle as the magnetron was only on for half of the 50 Hz cycle of the mains voltage. Similarly when one terminal of the step-down transformer, used to measure input voltage, was connected to ground only the positive half-cycle could be sampled. Therefore new data sets were generated by the sampling code every 40 ms and the control software sent a request for this data when it was required. The motivation behind the 40 ms delay between new data sets was to give the serial communication sufficient time to transfer the data. The baud rate was set to its maximum of 115200 baud and the amount of data that had to be sent was

100 comma separated samples per microcontroller, for both the input power and the microwave output power measurements.

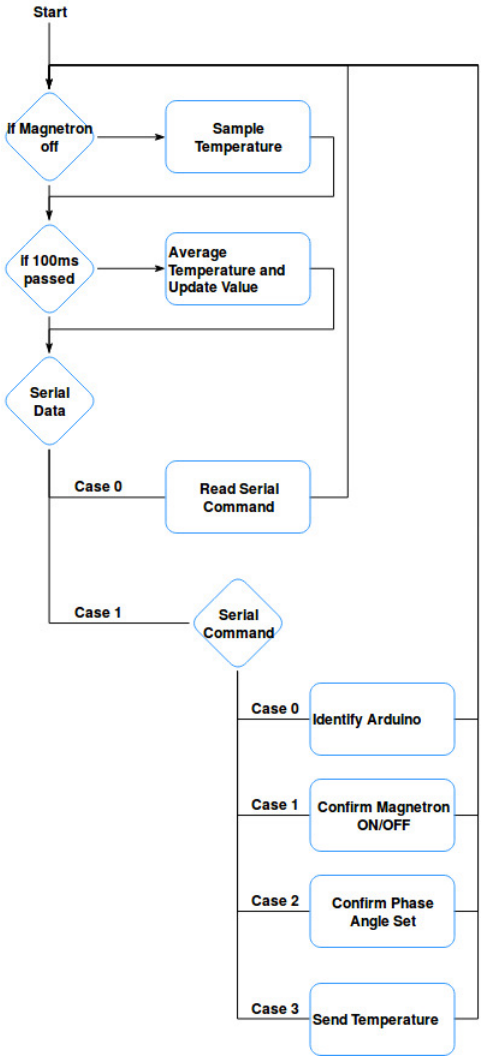

Figure 6.8: Flow diagram of Arduino power controller script.

The phase angle control for the magnetron input power was done with the controller script, the flow diagram is shown in Figure 6.8. Once the zero crossing hardware interrupt fired, (interrupts are not shown on the flow diagram in Figure 6.8 as they were only used to switch one output pin on and off) timer 0 and timer 1 of the Arduino were used to control the TRIAC. Timer 0 had a 10 bit resolution and timer 1 had a 16 bit resolution. Timer 1 was used to determine when the TRIAC would fire and timer 0 was used to switch off the

pin used to switch on the TRIAC. This script could also respond to several commands like switching the system on and off, changing the phase angle and sending back temperature readings when prompted by the master control program.

The temperature readings were made when the magnetron was off. The status of the magnetron was determined by the zero crossing signal: When the zero crossing signal was low the magnetron is on. The temperature was continuously sampled when the zero crossing signal went high and the magnetron was off. The temperature samples were averaged every 100 ms. The temperature value returned to the control program, when requested, was the latest averaged temperature value.

6.3.3 Microwave Dashboard Data Acquisition

The main control program or "Microwave Monitoring Dashboard" had functions to generate and manage the graphical user interface in order to make it user friendly and robust. When only looking at the critical parts of the code, it can be broken up into two loops.

The first loop requests the power measurements from the respective input and output power Arduinos. The flow diagram can be seen in Figure 6.9, where two threads were used to request the data at the same time. The data was processed by calculating the average power when integrating the discrete samples over the sampling period. The average power values for both the input power and microwave output power were continuously generated and appended to a set of arrays from the moment the magnetron was switched on. The loop is called recursively every 160 ms, giving enough time for data to be requested and processed before the next cycle starts.

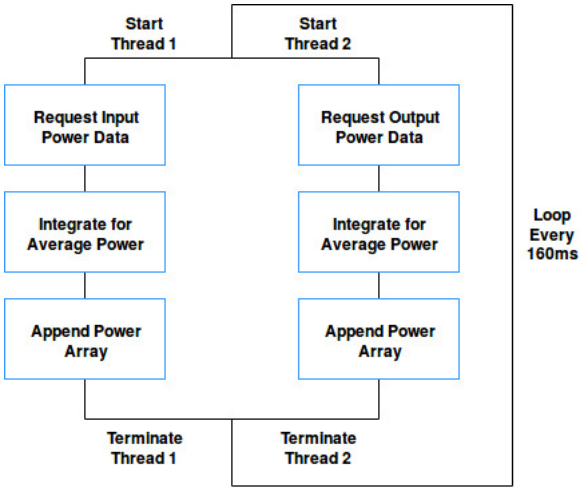

Figure 6.9: Data acquisition loop.

A second, slower loop executes once every second. This loop was used to update the plots, update the clock, get the average power for the previous second, calculate the sliding average for the last five seconds and calculate the new phase angle with the PID algorithm. The flow diagram for this loop is shown in Figure 6.10.

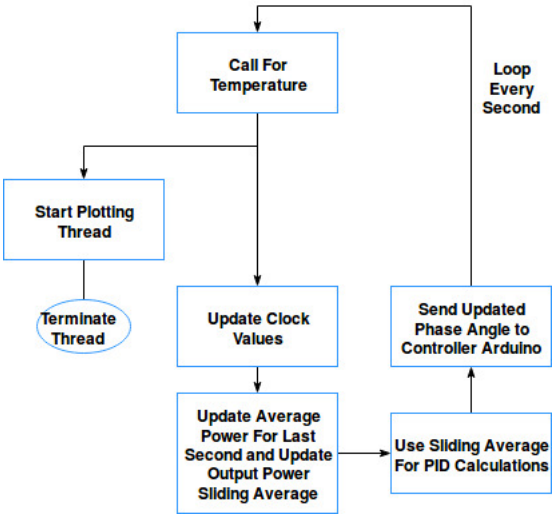

Figure 6.10: Plotting and control loop.

6.4 Chapter Conclusion

The "Microwave Monitoring Dashboard" program has multiple routines that executes in parallel. This created timing issues during the development of the software package. The fastest possible control feedback would have been to update the phase angle every 20 ms: 10 ms to sample the data and 10 ms to send the data and receive feedback from the controller.

Through a trial and error approach it was found that the shortest possible time to control the microwave output power and still maintain the functionality of the program was to use 160 ms sampling period for the two power measurements. This resulted in six input power and microwave output power measurements per second. The trade off could be made where less data points were sampled and therefore all other dependent programming time would have been reduced, but this would have lead to a compromise in resolution. Since the microwave power was randomly scattered around the set point due to the mode stirrer, the decision was made to use a sliding average for the last five seconds to determine what the next input to the actuator had to be.

In conclusion the sampled power waveforms were processed every 160 ms and appended to an array. The average power value is calculated and plotted every second. The PID algorithm uses a sliding average of the last 5 seconds to adjust the phase angle. The phase angle was therefore updated every second using the average microwave output power measured in the last 5 seconds. The design of the controllers is discussed further in Chapter 7.

Chapter 7

Controllers

7.1 Chapter Introduction

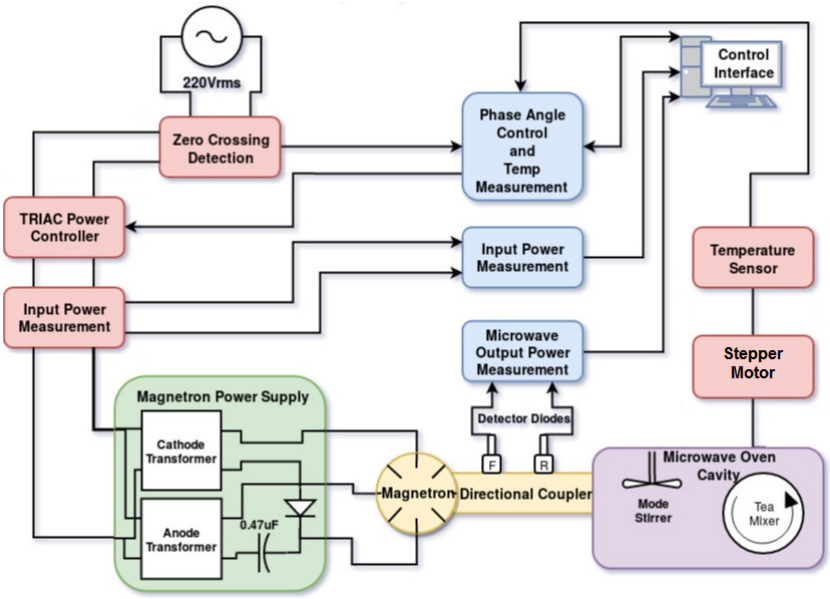

Figure 7.1: Complete system overview.

This chapter only focuses on the design of the control software used in the microwave monitoring dashboard program, as discussed in Chapter 6. The software package has the functionality to either be used as a temperature controller or a microwave output power controller. Both of these implementations

use different PID algorithms. The derivation of both these algorithms are explained. The first part of the chapter covers general control theory, which was used to explain design decisions and the derivation of the final algorithms implemented in software.

7.2 Control Theory

The aim of a good control system is to track the reference input, be resistant to external disturbances and always remain stable. On top of these three goals, the system should still adhere to these rules even if the theoretical model used to derive the transfer function is not completely accurate [58].

7.2.1 Closed Loop Transfer Function

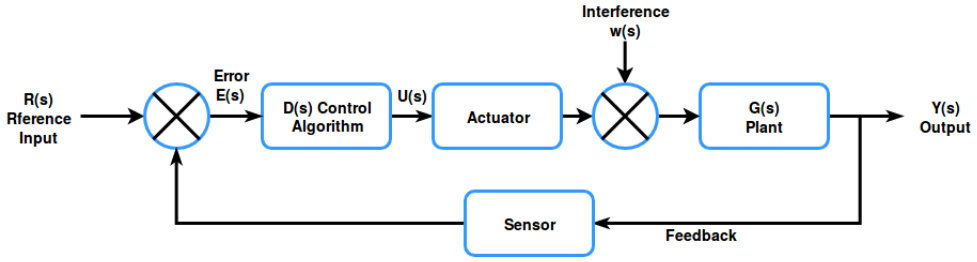

Figure 7.2: Block diagram of typical feedback control system [7].

The block diagram in Figure 7.2 was used to derive the closed-loop transfer function, which was later used to evaluate and tune the PID settings of the controller. Equations 7.2.1 and 7.2.2 can be derived from the block diagram:

$$Y(s) = G(s)(U(s) + w(s)) \tag{7.2.1}$$

$$U(s) = D(s)(R(s) - Y(s)) \tag{7.2.2}$$

Substituting Equation 7.2.1 into Equation 7.2.2, assuming that there is no interference so that $w(s) = 0$, resulted in Equation 7.2.3, which is the closed loop transfer function [7].

$$\frac{Y(s)}{R(s)} = \frac{D(s)G(s)}{1 + D(s)G(s)} \tag{7.2.3}$$

7.2.2 Determining The Plant

The step response of a temperature control problem has an s-shaped curve, which is characteristic of various other systems as well. The process reaction curve can therefore be approximated by a standard plant transfer function in Equation 7.2.4 [59].

$$P(s) = \frac{Ae^{st_d}}{(\tau s + 1)} \tag{7.2.4}$$

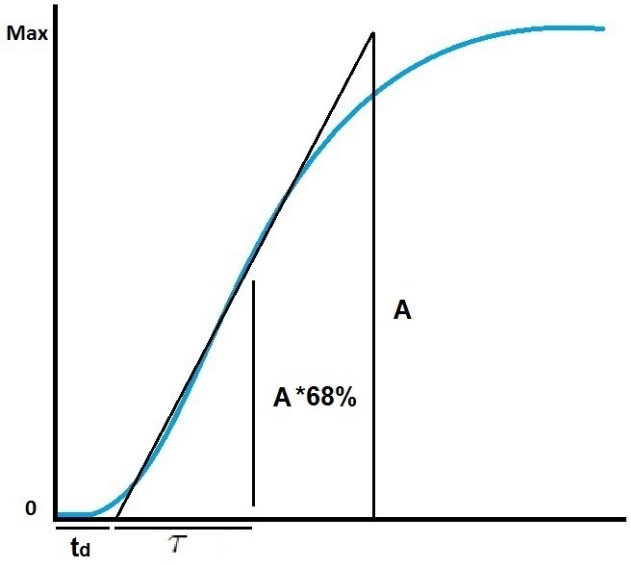

Figure 7.3: Typical S-shape process reaction curve.

Applying the plant transfer function to the step response in Figure 7.3, where A was the maximum change in the output of the step response, τ was the time constant and t_d is the time delay. The effect of the sampling delay T_s was also added. The total delay is as shown in Equation 7.2.5 [60]:

$$T_{delay} = \frac{T_s}{2} + t_d \tag{7.2.5}$$

The plant can then be approximated using Equation 7.2.6:

$$P(s) = \frac{A\frac{2}{T_{delay}}}{(\tau s + 1)(s + \frac{2}{T_{delay}})} \tag{7.2.6}$$

7.2.3 Implemented in Software

The software to implement the PID controller could be written without designing the actual controller, with arbitrary values being used for the PID controller. Knowing that the software was written correctly allowed for the continuous testing of the derived models. The PID software runs in a loop at a specified frequency that executes the discrete time PID algorithm in Equation 7.2.18.

A relationship between the discrete and continuous time PID algorithms was found to understand how the calculated PID values must be implemented in software. The derivation was started with the continuous time domain PID algorithm in Equation 7.2.7 [61].

$$u(t) = K(e(t) + \frac{1}{T_i}\int_0^t e(\tau)d\tau + T_d\frac{de(t)}{dt} \tag{7.2.7}$$

Converting the Equation 7.2.7 to the frequency domain using the Laplace transform results in Equation 7.2.8:

$$D(s) = \frac{U(s)}{E(s)} = K(1 + \frac{1}{sT_i} + sT_d) \tag{7.2.8}$$

Defining the PID parameters of Equation 7.2.8 as follow simplified the calculation of the z-transform:

$$K_p = K \tag{7.2.9}$$

$$K_i = \frac{K}{T_i} \tag{7.2.10}$$

$$K_d = KT_d \tag{7.2.11}$$

The z-transform is done using the backwards Euler method [62]:

$$s = \frac{1 - z^{-1}}{T_s} \tag{7.2.12}$$

Resulting in Equation 7.2.13:

$$\frac{U(z)}{E(z)} = (K_p + K_i\frac{T_s}{1 - z^{-1}} + K_d\frac{1 - z^{-1}}{T_s}) \tag{7.2.13}$$

sorting the terms in Equation 7.2.13 gives:

$$\frac{U(z)}{E(z)} = \frac{(K_p + T_sK_i + \frac{K_i}{T_s}) + (-K_p - 2\frac{K_d}{T_s})z^{-1} + K_dz^{-2}}{1 - z^{-1}} \tag{7.2.14}$$

Equation 7.2.13 can be further simplified by grouping the terms as follows:

$$K_1 = K_p + T_s K_i + \frac{K_d}{T_s} \tag{7.2.15}$$

$$K_2 = -K_p - 2\frac{K_d}{T_s} \tag{7.2.16}$$

$$K_3 = K_d \tag{7.2.17}$$

Multiplying out and converting back to discrete time, gives the difference equation as Equation 7.2.18 below.

$$u[k] = u[k-1] + K_1 e[k] + K_2 e[k-1] + K_3 e[k-2] \tag{7.2.18}$$

Equation 7.2.18 could then be implemented as the control algorithm in the controller software [61].

7.2.4 Ziegler-Nichols Tuning

Ziegler and Nichols derived a set of formulas that can be used to tune a PID controller. The quarter decay method has an approximate damping of $\zeta = 0.21$ and served as a good starting point for tuning a PID controller [63]. The Ziegler-Nichols method uses parameters from the step response of a plant, as discussed in Subsection 7.2.2, to find the parameters of Equation 7.2.18. The values of R and L, in Equations 7.2.19 and 7.2.20, are derived directly from the parameters of the plant shown in Figure 7.3 and then used to find the required PID values.

$$R = \frac{A}{\tau} \tag{7.2.19}$$

$$L = t_d \tag{7.2.20}$$

Where R is the slope or gradient of the step response and L is the lag in the system.

R and L can be used to find the parameters for either the P, PI or PID controller configurations shown below. The values can then be used to find K_1, K_2 and K_3 as derived in Subsection 7.2.3. The resulting controller can then be tuned by changing PID values in the discrete time PID algorithm of Equation 7.2.18 [63].

Proportional Control:

$$K_p = \frac{1}{RL} \tag{7.2.21}$$

Proportional Integral Control:

$$K_p = \frac{0.9}{RL} \tag{7.2.22}$$

$$T_i = \frac{L}{0.3} \tag{7.2.23}$$

Proportional Integral Derivative Control:

$$K_p = \frac{1.2}{RL} \tag{7.2.24}$$

$$T_i = 2L \tag{7.2.25}$$

$$T_d = 0.5L \tag{7.2.26}$$

7.3 Microwave Output Power Controller Design

The magnetron has the ability to change its microwave output power over one period of the 50 Hz power frequency. Therefore, after the actuator (TRIAC controller) changes value, the effect could be seen within 20 ms, making $t_d = 0.02\ s$. Chapter 6 explains that the average microwave output power was calculated with a sliding average over a 5 second period. After the first 5 seconds, the sliding average and PID algorithm updateds every second, therefore the sampling time t_s is then 1 second. With the hardware modifications, the maximum microwave output power was 200 W. The parameters used to determine the transfer function of the power controller is listed in Table 7.1.

Table 7.1: Parameters for the plant of the microwave output power controller.

Parameter	Value
A	200 $Watt$
τ	0.003 s
t_d	0.02 s
t_s	1 s

The transfer function of the plant was not obtained by measuring a reaction curve, as described in subsection 7.2.2, as the microwave output power changed too quickly. The plant was better represented by a step waveform that could vary between 0 W and 200 W. The plant in Equation 7.3.1 was determined through simulation, still using Equation 7.2.4 to describe the plant. The simulated plant can be seen in Figure 7.4; note that no sampling delays were added to the plant and that only the 20 ms period used to change the microwave output power is taken into account.

$$P(s) = \frac{200}{(0.003s + 1)} \tag{7.3.1}$$

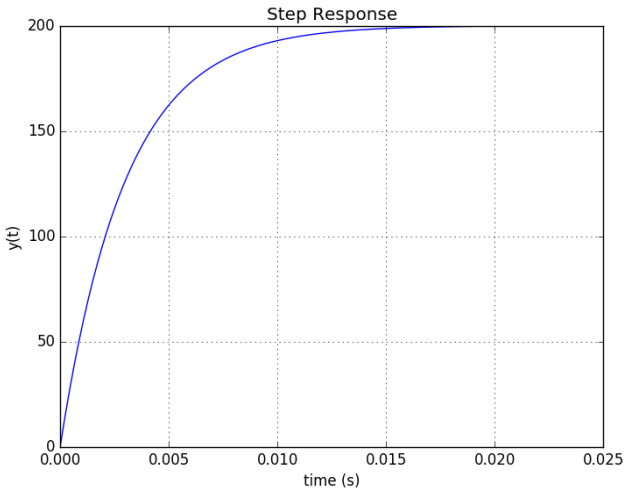

Figure 7.4: Step response of magnetron power controller plant.

The 1 second sampling delay was added to the plant $T_d = \frac{t_s}{2} + t_d = 0.52\ s$. The new plant is represented below by Equation 7.3.2. The resulting simulation of the added delay is shown in Figure 7.5.

$$P(s) = \frac{200\frac{2}{0.52}}{(0.003s + 1)(s + \frac{2}{0.52})} \tag{7.3.2}$$

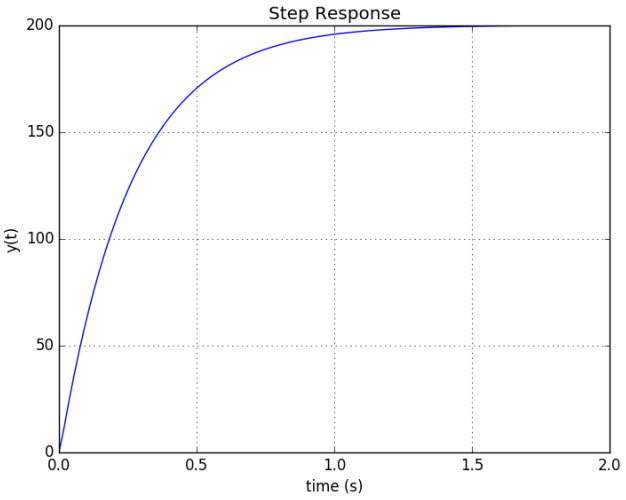

Figure 7.5: Step response of magnetron power controller plant with sampling delay.

Ziegler-Nichols tuning was not used to determine the PID values. The large A value over the small τ value resulted in a large R that did not give the expected quarter decay response, refer back to Subsection 7.2.4. The values for the PI controller was determined through software simulation and continuous testing with the PID software. The discrete PI control algorithm was implemented in software with Equation 7.3.3. The values for K_p and K_i are shown in Table 7.2.

$$u[k] = u[k-1] + 0.002137e[k] + 0.00187e[k-1] \tag{7.3.3}$$

Table 7.2: Parameters for the microwave output power PI controller.

PI Parameters	Value
K_p	0.00186
K_i	0.000267

The simulated result of the PI controller is shown in Figure 7.6.

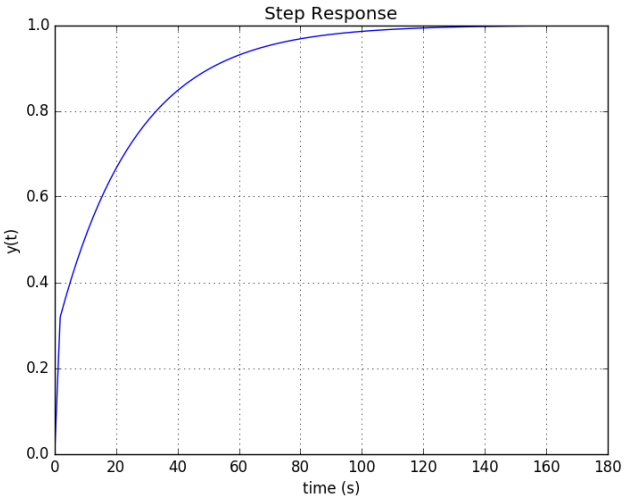

Figure 7.6: Simulated step response of the PI microwave output power controller.

The actual system response in Figure 7.7 shows the microwave output power for a reference set point of 150 W. These graphs were obtained from the software package, discussed in Chapter 6, during one of the Rooibos tea sterilization tests.

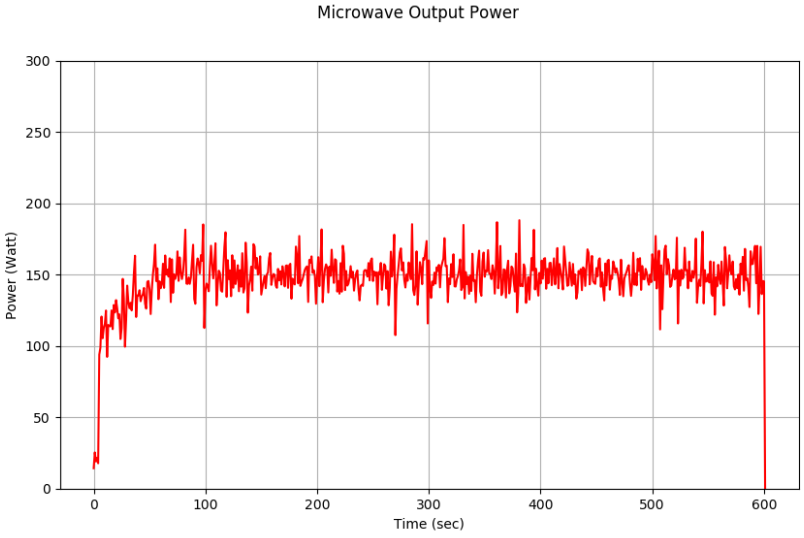

Figure 7.7: Microwave output power controlled at 150 W.

Figure 7.8 shows how the input power of the system was changed to control the 150 W microwave output power.

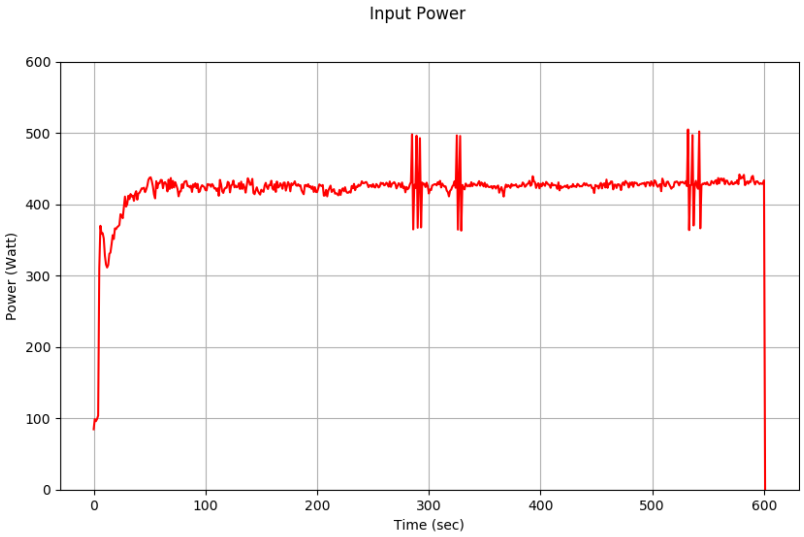

Figure 7.8: System input power to control at 150 W output power.

7.4 Temperature Controller Design

The temperature control algorithm was set up to request a new power reference from the power controller, instead of directly changing the phase angle on the TRIAC controller. The temperature control was therefore dependent on the microwave output power controller designed in Subsection 7.3. The transfer function of the plant was determined by setting the power to 200 W and evaluating the temperature response, as seen in Figure 7.9.

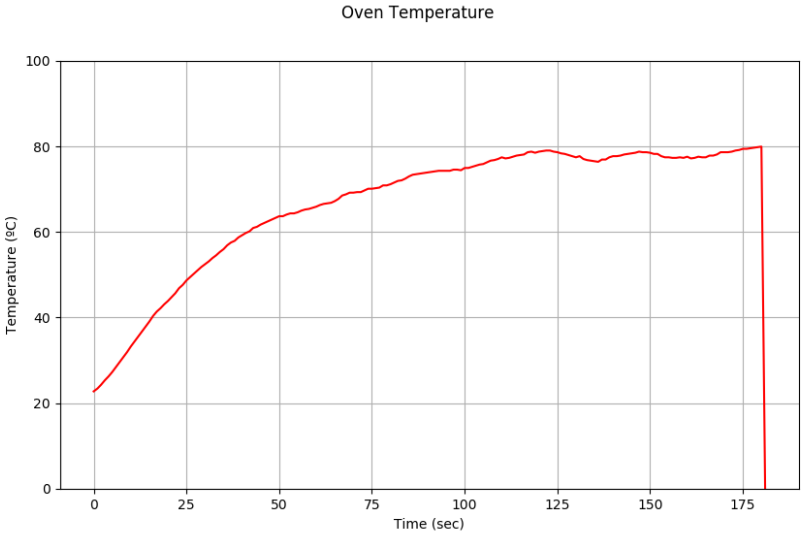

Figure 7.9: Temperature response at 200 W.

The plant values shown in Table 7.3 were determined from Figure 7.9.

Table 7.3: Parameters for the plant of the temperature controller.

Parameter	Value
A	$58\ ^{\circ}C$
τ	$25\ s$
t_d	$1\ s$
t_s	$1\ s$

The resulting transfer function was determined to be:

$$P(s) = \frac{58\frac{2}{1.5}}{(25s+1)(s+\frac{2}{1.5})} \tag{7.4.1}$$

The simulated step response of Equation 7.4.1 can be seen in Figure 7.10.

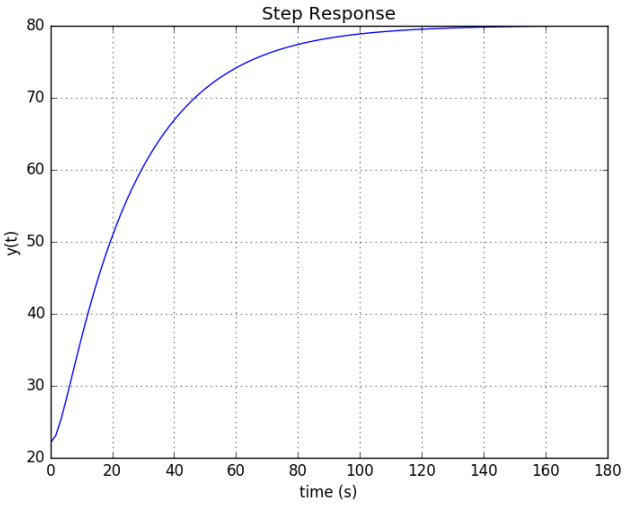

Figure 7.10: Step response for theoretical temperature plant.

The initial PID values for the controller was chosen using the Ziegler-Nichols method, after which the values were experimentally adjusted to give the desired response. Equation 7.4.2 was used in the control algorithm:

$$u[k] = u[k-1] + 0.08115e[k] + 0.0736e[k-1] \tag{7.4.2}$$

The Pi controller parameters are listedin Table 7.4.

Table 7.4: Parameters for the temperature PI controller.

PI Parameters	Value
K_p	0.0736
K_i	0.00755

The simulated closed-loop step response gives the resulting output in Figure 7.11.

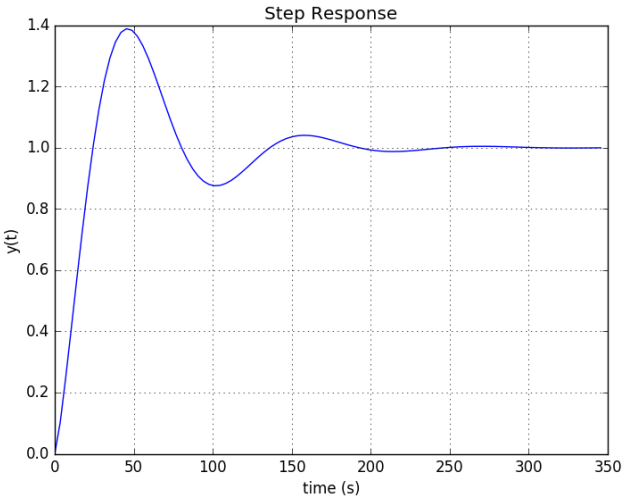

Figure 7.11: Simulated closed-loop step response for temperature PI controller.

The actual response, as seen in Figure 7.12, had a more damped response. This was due to the lag between the temperature controller's power set-point and the power controller adjusting to meet the new set point.

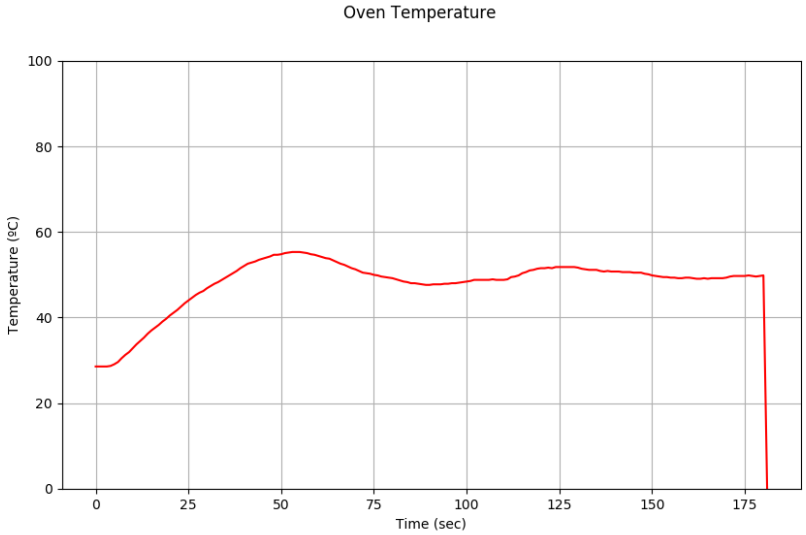

Figure 7.12: Temperature controlled at 50 °C

The microwave output power in Figure 7.13 shows how the controller adapted to maintain the temperature in Figure 7.12 at 50 °C.

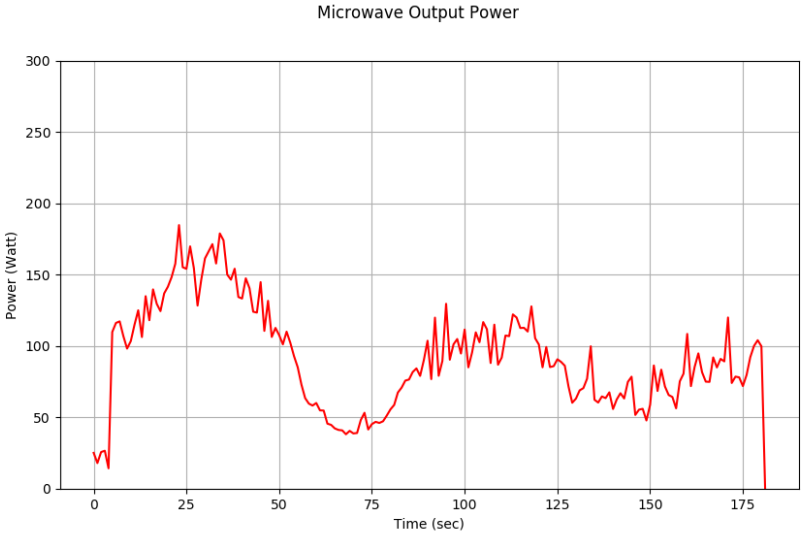

Figure 7.13: Microwave output power for temperature controlled at 50 °C

7.5 Chapter Conclusion

This chapter shows how two controllers were designed to give the software package in Chapter 6 the functionality to either track a reference temperature or microwave output power. The design had to take into account the timing enforced by the software package and the nature of the microwave power being measured. The choice to average the microwave power over five seconds was to ensure that the controller would be more resistant to reflections from the mode stirrer. The temperature controller could also have had a faster and less damped response if it was implemented independently, directly requested phase angle values from the actuator and not microwave power. However, the control system is accurate enough for the intended sterilisation process.

Chapter 8

Tea Experiments

8.1 Chapter Introduction

This chapter looks at the sterilisation tests performed on Rooibos tea with the developed microwave sterilisation system. The microbiology of the sterilisation problem was limited in the scope of this project. Some basic principles are explained in order to be used in further discussions of the sterilisation results. The experimental setup for each test as well as the significance of the tests are explained. The results are evaluated and further insights into Rooibos tea sterilisation by means of microwave irradiation are discussed.

8.2 Temperature Treatments

The term sterilisation refers to the removal of all living organisms in a medium. Temperature has been used as a sterilisation method for ages. Heat is effective as a sterilisation technique due to its ability to change the organic molecules inside of biological cells, resulting in their death. These changes involve the alteration of enzyme molecules and the structural breakdown of the cell membrane. Heat also releases moisture from cells and since all organisms depend on moisture, dehydration can have lethal effects [8].

There are various types of microorganisms, each with their own degree of resistance to temperature treatments. These resistances to heat have thoroughly been studied and documented. Figure 8.1 gives an overview of the typical temperatures used to sterilise different types of microorganisms.

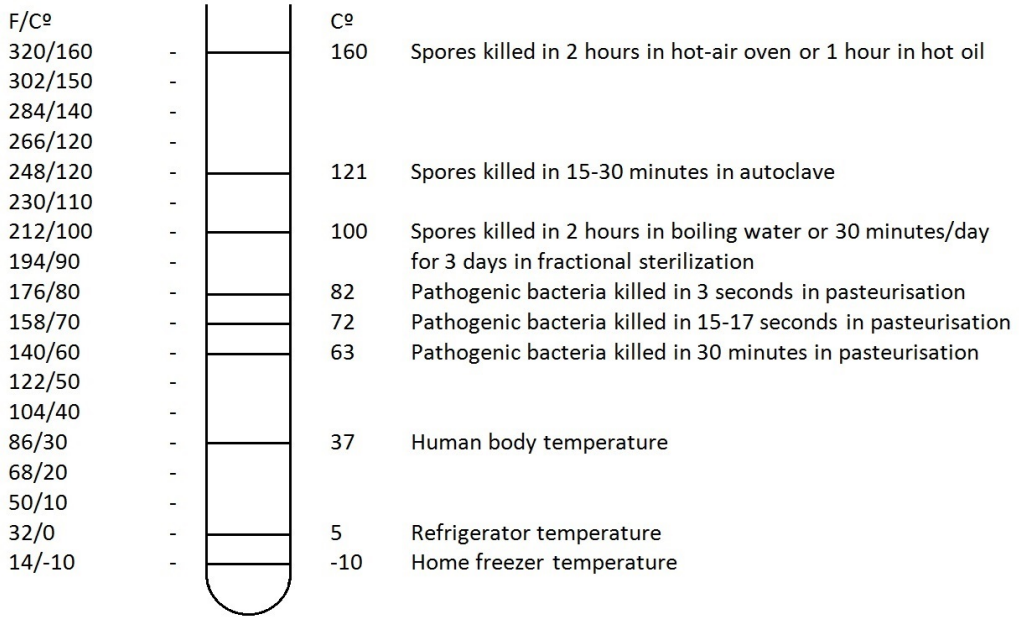

Figure 8.1: Temperature environments used in microorganism control [8].

One of the parameters used to describe a microorganism's resistance to heat is called its D-value. The D-value is a time parameter that indicates how long a batch, which is contaminated with a specific microorganism, must be exposed to a constant temperature to achieve a 90% reduction in its the CFU's (colony forming units) [9].

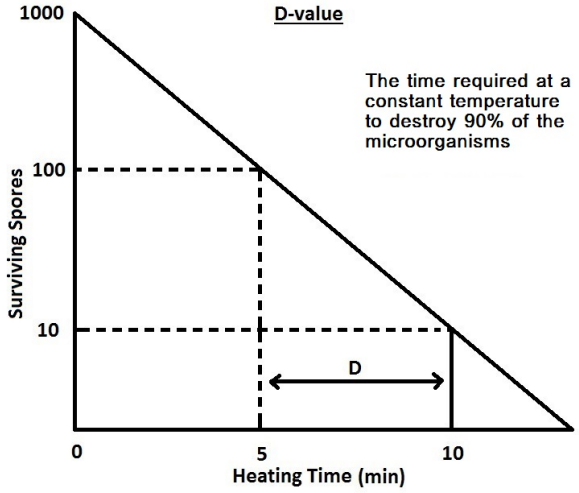

Figure 8.2: The D-value graph [9].

Similarly a Z-value, which is a temperature value, exists. The Z-value indicates the temperature required over a specific time interval to achieve a 90% reduction in microorganism activity. Then looking at the graphs in Figure 8.3 below, if the temperature is increased to 80 $°C$, the sterilisation would be just as effective over a 1 minute time period [9].

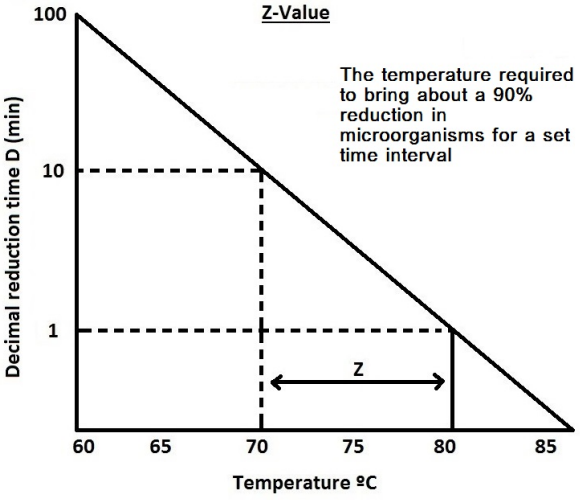

Figure 8.3: The Z-value graph [9].

8.3 Bacterial Reproduction and Growth

Bacteria reproduce by means of an asexual method called binary fission. This process allows the chromosomes to duplicate and separate. The cell wall grows inward at the middle and two new bacteria are formed. This method allows bacteria to never get "old" as new ones are formed at set time intervals. The time interval required for the bacteria to reproduce is unique to specific species of bacteria. Some occur at slow rates, like every 18 hours, and others at fast rates of up to once every 20 minutes in optimal conditions [10].

The duplication causes a logarithmic increase in population. To put this in perspective, if 1 rod of bacteria with a generation time of 20 minutes is placed in an optimal growth medium at 8:00 AM, it would have grown to 1 billion by 6:00 PM that evening. However, optimal growth is seldom possible as the surrounding elements limit the reproduction rate [10].

Figure 8.4 shows the typical effects of external factors on bacterial growth in a lab setup.

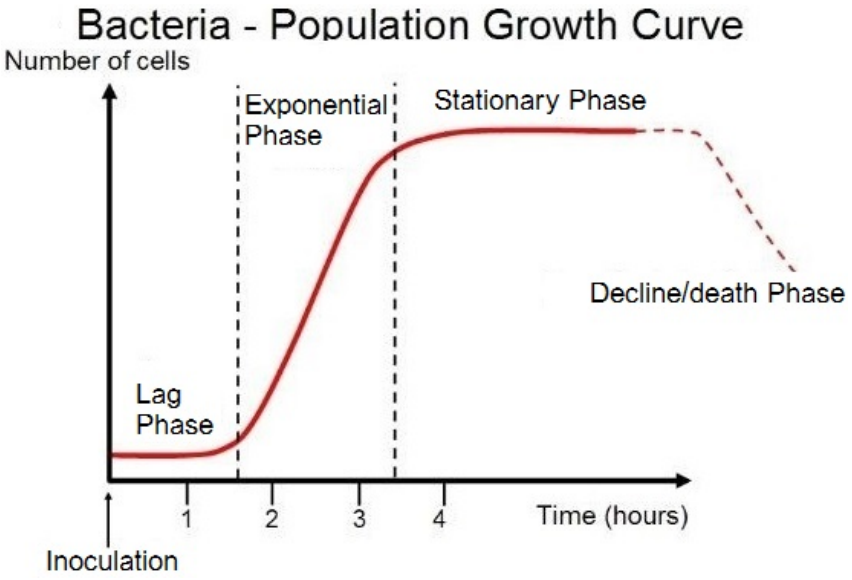

Figure 8.4: Bacterial population growth curve [10].

The lag phase is when the bacteria are initially introduced into the prepared nutrient rich growth medium. The initial shock of transferring and adapting to the new environment causes a halt in growth. The bacteria is also sourcing nutrients and preparing for binary fission [10].

Once reproduction starts, a log increase can be seen as the bacteria thrive in the nutrient rich environment. This can usually be observed in a change in colour of the growth medium, or isolated colonies start to form. Most research on microorganisms is performed during this period [10].

The saturation point is reached when the reproduction rate of the bacteria is the same as the death rate. This is due to an increase in population, which brings about a scarcity in nutrients and the bacteria must compete for resources [10].

The death phase is reached when more cells die than are being generated. This happens as the nutrients become depleted [10].

8.4 Sanitising the Experimental Environment

The Rooibos tea sterilisation and the microbiological tests were performed in two separate locations. The microbiological testing was performed in a laboratory at the Food Science Department and the sterilisation took place in a different laboratory at the Engineering Department. The laboratory at the Food Science Department is constantly being cleaned and kept in a relatively sterile state. The laboratory at the Engineering Department had to be steralised before testing began.

The Rooibos tea sterilisation itself took place in the laboratory where the microwave sterilisation system was built. This is typically not a clean environment and precautions had to be taken to avoid contamination after sterilisation. The microwave applicator itself was thoroughly sprayed with alcohol and wiped with sterile wipes. All working surfaces were washed with bleach and then wiped with alcohol. The container that the tea was placed in during sterilisation was also treated with alcohol and then rinsed in sterilised water. Gloves were worn throughout the procedure. Sterilised samples were directly placed inside the stomacher bag from which the solution series would be made. The bag was sealed with tape and kept closed until the microbiological tests could be performed. Microbiological tests were performed within one day of sterilisation.

Before microbiological tests were performed in the laboratory extra precaution was taken and all working surfaces were wiped down with a 60% alcohol solution. Equipment was sterilised in an autoclave before use. Gloves had to be worn throughout the testing procedure. A bunsen burner was used to work anaerobically, therefore all containers were put over the open flame to remove most of the oxygen before they were sealed.

8.5 Dilution Series

A dilution series can be made to determine the concentration of CFU's in a sample. More diluted samples makes counting the colonies that form on the growth medium easier. The counted colonies can then be worked back directly

to the number of colonies per gram or milliliter in the original sample.

The dilution series made for the tea tests required 10 g of tea and 90 ml of solution. The solution therefore had a concentration of 10^{-1}. Removing 1 ml and adding it to 9 ml of solution would make it a 10^{-2} dilution. Removing 1 ml from the second solution and adding it to 9 ml of solution would make 10^{-3}. This can be continued until the correct dilution range is achieved, as seen in Figure 8.5.

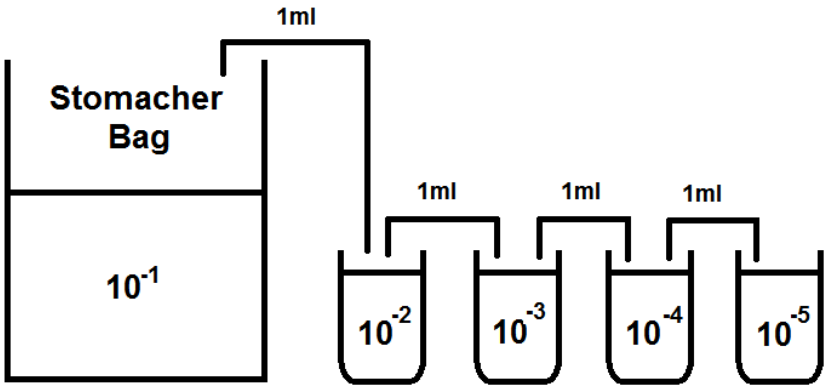

Figure 8.5: Process of making a dilution series.

8.6 Salmonella

Salmonella is one of the most common causes of food poisoning in the world. The bacteria can be found in almost all food types.

8.6.1 Significance of Tests

Salmonella has proven to have a high resistance to drying and once dried it has also shown a high resistance to temperature. These properties make it a problematic contaminant in food processing, especially in dry and semi-dry products.

Symptoms of infection start to show after 12 to 72 hours and may include diarrhoea, fever and abdominal pain. The symptoms usually pass after about 4 to 7 days and a majority of infected individuals recover without treatment

[64]. Several cases have, however, turned out to be fatal and the symptoms should not be taken lightly. Therefore, strict regulations exist world-wide for all food processing [65]. The Rooibos tea standard is no exception, a zero tolerance stance is taken on the presence of Salmonella [12].

8.6.2 Experimental Setup

The experimental setup did not use the final microwave sterilisation system. The Salmonella test was the first to be performed. This test was done differently from the aerobic count and E.Coli/Coliforms tests, as it was used as an initial indication of the viability of microwave sterilisation. The microwave output power of the magnetron was controllable. The Rooibos tea was placed in a sterile glass container on the turntable of the microwave applicator. No further modifications were added. The main aim of this test was to establish what power levels could be used and to get a better idea of the sterilisation potential of microwaves. The setup can be seen in Figure 8.6.

Sterile rooibos tea, doped with Salmonella, was used. Batches of 25 g each were weighed out into sterile bags for each test. The Rooibos standard states that 25 g is the minimum batch size allowed to be sterilised for microbial testing [66]. The tea was placed in a sterile beaker in the middle of the microwave oven. The power levels were chosen to be 600 W, 200 W and 100 W respectively. The tests were run over 2 minutes, where it was paused halfway to be stirred. The temperature was measured using a laser thermometer at the 1 minute mark and the 2 minute mark. After sterilisation the tea was placed in new sterile bags and sealed for microbial testing.

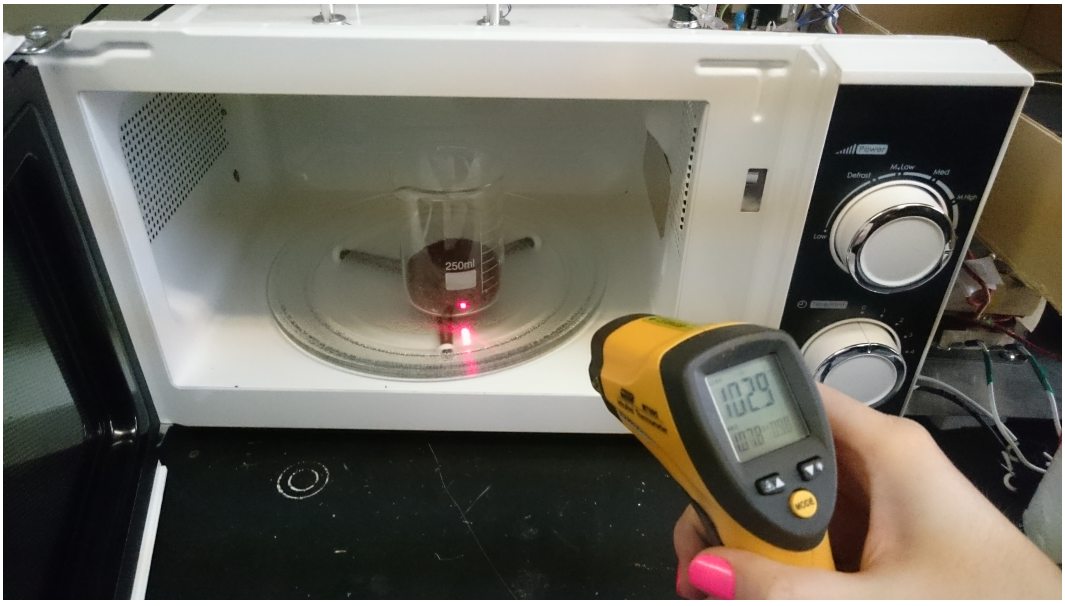

Figure 8.6: Experimental setup for salmonella sterilisation test.

8.6.3 Microbial Testing Methods

The following method was set out by SANS (South African National Standards) as the procedure to follow when testing for Salmonella in food.

8.6.3.1 Principle

The detection of Salmonella requires four stages. It is started by pre-enriching the sample in a non-selective liquid medium. The identified salmonella sample is then enriched in a selective medium. The last two steps require plating out the sample growth, then identifying and confirming the plated bacteria [67].

8.6.3.2 Method

The steps in Table 8.1 were followed to test for the presence of salmonella in the sterilised Rooibos tea samples [67].

Table 8.1: Steps followed to test for the presence of salmonella.

Salmonella Testing Procedure	
Steps	Procedure
1.	225 ml of buffered peptone water was placed in the autoclave for sterilisation. 25 g of contaminated sample was added to the sterile mixture. The mixture was then incubated for 16 to 20 hours at 35 $°C$.
2.	10 ml of salmonella enrichment broth was prepared, as indicated by the manufacturer, for each test sample.
3.	0.1 ml of the pre-enriched sample was transferred into a test tube containing 10 ml of salmonella enrichment broth. The solution was then incubate at 42 $°C$ for 24 hours.
4.	The surface of a pre-dried agar plate was inoculate using the cultures obtained from salmonella enriched broth, after incubation for 24 hours.
5.	The plate was then inverted and incubate at 35 $°C$ for 20 to 24 hours.
6.	After incubation, the plates were examined for typical colonies of Salmonella. If growth was slight and no typical colonies were present, the sample was incubated for another 24 hours.
7.	The typical colonies obtained in the steps above was streaked out onto plates of nutrient agar and incubate at 35 $°C$ for 24 hours.
8.	These colonies were used to confirm and identify the Salmonella present in the sample.

8.6.4 Results

A photo of the salmonella agar plates can be seen in Appendix C. The results are summarised in Table 8.2. (Note that the microbiological tests were performed in duplicate to ensure the reliability of the results. Batch "A" and "B" are therefore from the same sterilisation sample, but different agar plates.)

Table 8.2: Salmonella test results.

Power	Batch	1 min Temperature (°C)	2 min Temperature (°C)	Salmonella	Total CFU's
600 W	A	96	103	None	200
	B	98	105	None	0
200 W	A	88	104	None	0
	B	90	104	None	300
100 W	A	86	105	None	100
	B	88	103	None	0

This test was not done with the final system and it was only used as an initial indicator. The test was performed with a microwave system that was built for another purpose, therefore the tea was not constantly mixed and high temperatures were reached in the mass of stationary tea. The tea used in this experiment was already sterile and only doped with salmonella. Therefore the amount of CFU's were expected to be very low, since the tea has already been treated with steam.

Table 8.2 indicates that the recorded temperatures at 1 min and 2 min were all relatively similar for the different power levels and no salmonella was found after sterilisation. As an initial test, this was seen as a positive result. No salmonella colonies were growing on the agar plates after incubation, as can be seen in the agar plates shown in Figure C.1. These results also indicated that sufficiently high temperatures could be achieved with much lower microwave output power levels. This influenced design decisions for the final tea sterilisation system as well as triggering an interest in the "non-thermal" effects of microwave irradiation.

8.7 Aerobic Plate Count and Coliforms

Sterilisation tests were done on untreated Rooibos tea with the developed microwave sterilisation system. The aerobic plate count and E.Coli/Coliforms were tested for in these treated samples. The significance of doing the tests, experimental setup, microbial methods and results are discussed in this section.

8.7.1 Significance of Tests

The aerobic plate count, also called the total viable count (TVC), is an indicator of bacterial growth in a sample. Coliform bacteria are found in the digestive tract of all mammals and is therefore an indicator of fecal pollution.

8.7.1.1 Aerobic Plate Count

The test does not represent the entire bacterial population of the sample. The test is a non-specific indicator of the organisms in the sample that grow aerobically (require oxygen) at mesophilic temperatures (25 - 40 °C). The test can therefore not be used to identify specific types of bacteria. The test is, however, very useful to indicate unhygienic practices in processing and predicted shelf life of a product. Note that there is no correlation between the TVC numbers and pathogenic activity. A low TVC does not necessarily mean that the food is safe for consumption [68].

The interpretation of TVC numbers requires knowledge of the product. For example, products that have undergone fermentation is known to have high counts. Raw farm products are also known to have varying counts for different samples. The test can therefore be seen as a good indication of bacterial activity, which might be interpreted as a "red flag" in food processing. Further screening of the bacteria must be done to identify the safety of the food [68].

8.7.1.2 E.Coli/Coliform Plate Count

This strand of bacteria has the ability to survive for extended periods of time in an outdoors environment. The majority of these bacteria are harmless, but some strands can cause diarrhoea and even kidney failure. This can prove fatal. Strict regulations on Coliform counts are put in place for food and water processing to prevent human consumption. Escherchia Coli (E.Coli) is the most important indicator in the Coliform group and is commonly used as a sign of contamination [69].

8.7.2 Experimental Setup

The tests for TVC and E.Coli/Coliforms were done using the microwave sterilisation system with modifications as discussed in Subsection 5.2. The microwave power was therefore accurately controlled, a mode stirrer was implemented with the tea mixer and the temperature was measured throughout.

Each test was done by putting 25 g of Rooibos tea in the mixer. The microwave power levels and the exposure time were varied for each test. After a test was performed, the sample was placed in a sterile stomacher bag and sealed. The microwave applicator was cleaned with alcohol between sequential sterilisation tests. The microbial testing was done within 24 hours after the sterilisation test took place. The tea used was unsterilized, straight from the fermentation heap with no doping or tampering.

8.7.3 Microbial Testing Methods

The TVC and E.Coli/Coliforms testing for this project was simplified and sped up by making use of 3M Petrifilm. The 3M Pertifilm method excludes the preparation of the growth medium for the tested bacteria. This leaves a simple set of steps to be completed for testing, which does not only cut down lab work but also reduces the margin for error. The procedure for both tests are listed in Table 8.3 [70].

Table 8.3: Steps followed to perform 3M petrifilm E.Coli and TVC tests.

3M Petrifilm Method	
Steps	Procedure
1.	A test sample was added to a stomacher bag with sterilised salt water to make a 10% dilution.
2.	A stomacher machine was used to ensure that the solution was mixed evenly, the result of which can be seen in Figure 8.8.
3.	A dilution series was created depending on the amount of microbial growth expected, as shown in Figure 8.8.
4.	The 3M petrifilm was placed on a flat surface and 1 ml of the dilution was put onto the film.
5.	The film was gently closed, ensuring that the solution did not slide off the film or trap any air bubbles.
6.	The 3M spreader was used to gently spread the solution across the film, as instructed.
7.	The pertifilm was placed in an incubator for the specified time, depending on the test performed.
8.	The CFU's were counted after incubation and worked back to the amount per gram from the dilution.
9.	Further analysis could then be done by examining isolated colonies.

Figure 8.7: Initial dilution in stomacher bag after mixing.

Figure 8.8: Dilution series from 10^{-2} to 10^{-4}.

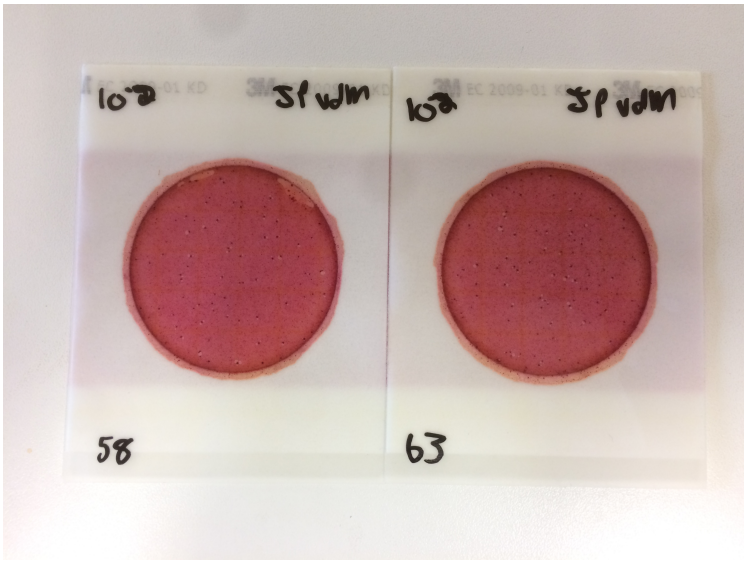

Figure 8.9: 3M Petrifilm with 10^{-2} dilution for coliforms.

For E.Coli/Coliforms, seen in Figure 8.9, all specks with bubbles around it were counted.

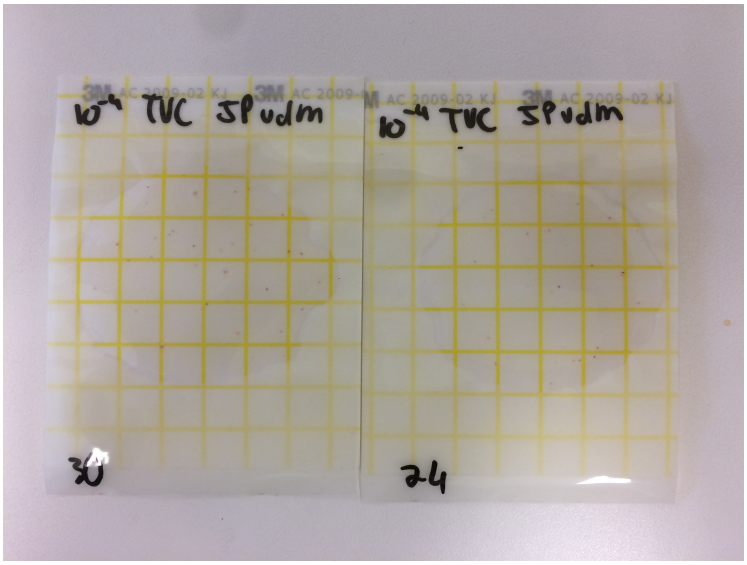

Figure 8.10: 3M Petrifilm with 10^{-3} dilution for TVC's.

For the TVC, seen in Figure 8.10, all pink dots were counted.

8.7.4 Results

All of the tests were performed with the experimental setup and 3M petrifilm method described in Subsection 8.7.3. (Note that TMC stands for "Too Many to Count" in all the tables in this section.)

8.7.4.1 Range of Dilution Series

Before any sterilisation tests could be performed, the level of microbial activity in the sample had to be determined. The Rooibos tea was put into a dilution series ending at 10^{-5}. The dilution series was plated out in duplicate to ensure the reliability of the result.

The CFU's for the TVC was considered countable at a dilution of 10^{-4}, therefore all further series were diluted up to this point. The E.Coli/Coliforms tests showed that a dilution of 10^{-3} would be sufficient to determine the Coliform activity. Tables 8.4 and 8.5 show the CFU counts of unsterilised Rooibos tea for TVC and E.Coli/Coliforms respectively.

Table 8.4: Raw data for TVC dilution series range test.

TVC Control Series			
Dilution	Set 1	Set 2	Average
10^2	TMC	TMC	TMC
10^3	420	380	400.0
10^4	67	44	55.5
10^5	6	4	5.0

Table 8.5: Raw data for E.Coli/Coliforms dilution series range test.

E.Coli/Coliforms Control Series			
Dilution	Set 1	Set 2	Average
10^2	58	63	60.5
10^3	9	7	8.0

8.7.4.2 Sterilisation Test 1

The Rooibos tea was irradiated at three different power levels for 5 minutes at a time. The power level was controlled instead of the temperature, since this would be the figure of merit should any "not-thermal" effects have been observed.

The salmonella test revealed that 150 W was sufficient to sterilise and was therefore used as the maximum output power in Test 1. The other two microwave output power levels were chosen to evenly split the power range into 50 W intervals. Therefore, the power levels used was 150 W, 100 W and 50 W. The microwave output power and temperature measurements taken during the tests are shown in Figures 8.11 and 8.12. The data for both the TVC and the E.Coli/Coliform counts are represented in Tables 8.6 and 8.7.

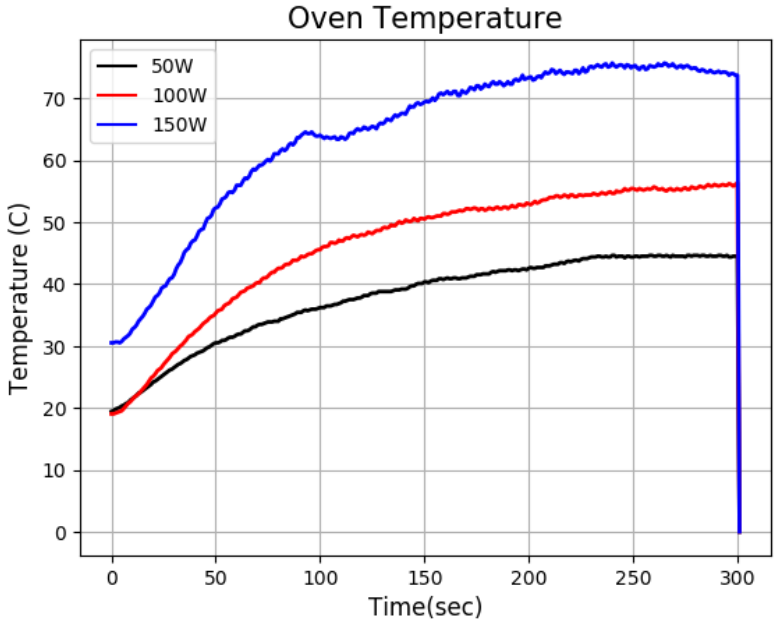

Figure 8.11: Temperature profiles for sterilisation Test 1.

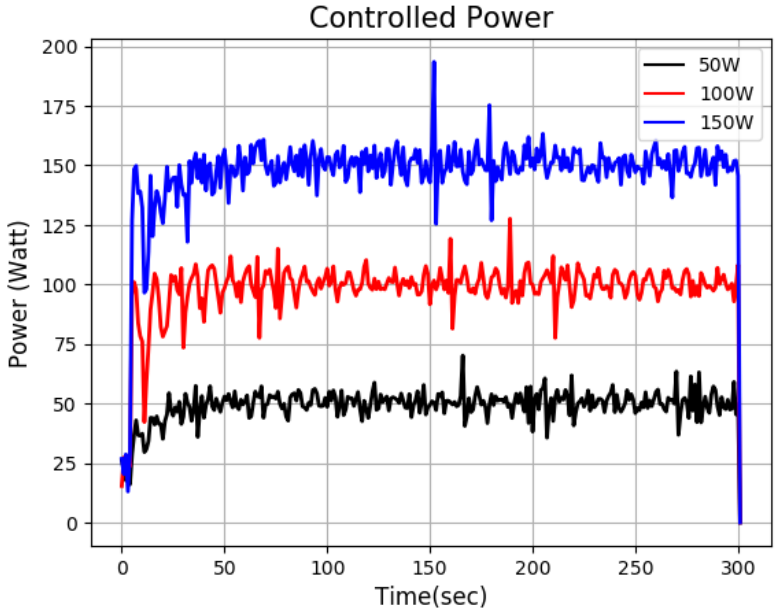

Figure 8.12: Controlled microwave output power for sterilisation Test 1.

Table 8.6: First sterilisation test results for TVC's.

TVC's after 5 min				
Power Level	Dilution	Set 1	Set 2	Average
Control	10^3	180*	186*	183.0
	10^4	19	14	16.5
50 Watt	10^3	TMC	TMC	TMC
	10^4	36	32	34.0
100 Watt	10^3	TMC	TMC	TMC
	10^4	41	33	37.0
150 Watt	10^3	TMC	TMC	TMC
	10^4	10	15	12.5

Table 8.7: First sterilisation test results for E.Coli/Coliforms counts.

E.Coli/Coliforms after 5 min				
Power Level	Dilution	Set 1	Set 2	Average
Control	10^2	20	29	24.5
	10^3	5	4	4.5
50 Watt	10^2	52	44	48.0
	10^3	17	18	17.5
100 Watt	10^2	23	24	23.5
	10^3	4	5	4.5
150 Watt	10^2	9	10	9.5
	10^3	2	3	2.5

The results showed that, for the 100 W and 50 W tests, the microbial activity was higher in the treated samples than the control series. Therefore no signs of sterilisation were seen in sterilisation Test 1. The 150 W test had the lowest microbial activity, but it was still within the same range as the control series. This could be due to the short exposure time and the low temperatures used to try and sterilise the Rooibos tea.

8.7.4.3 Sterilisation Test 2

The first set of tests showed that the lower power levels were not successful in sterilising the Rooibos tea. The second set of sterilisation tests were then set up to still use 150 W but increase the exposure time to 10 min and 20 min respectively. The rest of the experimental setup was kept exactly the same as before. Only one temperature and one power profile is displayed in Figures 8.13 and 8.14, because both tests were done at the same power level. The sample irradiated for 10 min reached a maximum temperature of 101.32 $°C$, where the sample irradiated for 20 min reached 116.86 $°C$.

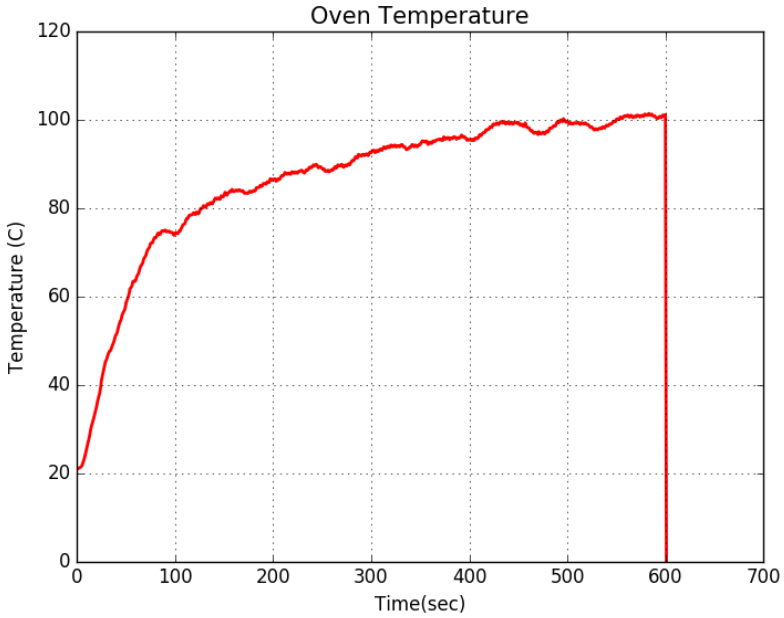

Figure 8.13: Temperature profile for sterilisation Test 2.

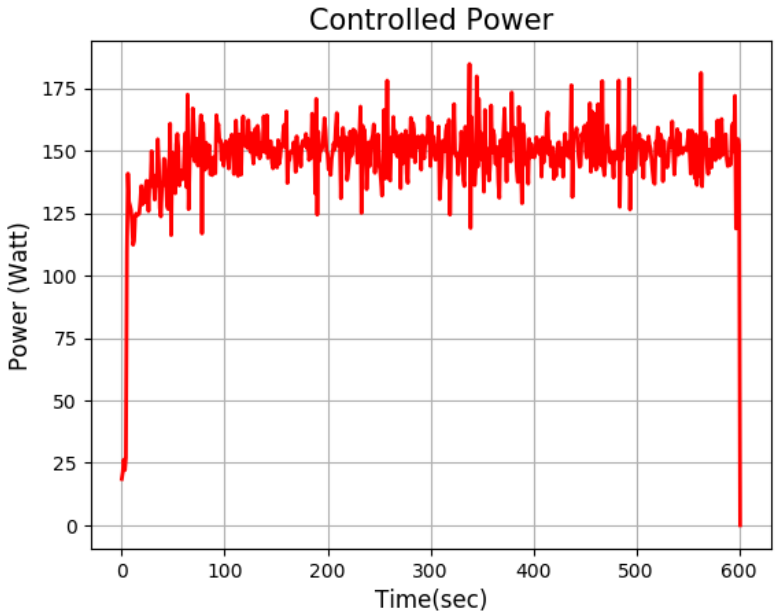

Figure 8.14: Controlled microwave output power profile for sterilisation Test 2.

Table 8.8: Second sterilisation test for TVC's.

TVC's at 150 Watt				
Exposure Time	Dilution	Set 1	Set 2	Average
Control	10^2	TMC	TMC	TMC
	10^3	210	195	TMC
	10^4	14	12	13.0
10 min	10^2	TMC	TMC	TMC
	10^3	TMC	TMC	TMC
	10^4	69	64	66.5
20 min	10^2	TMC	TMC	TMC
	10^3	86	89	87.5
	10^4	5	4	4.5

Table 8.9: Second sterilisation test for E.Coli/Coliforms counts.

E.Coli/Coliforms at 150 Watt				
Exposure Time	Dilution	Set 1	Set 2	Average
Control	10^2	31	36	33.5
	10^3	9	12	10.5
10 min	10^2	58	71	64.5
	10^3	18	18	18.0
20 min	10^2	9	26	17.5
	10^3	2	5	3.5

The range of temperatures reached and the time of exposure should have resulted in effective sterilisation of most microorganisms. These temperatures are similar to those of steam sterilisation, but with a longer exposure time. Looking at the raw data of the results obtained from the second sterilisation test in Tables 8.8 and 8.9, it is clear that there were varying amounts of microorganisms in the different batches.

The batch of Rooibos tea irradiated at 150 W for 10 min in sterilisation Test 2 had the highest count rate recorded with the sterilisation tests thus far. None of the untreated control sets showed counts this high. All the previously treated samples had lower counts than this sample, even though it was treated with the highest temperature up to this point. This can be observed in both the TVC values and the E.Coli/Coliform counts. This brings up the issue of batching, a known problem with raw farm products that come into contact with a variety of contamination sources during processing [71].

8.7.4.4 Sterilisation Test 3

In order to confirm that the problem was indeed a batching problem, sterilisation Test 2 was repeated. However, for this iteration, enough tea was sterilised to make five batches. Five batches for each test would be enough to statistically identify a batching problem or rule out the suspicion that this might have been the problem. Therefore 50 g of dry tea was required to make 5 dilution

series, the tea was sterilised in two batches of 25 g for 10 min and again in two batches of 25 g for 20 min. This was to keep the dosage of microwave irradiation the same as in sterilisation Test 2.

Table 8.10: Third sterilisation test results for TVC's

TVC's at 150 Watt							
Exposure Time	Dilution	Batch 1	Batch 2	Batch 3	Batch 4	Batch 5	Average
Control	10^3	160	240	320	200	440	272.0
	10^4	15	23	40	17	98	38.0
10 min	10^3	230	150	200	160	210	190.0
	10^4	15	15	22	14	12	15.6
20 min	10^3	44	59	194	91	35	84.6
	10^4	4	7	32	4	4	10.2

Table 8.11: Third sterilisation test results for E.Coli/Coliforms

E.Coli/Coliforms Count at 150 Watt							
Exposure Time	Dilution	Batch 1	Batch 2	Batch 3	Batch 4	Batch 5	Average
Control	10^2	40	40	30	39	33	36.4
	10^3	6	7	6	8	29	11.2
10 min	10^2	34	29	46	8	2	23.8
	10^3	2	2	25	2	1	6.4
20 min	10^2	14	38	32	30	23	27.4
	10^3	2	3	8	6	4	4.6

The sterilised tea was then recombined into bags for the 10 min, 20 min and the control tests. Each bag had 50 g of tea and was mixed again before the 10 g samples were weighed out to make the dilution series for each batch. Therefore, five separate dilution series were made for the control, 10 min exposure time and 20 min exposure time. Each 10 g sample of Rooibos tea is referred

to as a batch in Tables 8.10 and 8.11.

The dilution series for each of these tests was not plated out into duplicate agar sets, because the results have proven to be reliable. For a large scale test like this it also helped to cut down on lab work. The sterilisation temperature and power profiles remained the same as in sterilisation Test 2.

The results in Tables 8.10 and 8.11 show at least one outlier in each of the test variations. Batches 3 and 5 of the control series for TVC's showed significantly higher counts than the rest of the batches. Similarly, for the 10 min and the 20 min tests, Batch 3 was higher in both the TVC and for the E.Coli/Coliform count. The results for the control series were also higher than the previous control series. This might have been due to the tea being thoroughly mixed before the samples were selected.

This test shows that a batching problem was definitely present with the Rooibos tea samples used for testing and that it must be taken into account with any further testing.

8.8 Analysis of Test Results

This section will provide further insight and analysis of the observations made during all the sterilisation tests performed in this section.

8.8.1 Salmonella Test

The salmonella tests that were performed gave a successful outcome. All three power levels that were tested managed to eliminate the presence of salmonella. The number of other CFU's that was still present after sterilisation was also very low. This was to be expected, since the tea was sterilised before doping it with salmonella. This result triggered the interest in the so called "non-thermal" effects of microwave sterilisation, since the salmonella was eliminated at such low power levels.

8.8.2 Aerobic Plate Count and E.Coli/Coliform Tests

The problem of batching was identified when the untreated Rooibos tea was used in the sterilisation tests. Since Rooibos tea undergoes fermentation in an open air environment there are a large variety of possible contamination sources. Both the fermentation and open air environment contributes to the batching problem [12].

A summary of all the control series used during the sterilisation tests is shown in Figure 8.15, where the red bars indicate TVC at a concentration of $10^4\ CFU \cdot g^{-1}$ and the blue bars indicate E.Coli/Coliforms at a concentration of $10^2\ CFU \cdot g^{-1}$. The figure shows how there were different concentrations of microorganisms in each batch of Rooibos tea and that a number of batches had to be tested in order to make a proper statistical evaluation of the CFU's in a large batch of tea.

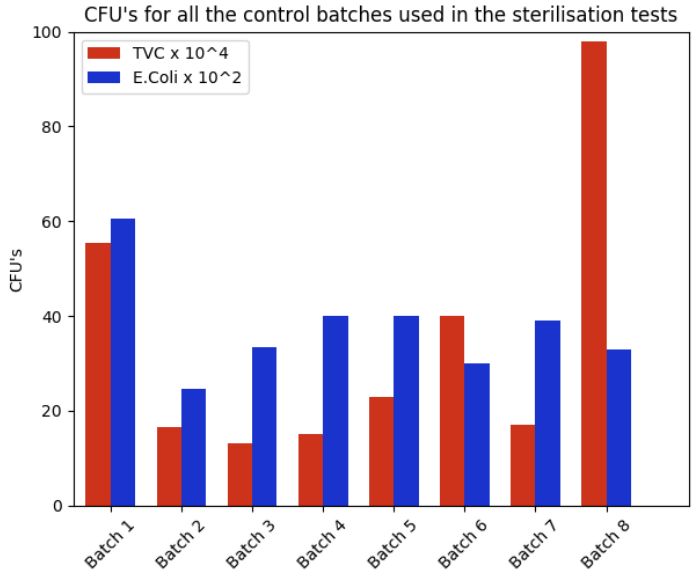

Figure 8.15: Microbiological tests for TVC and E.Coli/Coliforms on eight different untreated Rooibos tea samples.

The effect of varying exposure times to microwave irradiation is summarised in Figure 8.16. The values were determined by averaging all the data gathered from the sterilisation tests and averaging the results. Therefore the 5 min

average only consists of one batch, where the 10 min and 20 min values are averages of six different batches. All of the batches were irradiated at 150 W.

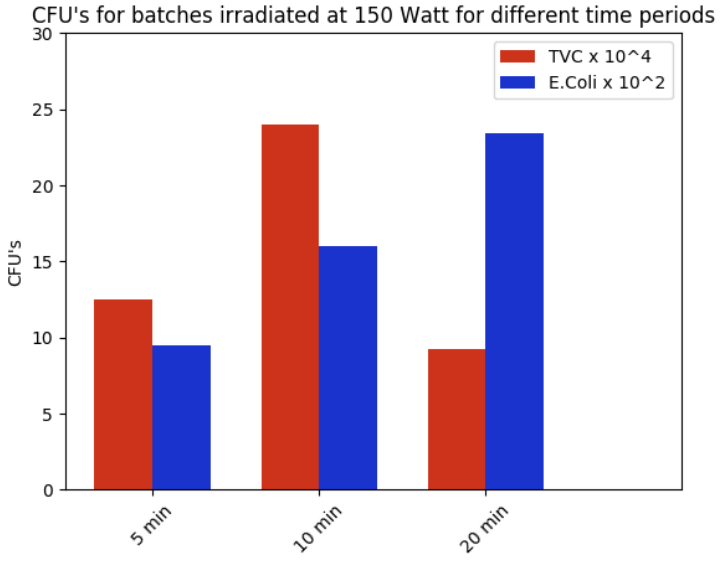

Figure 8.16: Average TVC and E.Coli/Coliforms for varying microwave exposure times.

The average values in Figure 8.16 seem to be the opposite of what was expected from the sterilisation tests. The shortest exposure time had the lowest CFU values and the longer exposure times showed higher values. The TVC for 20 min exposure time was the only value that behaved as expected.

The individual batches of all the sterilisation tests, where Rooibos tea was irradiated at 150 W for 10 min and 20 min, are plotted in Figures 8.17 and Figure 8.18 respectively. These figures give a better evaluation of the sterilisation effect that microwave irradiation had on the Rooibos tea samples.

The TVC values for the control series in Figure 8.15 vary between 130 000 $CFU \cdot g^{-1}$ and 400 000 $CFU \cdot g^{-1}$, if the outliers are removed. Figure 8.17 shows that these values reduced to between 220 000 $CFU \cdot g^{-1}$ and 120 000 $CFU \cdot g^{-1}$, if the outlier is removed. Finally, Figure 8.18 shows that these values have further reduced to between 70 000 $CFU \cdot g^{-1}$ and 40 000 $CFU \cdot g^{-1}$, if the outlier is removed. This is a positive result as the South African Rooibos standard requires the TVC to be below 75 000 $CFU \cdot g^{-1}$ [12].

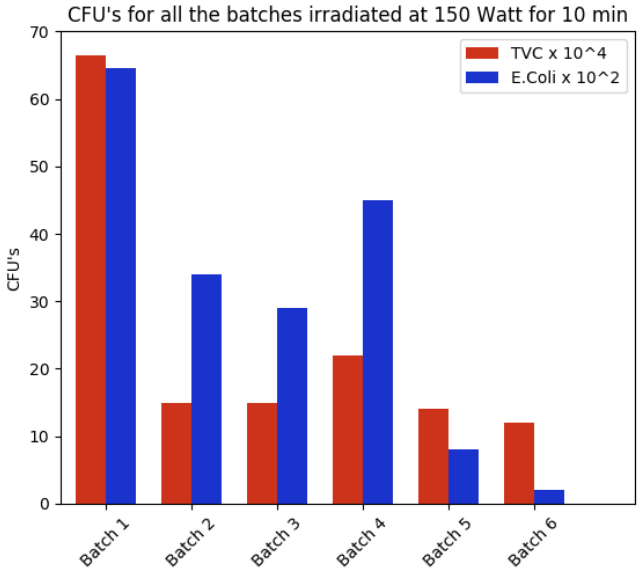

Figure 8.17: All the TVC and E.Coli/Coliforms test results for a 10 minute exposure time at 150 W.

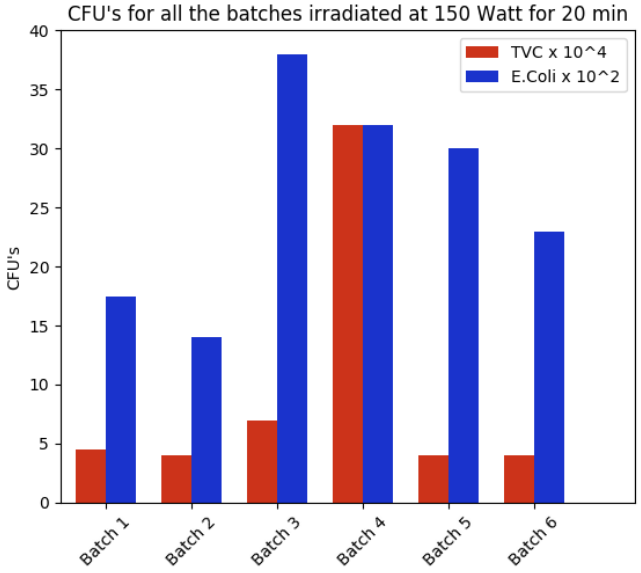

Figure 8.18: MAll the TVC and E.Coli/Coliforms test results for a 20 minute exposure time at 150 W.

The sterilisation effect on E.Coli/Coliforms was not as effective. The control series in Figure 8.15 vary between 4000 $CFU \cdot g^{-1}$ and 2450 $CFU \cdot g^{-1}$,

if the outlier is removed. Figure 8.17 shows that these values vary between 4500 $CFU \cdot g^{-1}$ and 200 $CFU \cdot g^{-1}$, if the outlier is removed. Finally, Figure 8.18 shows that these values remain between 3800 $CFU \cdot g^{-1}$ and 1400 $CFU \cdot g^{-1}$, with no outliers. The sterilisation result does not comply with the South African Rooibos standard, where an E.Coli/Coliforms count below 20 $CFU \cdot g^{-1}$ is required [12].

The results made it clear that more tests must be performed with the microwave sterilisation system. The TVC's have shown a clear drop after 20 min exposure at 150 W, these count values will most probably decrease even more with extended exposure time or increased microwave power levels.

The E.Coli/Coliform tests give rise to an interesting microbiology problem, where a heat resistant microorganism is present in the Rooibos tea samples. A solution must be found where a clear drop in CFU values can be observed. This can be done by plating out the microorganisms present after sterilisation and identifying them. This would give an indication of the D-value or Z-value associated with the microorganisms and the microwave system can be adjusted to meet this power and temperature demand to sterilise these microorganisms.

8.8.3 Non-thermal effects

The "non-thermal" effects described in Chapter 2.5 was one of the points of interest in the microbiological testing. Chapter 2.5 states that the "non-thermal" effects are in fact all thermal in nature. The reviewed "non-thermal" model uses the term "bulk temperature" for conventional heat and "instantaneous temperature" for the heat generated at molecular level, due to the fast reorientation of the polar molecules. This "instantaneous temperature" is used to explain why some studies have shown that microwave sterilisation works better than conventional heating.

The sterilisation tests performed in this chapter were done at low power levels. This reduced the temperature gradient and prevented the Rooibos tea from burning. The "bulk temperatures" reached in the Rooibos tea samples during irradiation was still sufficient for sterilisation. The results did not produce any surprisingly effective sterilisation, which can only be explained by the "instan-

taneous temperature" generated with microwave heating. Therefore, no signs of "non-thermal" effects were recorded during these tests.

8.9 Chapter Conclusion

This chapter showed that the microwave sterilisation system worked. The initial salmonella tests were successful. The TVC values were below the required limit, as set out by the South African Rooibos standard. However, the system was not as effective as it could be. Further sterilisation tests must be performed to find the required microwave power and temperature profiles to eliminate E.Coli/Coliforms.

No signs of "non-thermal" effects were observed during testing. The chapter also pointed out the importance of working with multiple batches of Rooibos tea when conducting microbiological testing. Finally, the microbiological testing was time consuming, as it took 72 hours to get the results for a sterilisation test. This chapter is therefore a good foundation to work from, for any further microwave sterilisation tests performed on Rooibos tea.

Chapter 9

Conclusion

This chapter will revisit the objectives, laid out in Chapter 1, and discuss the outcomes of each objective. The discussion will highlight the parts of the objective that worked well and the areas that can be improved on. The insights gained into the various fields of study during this project will also be highlighted.

9.1 Microwave Sterilisation System

The main objective of this project was to build a microwave sterilisation system from readily available domestic microwave oven parts. In order to achieve this objective, an accurate magnetron output power control strategy had to be implemented. The second important component was to measure the internal temperature of the microwave applicator. Having accurate power control and temperature measurements allowed for reliable scientific research to be performed using the microwave sterilisation system.

All of the stated requirements in the main objective was met. A microwave sterilisation system was developed from domestic microwave oven parts. A microwave output power controller was developed to reliably control the microwave power delivered to the applicator. Custom hardware had to be developed to achieve this outcome. A magnetron power supply, that can cope with the fast switching speeds of the TRIAC controller, had to be designed. The PT100 was implemented to measure the internal temperature of the microwave applicator. A software package was developed to control the microwave steril-

isation system. The software package combined the controller software with a graphical user interface to easily change system settings as well as monitor all the power and temperature waveforms in real time.

9.2 Rooibos Tea Sterilisation

The second objective was to ensure that the microwave sterilisation system is specifically suited for Rooibos tea sterilisation. This required the system to be able to cope with a relatively dry load, which has an effect on microwave power control as well as ensuring that the tea does not burn. The small scale setup had to be capable of sterilising at least 25 g of Rooibos tea at a time.

A tea mixer made of glass and Teflon was built and installed inside the microwave applicator. The effects of the changes made in the applicator was investigated to ensure that the majority of the microwave power was applied to the Rooibos tea. The effects of a dry load, such as tea, was investigated and the control system was designed to compensate for the resulting microwave power reflections. A fast spinning mode stirrer was installed, reducing the heating time constant, to ensure that the Rooibos tea does not burn. The second objective was therefore achieved as the system changes allowed the irradiation of Rooibos tea for extended periods of time.

9.3 Sterilisation Tests

The final evaluation of the system required testing the sterilisation effect it has on Rooibos tea. This was done by following standard microbial testing procedures to evaluate the TVC and E.Coli/Coliform counts for a batch of Rooibos tea. These counts were compared to the maximum allowable CFU values set out in the South African Rooibos standard to evaluate its effectiveness.

The microwave sterilisation system was able to sterilise salmonella in its initial testing phase. The final system was able to successfully reduce the TVC to adhere to the South African Rooibos tea standard. The E.Coli/Coliform counts were not below the maximum allowable microbial count as set out by the South African Rooibos standard. Therefore, it cannot be conclusively stated

that the microwave sterilisation system works on Rooibos tea. Further testing is required to adjust the system to successfully sterilise Rooibos tea, so that it adhere to all the needed requirements. The result did however raise questions about the nature of Rooibos tea sterilisation and gave valuable insight into the batching problem experienced with raw farm products. This study provides a good foundation for further work on microwave sterilisation of Rooibos tea.

Chapter 10

Recommendations

This chapter discusses improvements that can be made to the existing microwave sterilisation system. The sections are broken up into the major topics covered in the project to put the suggestions in context. The recommendations are meant to round off some of the work that was done in this project, but also to lead the project to new research topics.

10.1 Hardware

Possible microwave output power and temperature measurement improvements will be discussed below.

10.1.1 Increase Microwave Output Power

The microwave sterilisation system had a maximum microwave output power of 200 W. This output power limit can easily be adapted by changing the high voltage capacitor in the voltage doubler circuit of the magnetron power supply. The 200 W power limit was very conservative and the system has the capability of running at a higher microwave output power. An increased microwave power level would allow for more variations and possibly better results in the sterilisation tests.

10.1.2 Temperature Measurement

The temperature reading inside the microwave applicator was done with a PT100. The metal probe used for the reading introduced a concentrated e-field

into the Rooibos tea sample. Using an infrared thermometer to measure the temperature can possibly be a better solution inside a microwave applicator.

10.2 Software

Possible simulation and control software changes will be discussed below.

10.2.1 LTSpice Model

The LT-Spice model that was developed worked well for the snubber circuit design and evaluating voltage waveforms in the system. However, the model can be improved by using a transformer model that simulates the effect of a saturating core. The current and high voltage waveforms can be improved to represent the measured values more closely.

10.2.2 Controller

The microwave control dashboard interfaces with three separate Arduinos to get all its inputs and timing correct. This can be improved by making use of a more powerful microcontroller. Using a raspberry pi would be a better solution as its clock speed is 2 GHz compared to the 16 MHz of the Arduino. Making use of better external ADCs and computing the power values directly on the processor will not only make it easier to interface with the GUI, but also improve the response time of the microwave output power control.

10.2.3 Types of Microwave Power Control

The microwave sterilisation system only made use of continuous power control. A feature can be added to the controller software to pulse the microwave power. The power delivered by each pulse can then also be set and controlled. This feature would offer possible alternative solutions to the sterilisation tests.

10.3 Microwave Applicator

Possible improvements on the tea mixer will be discussed below.

10.3.1 Tea Mixer

The tea mixer can be improved by making use of more robust materials in a smart configuration that automatically mixes the tea. Glass is fragile and continuous removal of the glass tube for sterilisation, between consecutive tests, is risky. Teflon has shown to be the best material to use inside the microwave applicator. The best solution would then be to build a tea mixer entirely from Teflon.

10.4 Sterilisation Tests

Variations on possible sterilisation tests will be discussed below.

10.4.1 Microwave vs Steam Sterilisation

Further work can be done by using the microwave sterilisation system that was developed in this project. Continuing from the sterilisation tests that were performed, the microwave output power used in sterilisation Test 3 must be increased until more effective sterilisation is observed. The same batch of Rooibos tea can then be sterilised using steam and microwave irradiation. The results will show which method is more effective whether if the batching problem persists for both methods.

10.4.2 Sterilise Specifically Doped Rooibos Tea

The microorganisms that were not successfully sterilised by the microwave sterilisation system can be isolated and identified. Sterilised tea can then be doped with these specific microorganisms and irradiated using different microwave power control methods until a solution is found to the sterilisation problem.

10.5 Non-thermal Effect

The microwave sterilisation system can be modified to perform tests to specifically address the topic of "non-thermal" effects. This can be done by developing

a conventional oven that has accurate temperature control and saves its temperature profiles to a file. The modified microwave sterilisation system can use the saved temperature profile of the conventional oven as the input to the temperature controller of the microwave sterilisation system. The reference temperature of the microwave sterilisation system will then follow the same temperature gradient as the conventional heating system. Comparing the sterilisation effects of the microwave system to the conventional heating system, while both follow the same temperature gradient, should offer great insight into the "non-thermal" effects of microwave heating.

Appendices

Appendix A

PCB Layouts

A.1 TRIAC

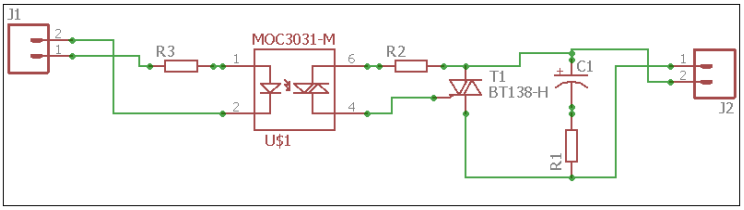

Figure A.1: The schematic for the TRIAC light dimmer circuit.

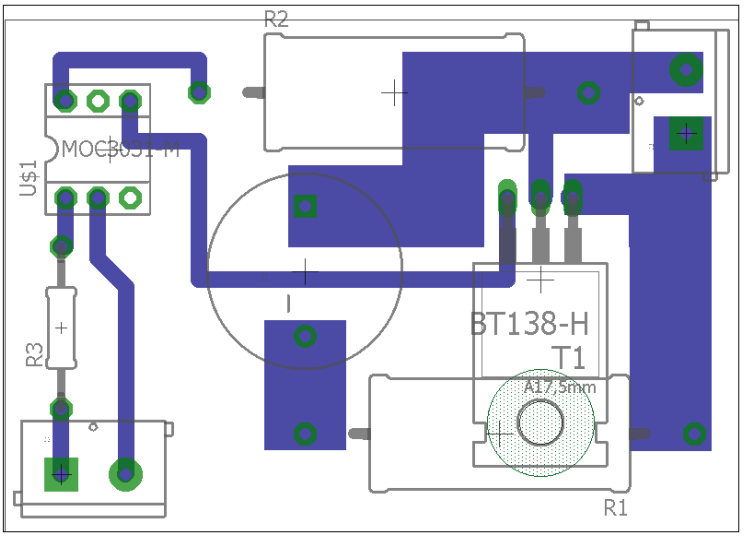

Figure A.2: The PCB for the TRIAC light dimmer circuit.

A.2 Zero-Crossing

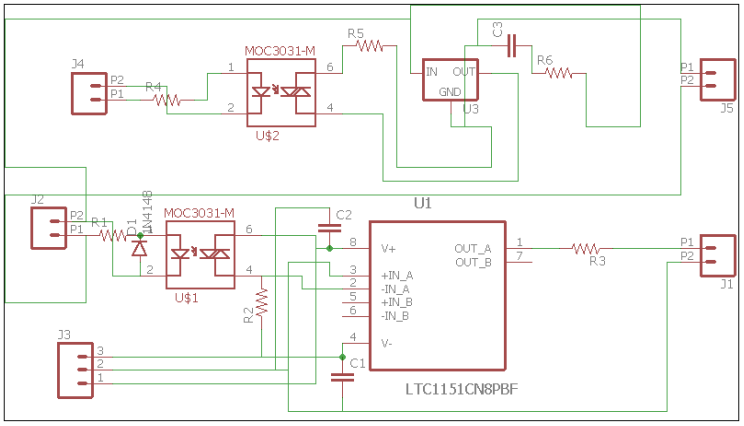

Figure A.3: The schematic for the zero-crossing detection circuit.

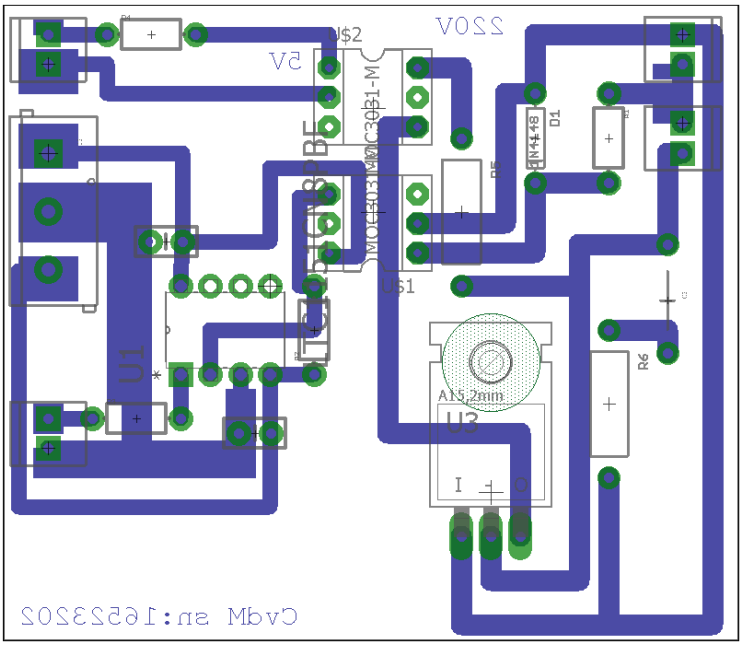

Figure A.4: The PCB for the zero-crossing detection circuit.

A.3 Temperature Probe

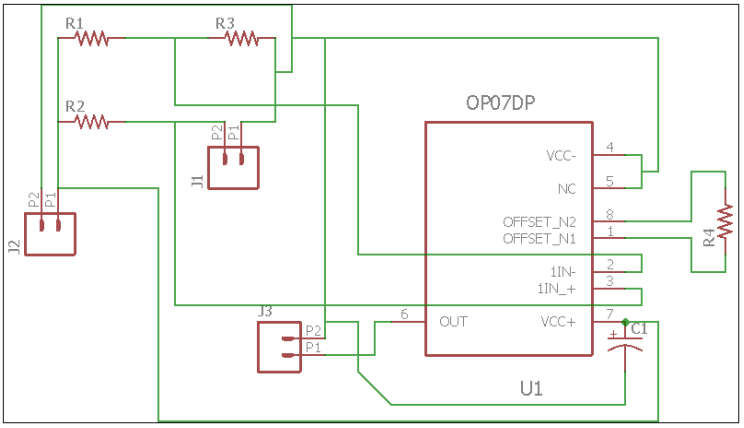

Figure A.5: The schematic for the temperature measurement circuit.

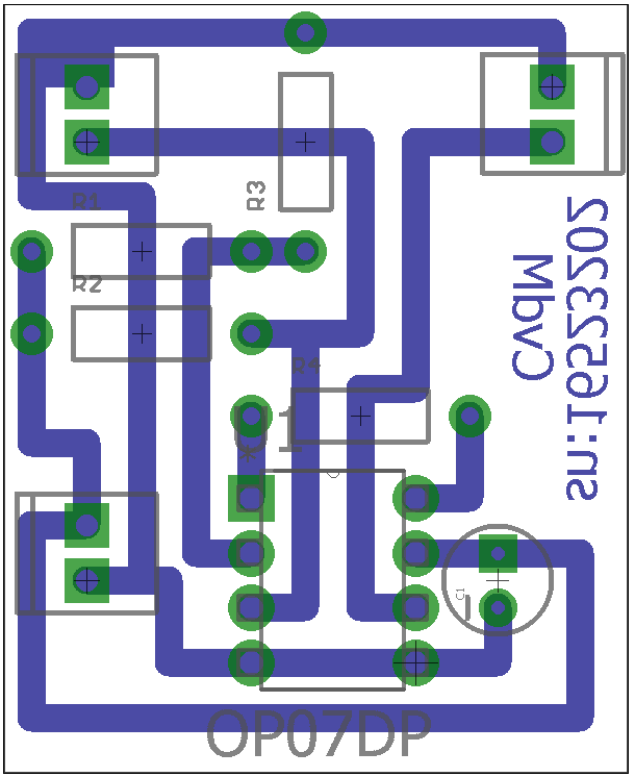

Figure A.6: The PCB for the temperature measurement circuit.

A.4 Current Sensor

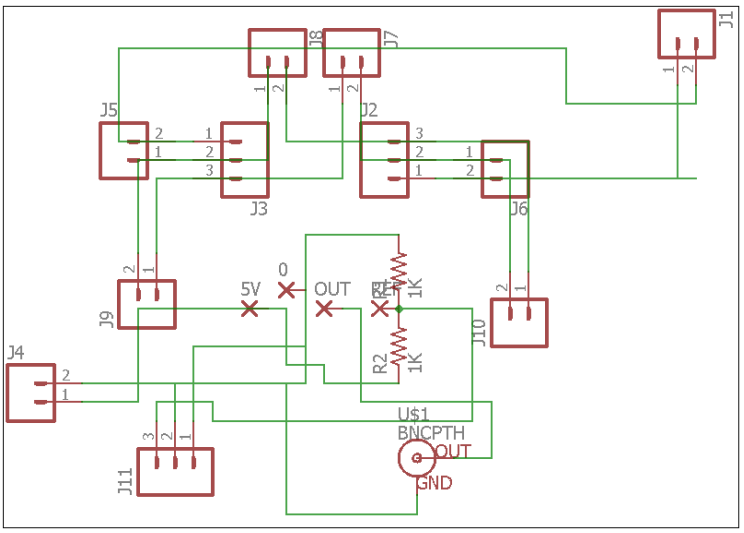

Figure A.7: The schematic for the current sensor circuit.

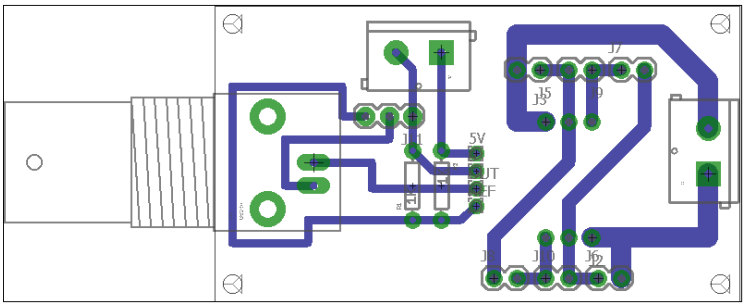

Figure A.8: The PCB for the current sensor circuit.

A.5 DC Power Supply

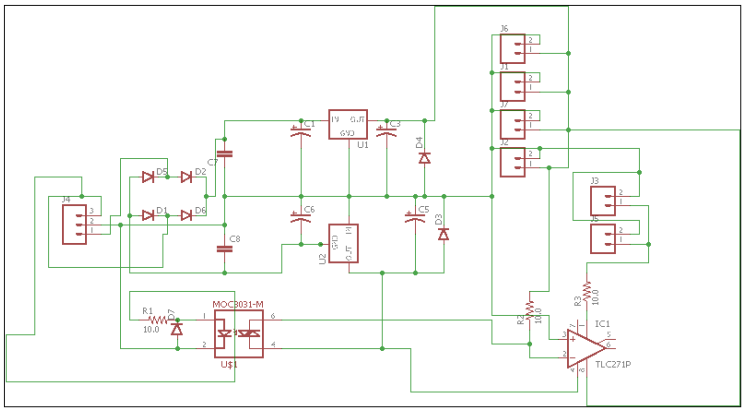

Figure A.9: The schematic for the DC power supply circuit.

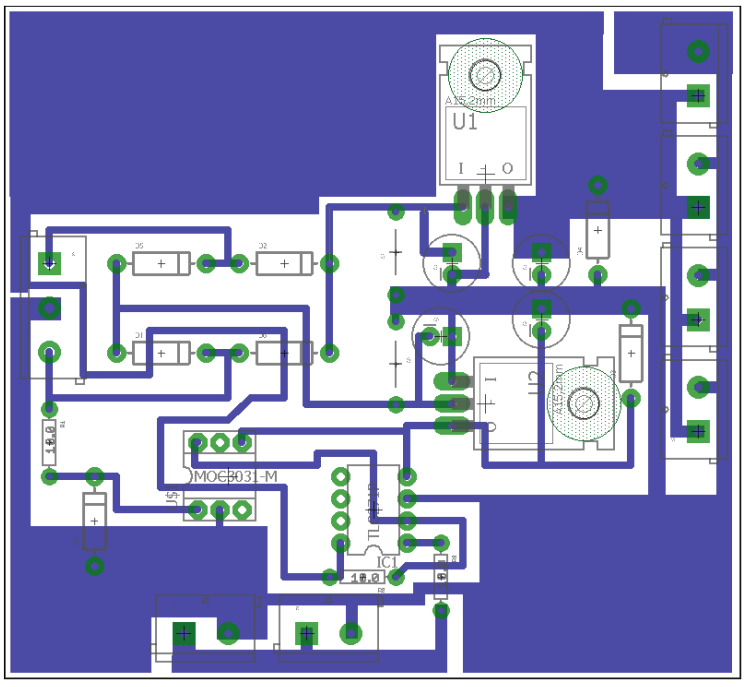

Figure A.10: The PCB for the DC power supply circuit.

Appendix B

Simulation Waveforms

This page was left open intentionally.

B.1 Anode Transformer Input Current

Table B.1: Comparing LT-Spice simulated and actual measured anode transformer input current waveforms.

Measured vs LT-Spice Simulated Current Waveforms.		
Phase Angle	Measured Waveforms	Simulated Waveforms
18°	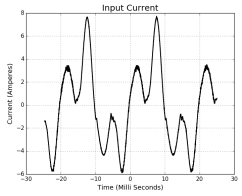	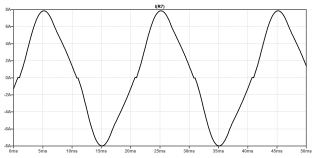
36°	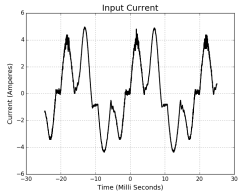	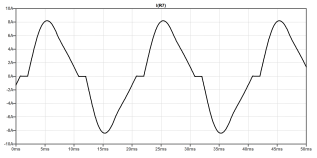
54°	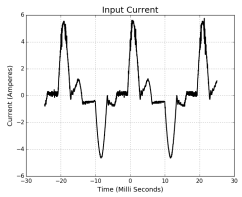	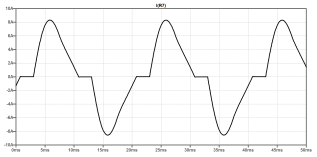
72°	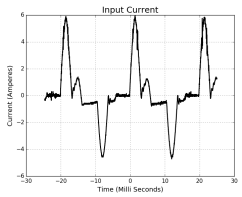	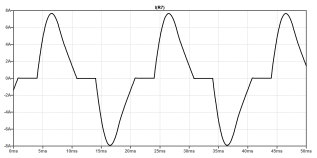
90°	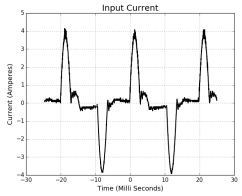	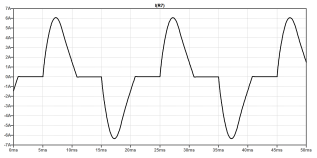
108°	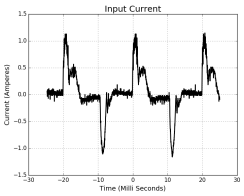	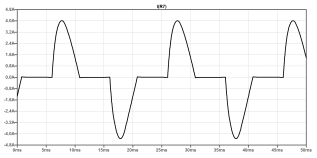
126°	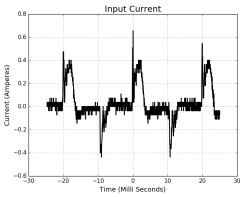	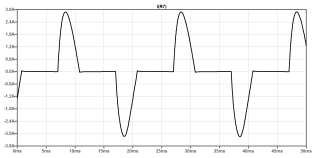

B.2 Magnetron Output Power

Table B.2: Comparing LT-Spice simulated magnetron anode current and actual measured magnetron output power pulses.

Measured vs LT-Spice Simulated Magnetron Output Power Pulses		
Phase Angle	Measured Waveforms	Simulated Waveforms
18°	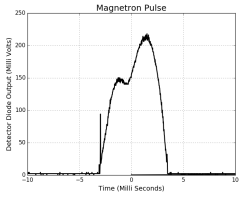	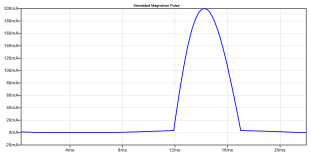
36°	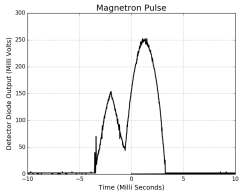	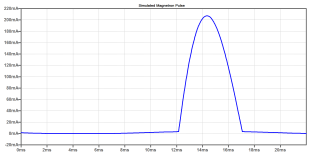
54°	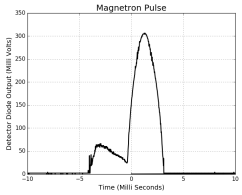	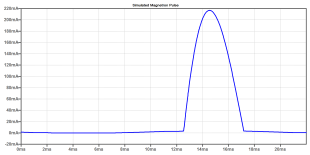
72°	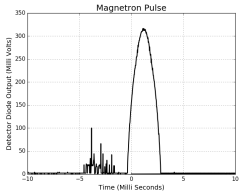	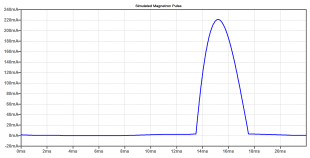
90°	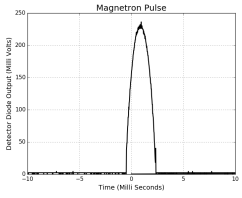	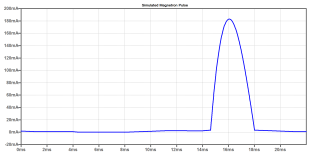
108°	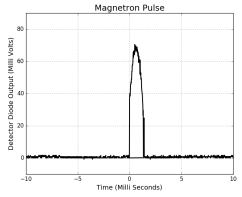	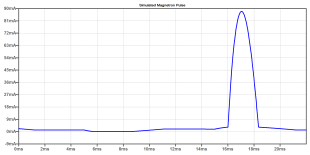
126°	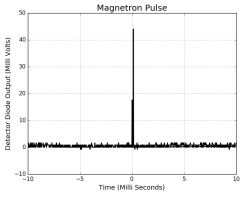	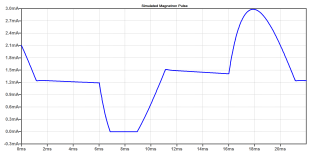

Appendix C

Microbiology Tests

C.1 Salmonella Test

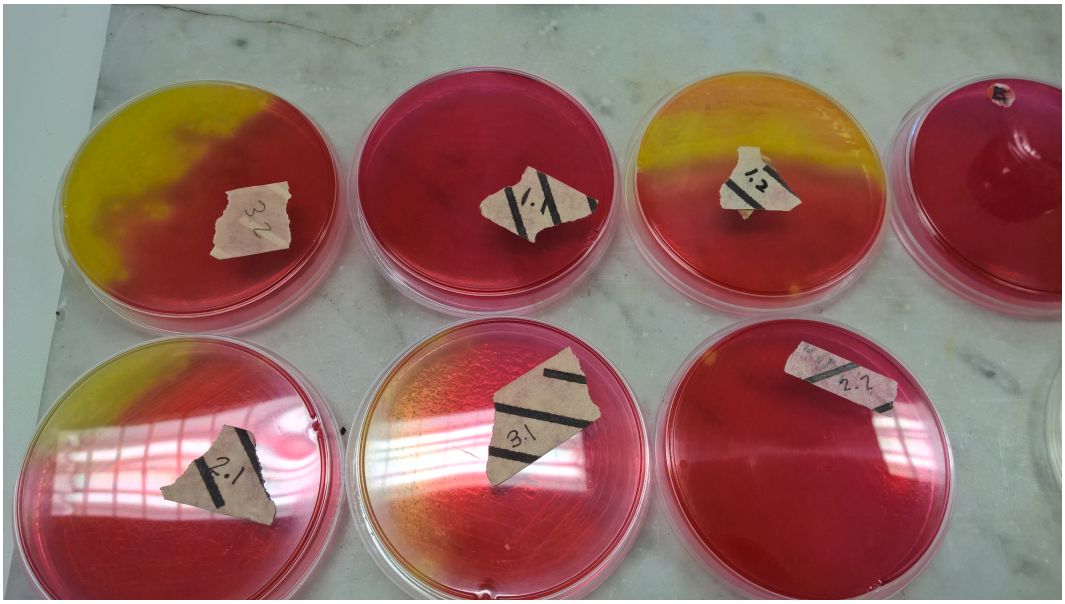

Figure C.1: Salmonella sterilisation test results.

C.2 Sterilisation Test 1

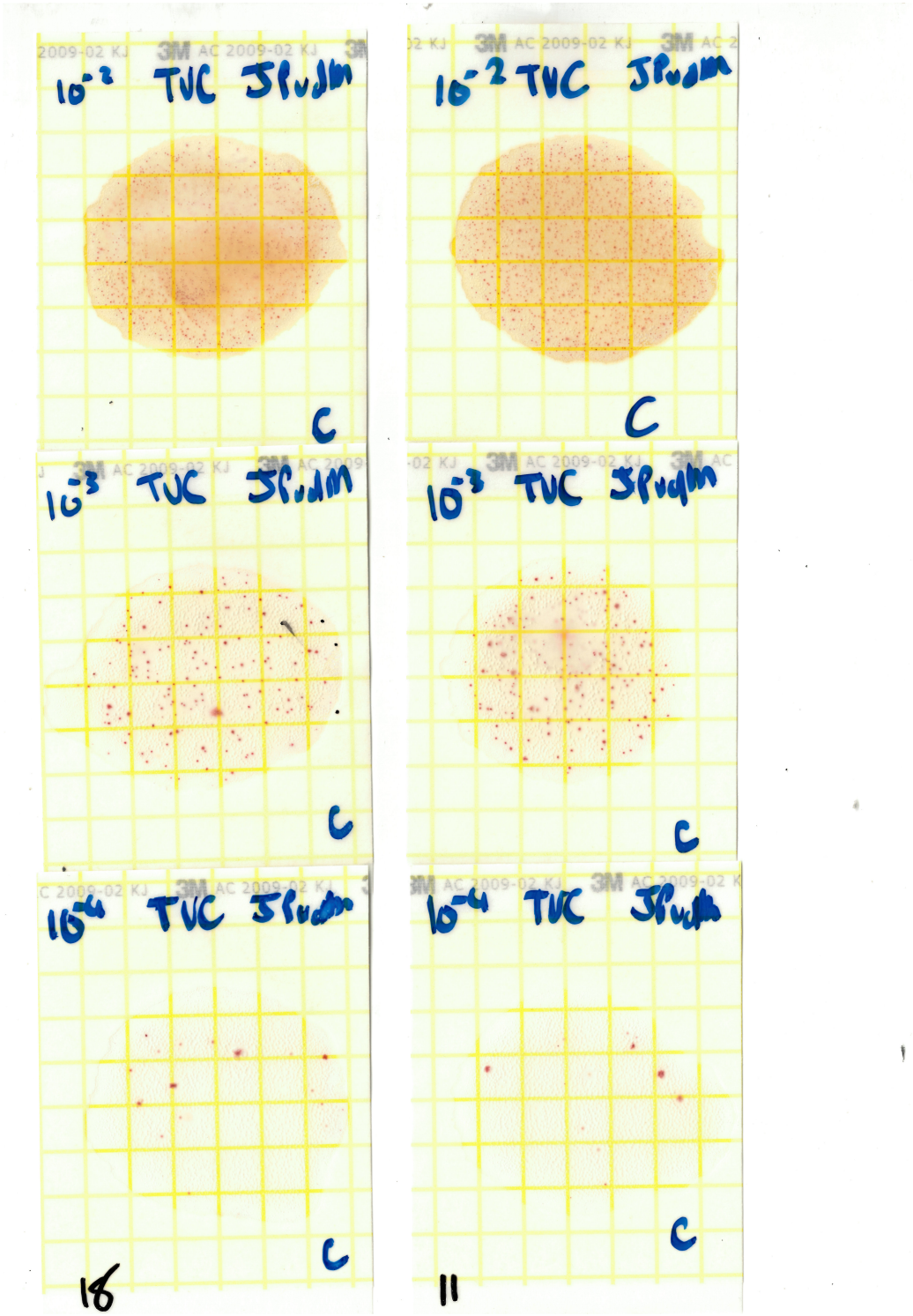

Figure C.2: Aerobic plate count control batch for sterilisation Test 1 results.

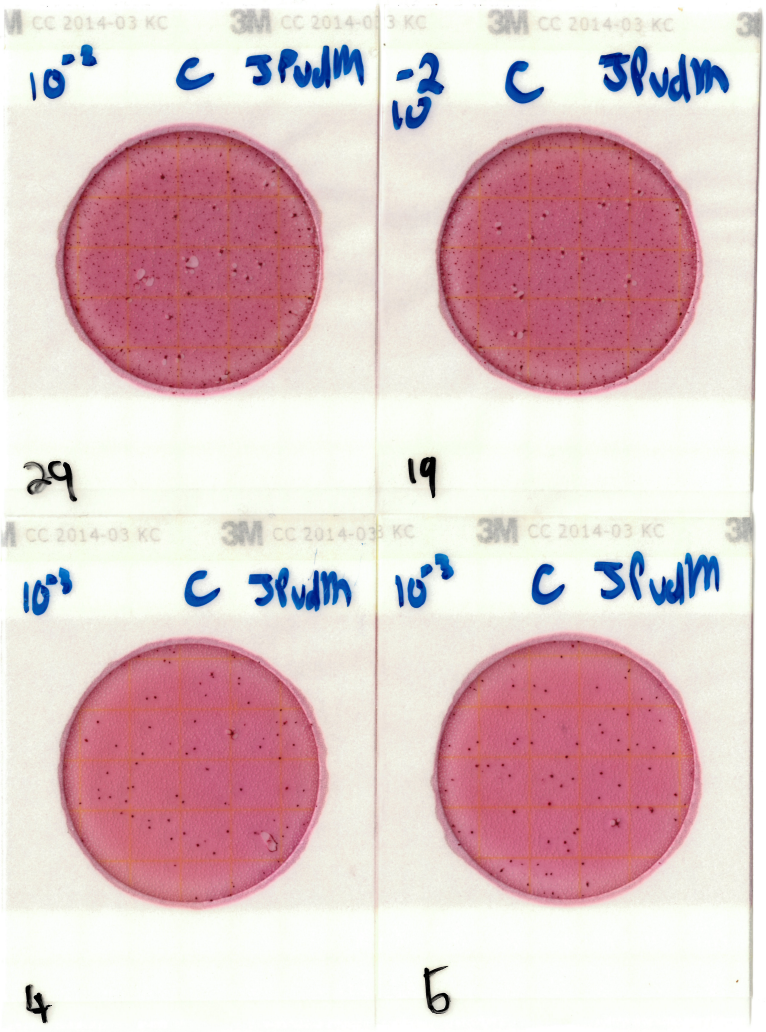

Figure C.3: E.Coli count control batch for sterilisation Test 1 results.

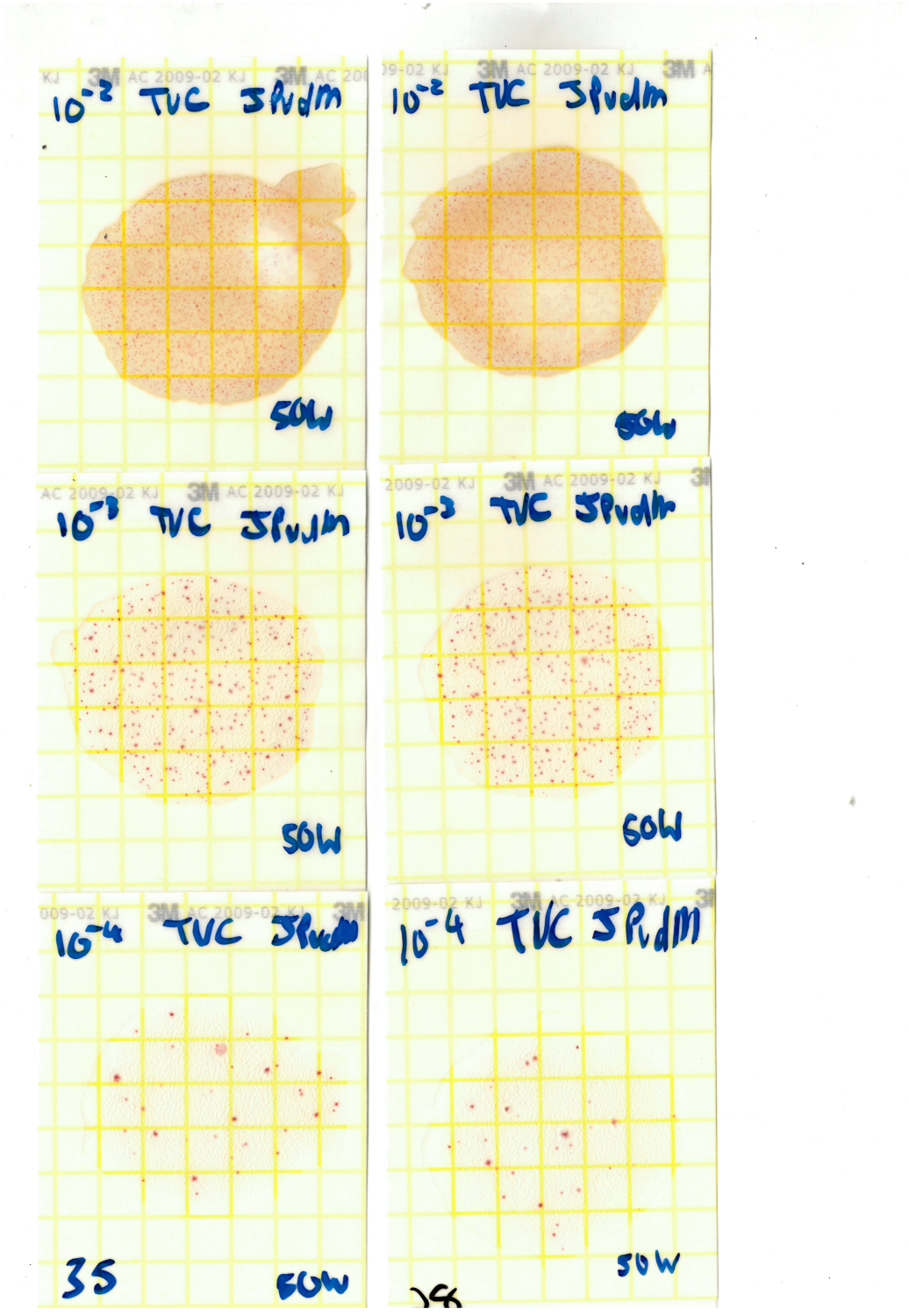

Figure C.4: Aerobic plate count for 5 min at 50 W for sterilisation Test 1 results.

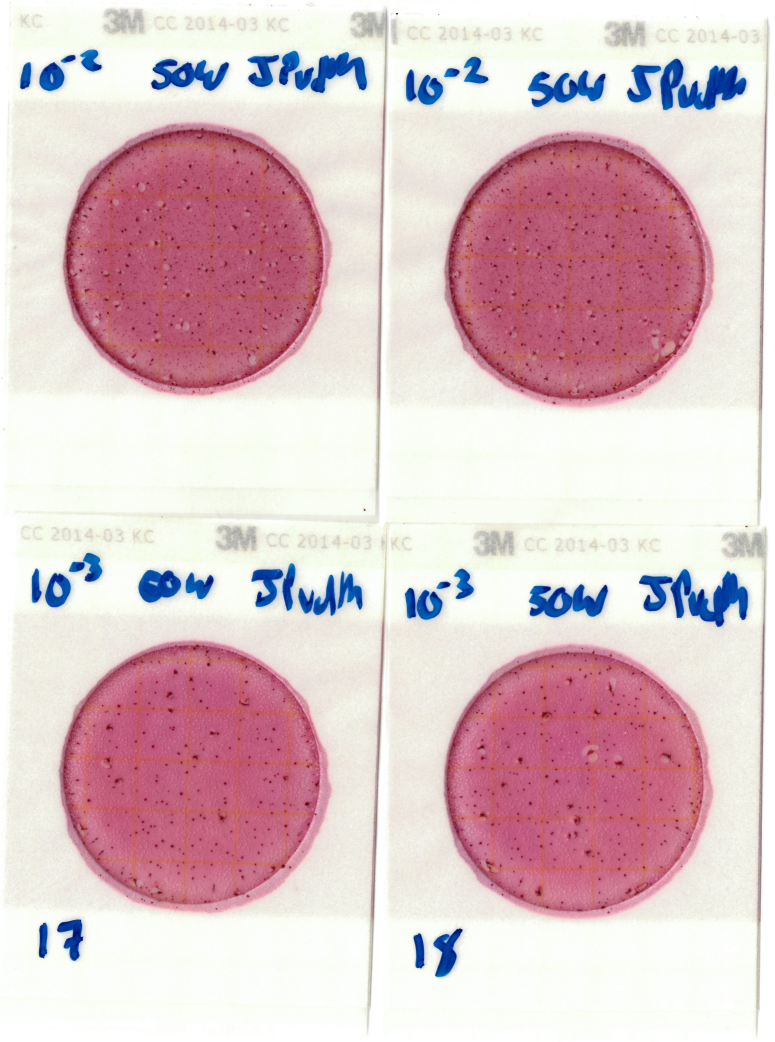

Figure C.5: E.Coli count for 5 min at 50 W for sterilisation Test 1 results.

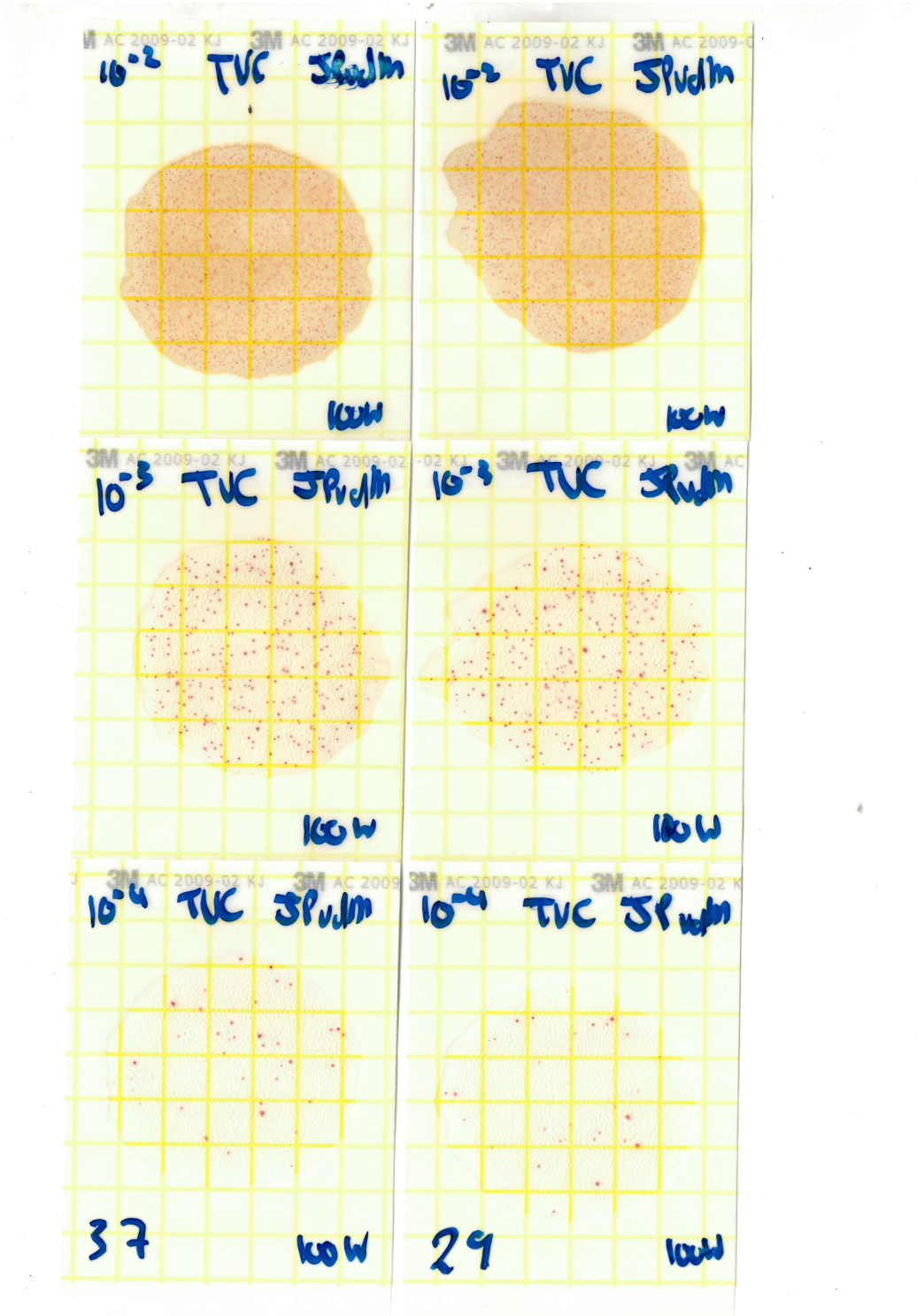

Figure C.6: Aerobic plate count for 5 min at 100 W for sterilisation Test 1 results.

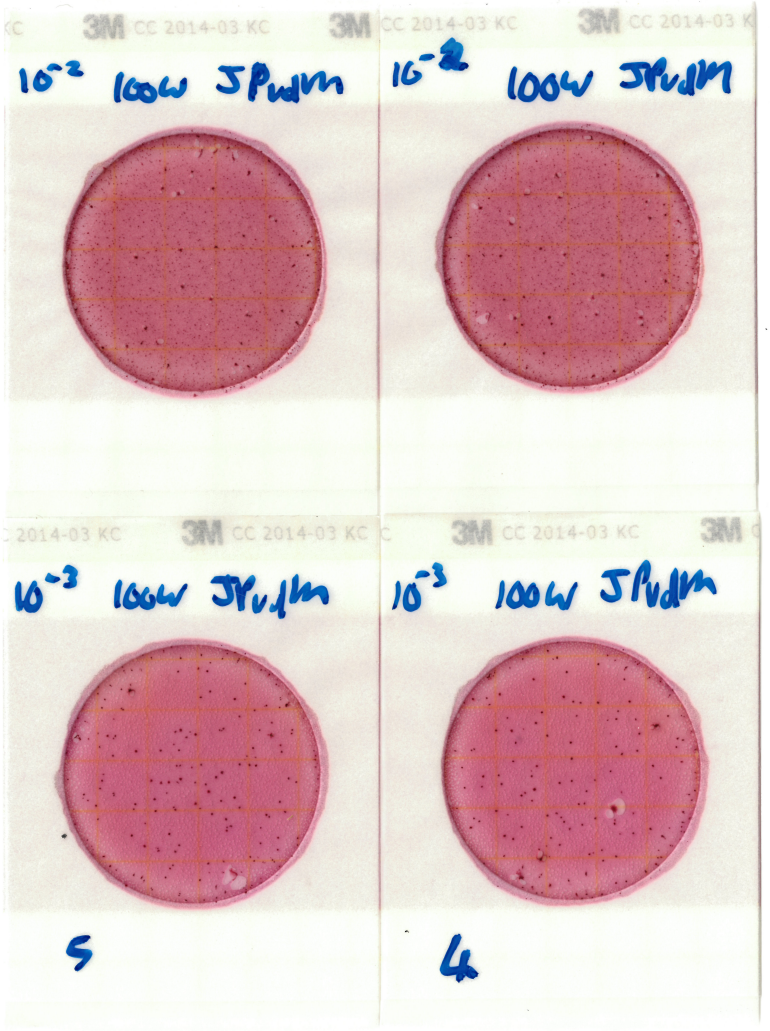

Figure C.7: E.Coli count for 5 min at 100 W for sterilisation Test 1 results.

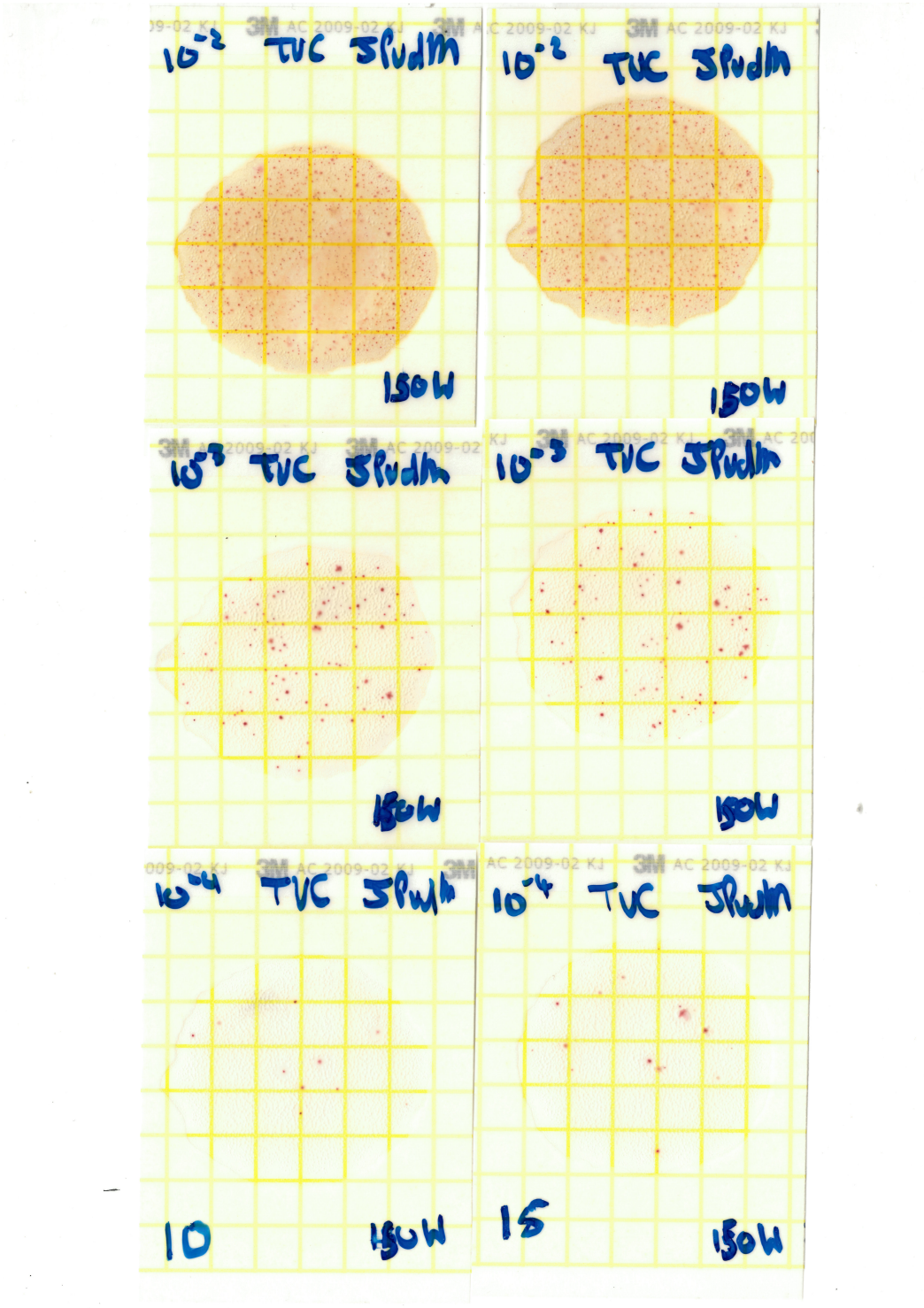

Figure C.8: Aerobic plate count for 5 min at 150 W for sterilisation Test 1 results.

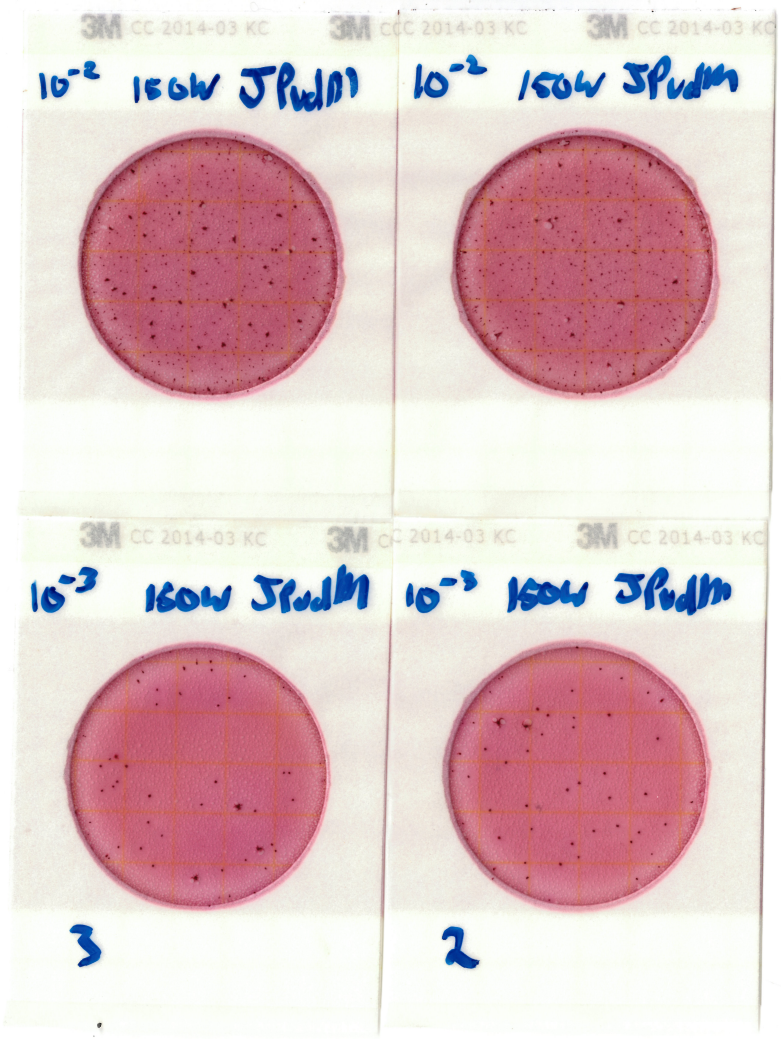

Figure C.9: E.Coli count for 5 min at 150 W for sterilisation Test 1 results.

C.3 Sterilisation Test 2

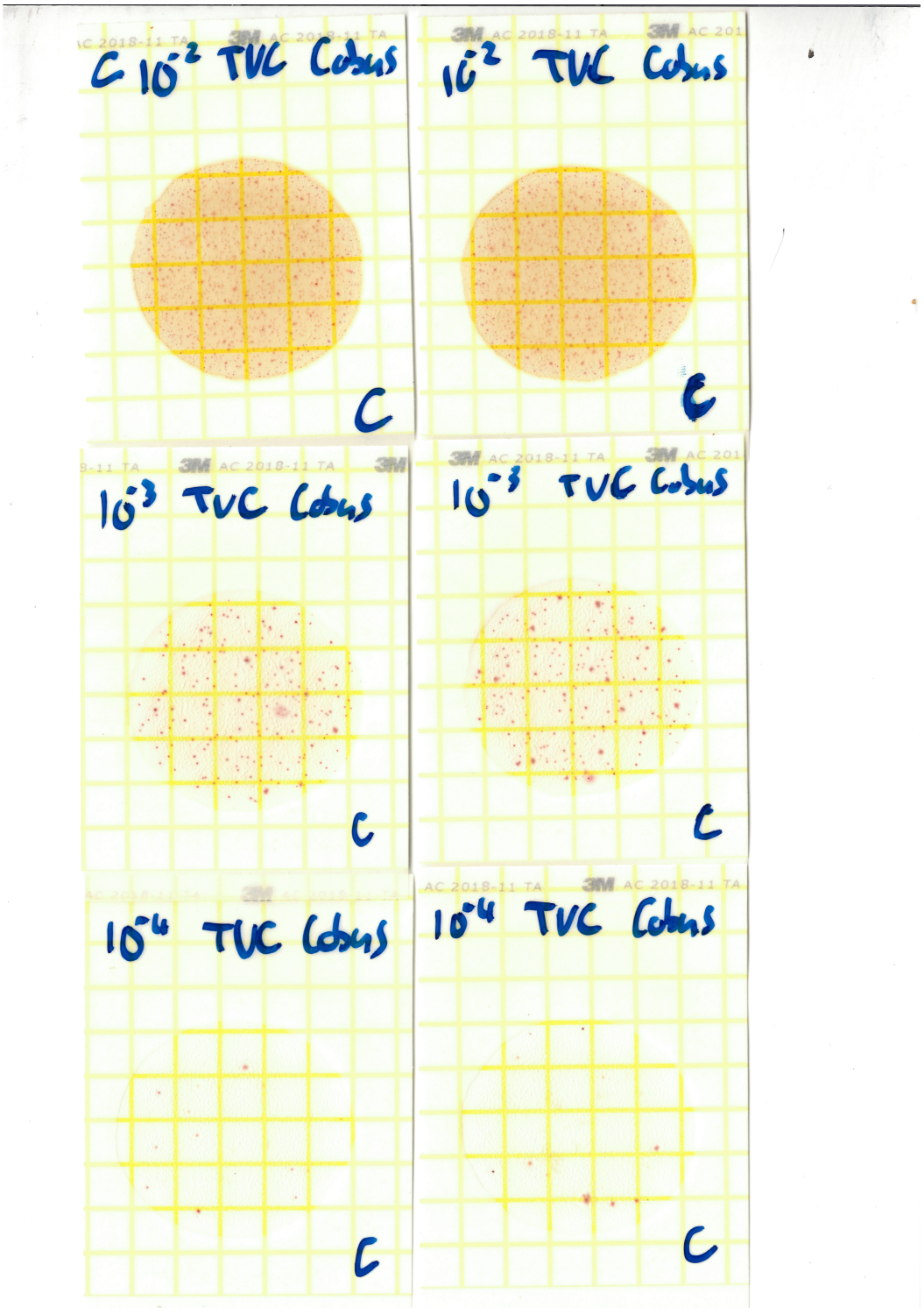

Figure C.10: Aerobic plate count control batch for sterilisation Test 2 results.

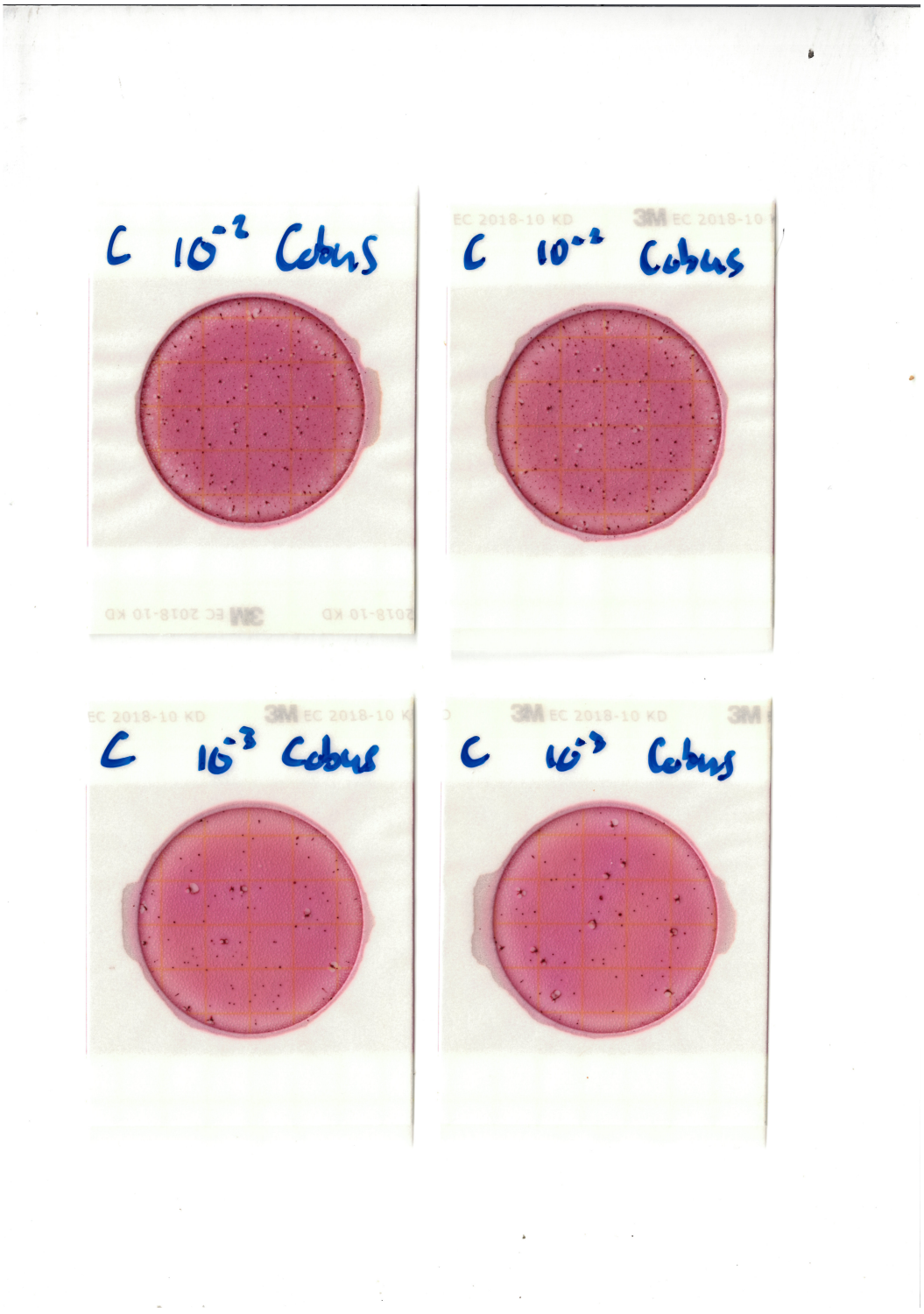

Figure C.11: E.Coli count control batch for sterilisation Test 2 results.

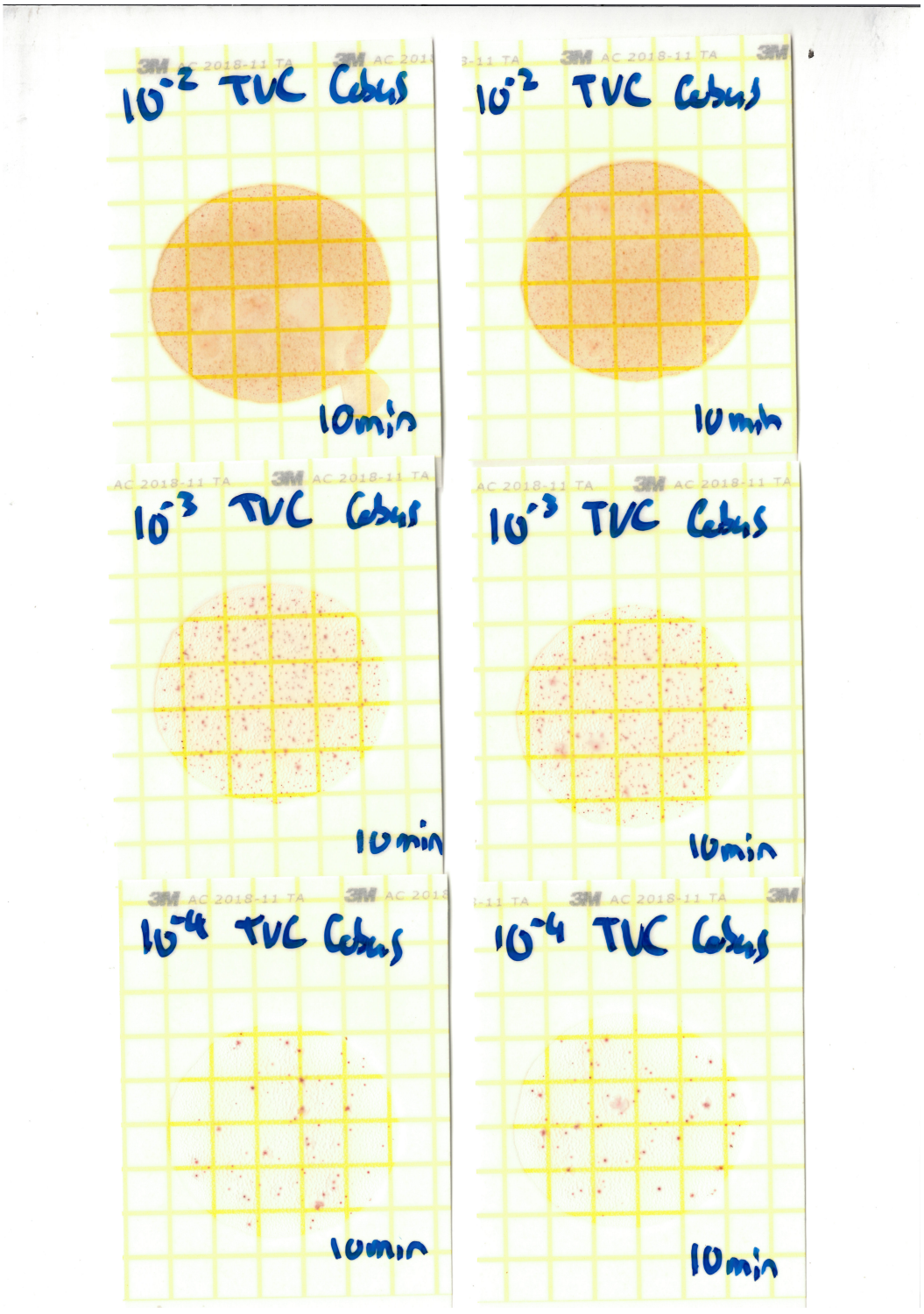

Figure C.12: Aerobic plate count for 10 min at 150 W for sterilisation Test 2 results.

Figure C.13: E.Coli count for 10 min at 150 W for sterilisation Test 2 results.

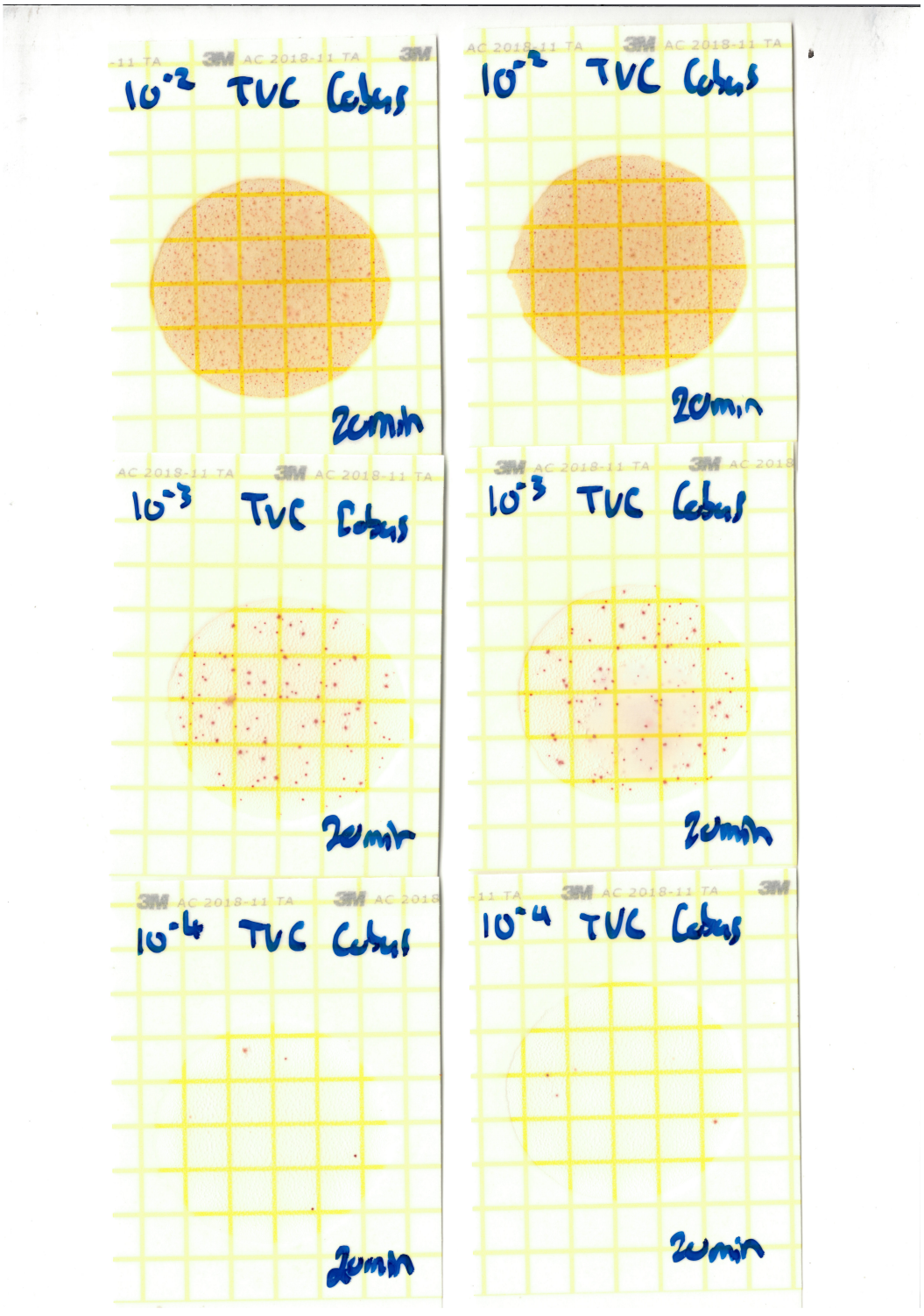

Figure C.14: Aerobic plate count for 20 min at 150 W for sterilisation Test 2 results.

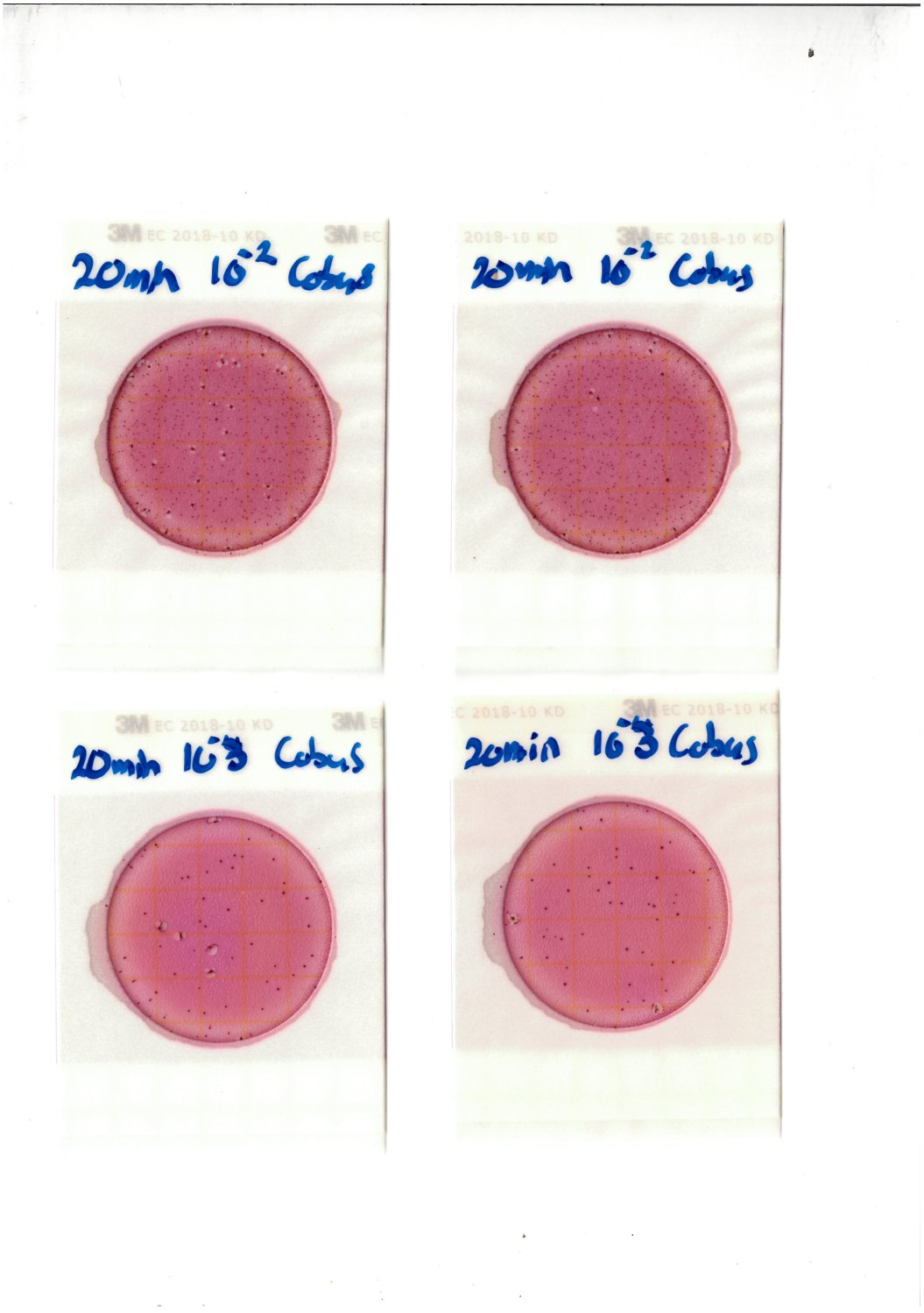

Figure C.15: E.Coli count for 20 min at 150 W for sterilisation Test 2 results.

C.4 Sterilisation Test 3

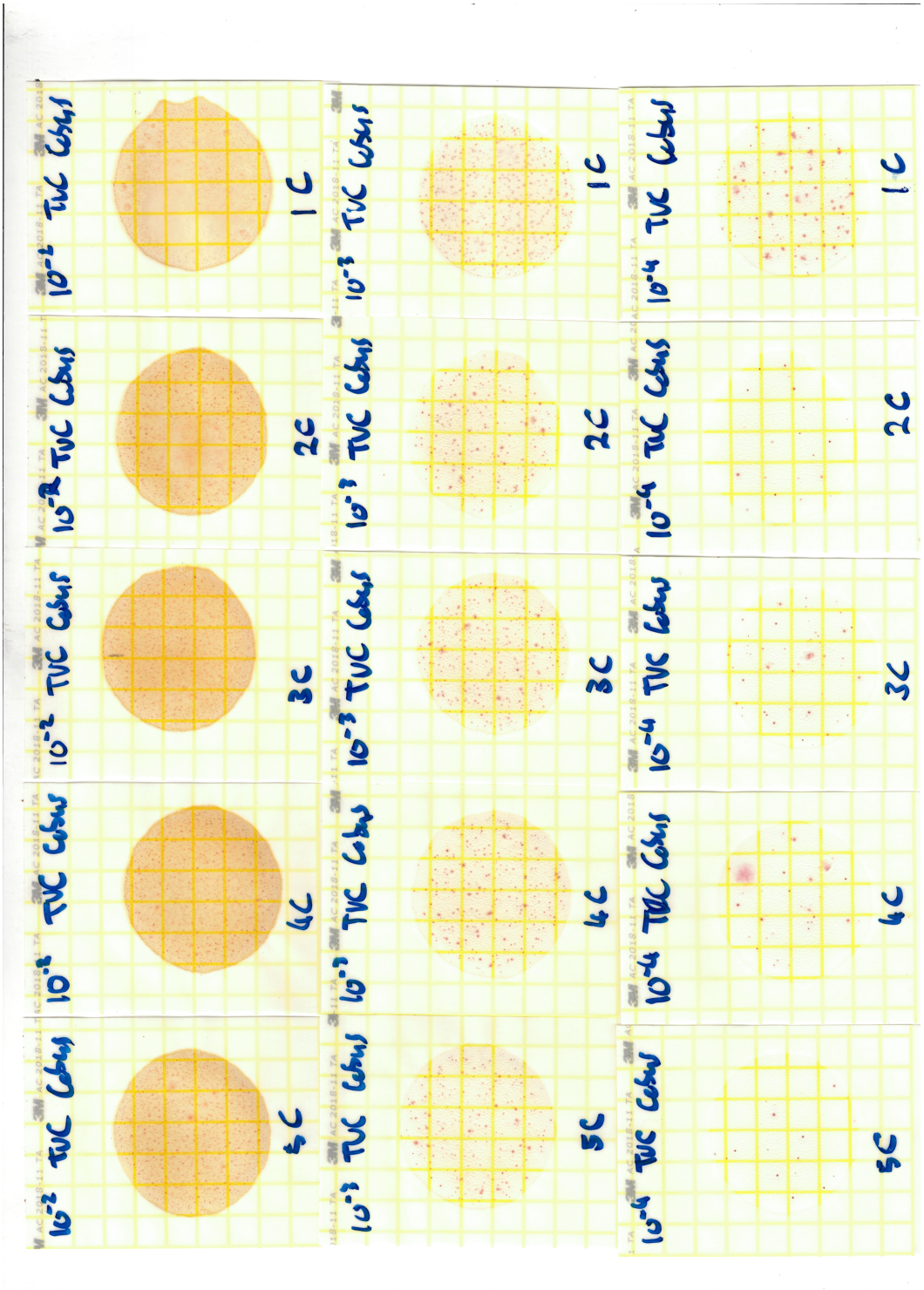

Figure C.16: Aerobic plate count control batch for sterilisation Test 3 results.

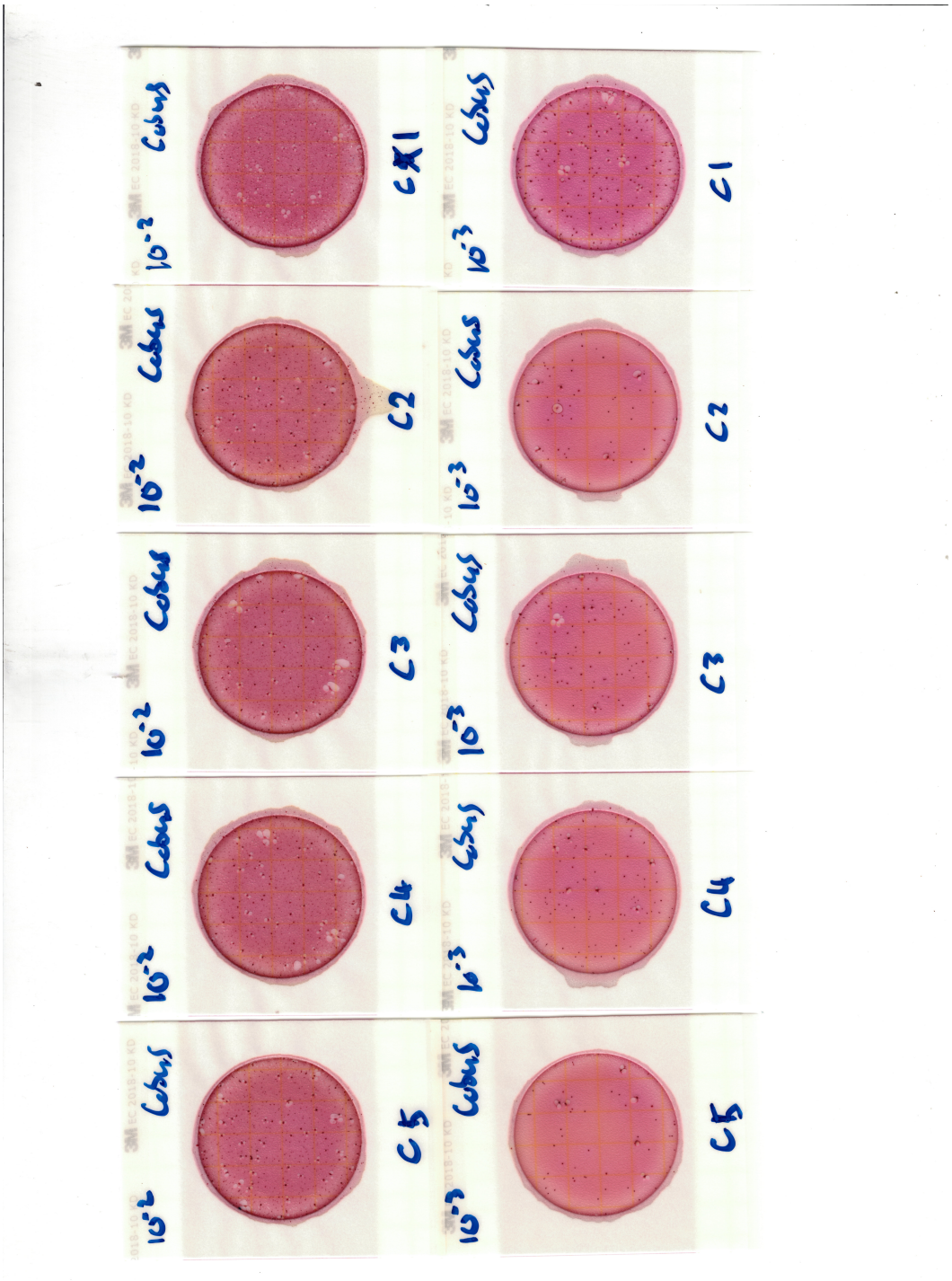

Figure C.17: E.Coli count control batch for sterilisation Test 3 results.

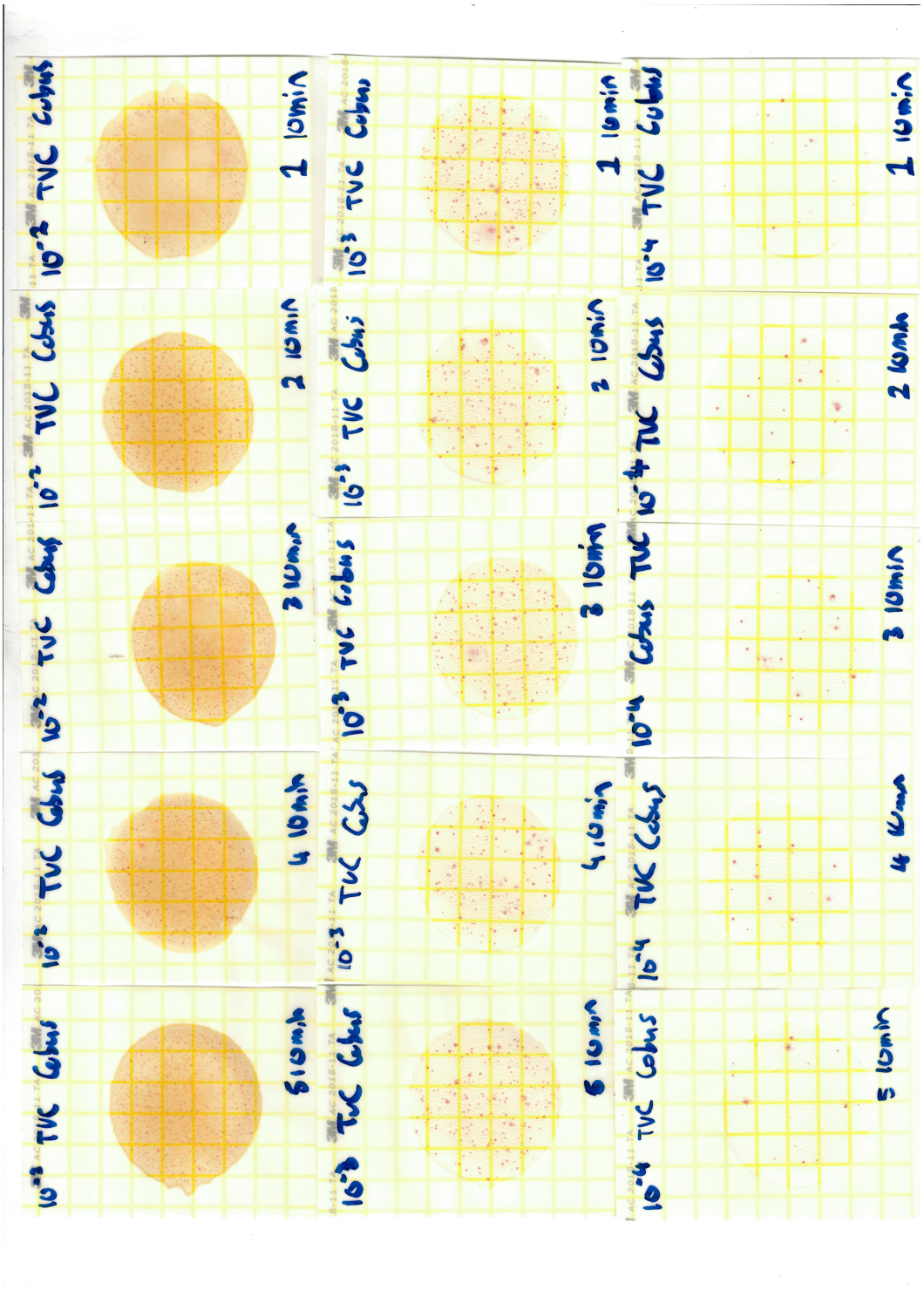

Figure C.18: Aerobic plate count for 10 min at 150 W for sterilisation Test 3 results.

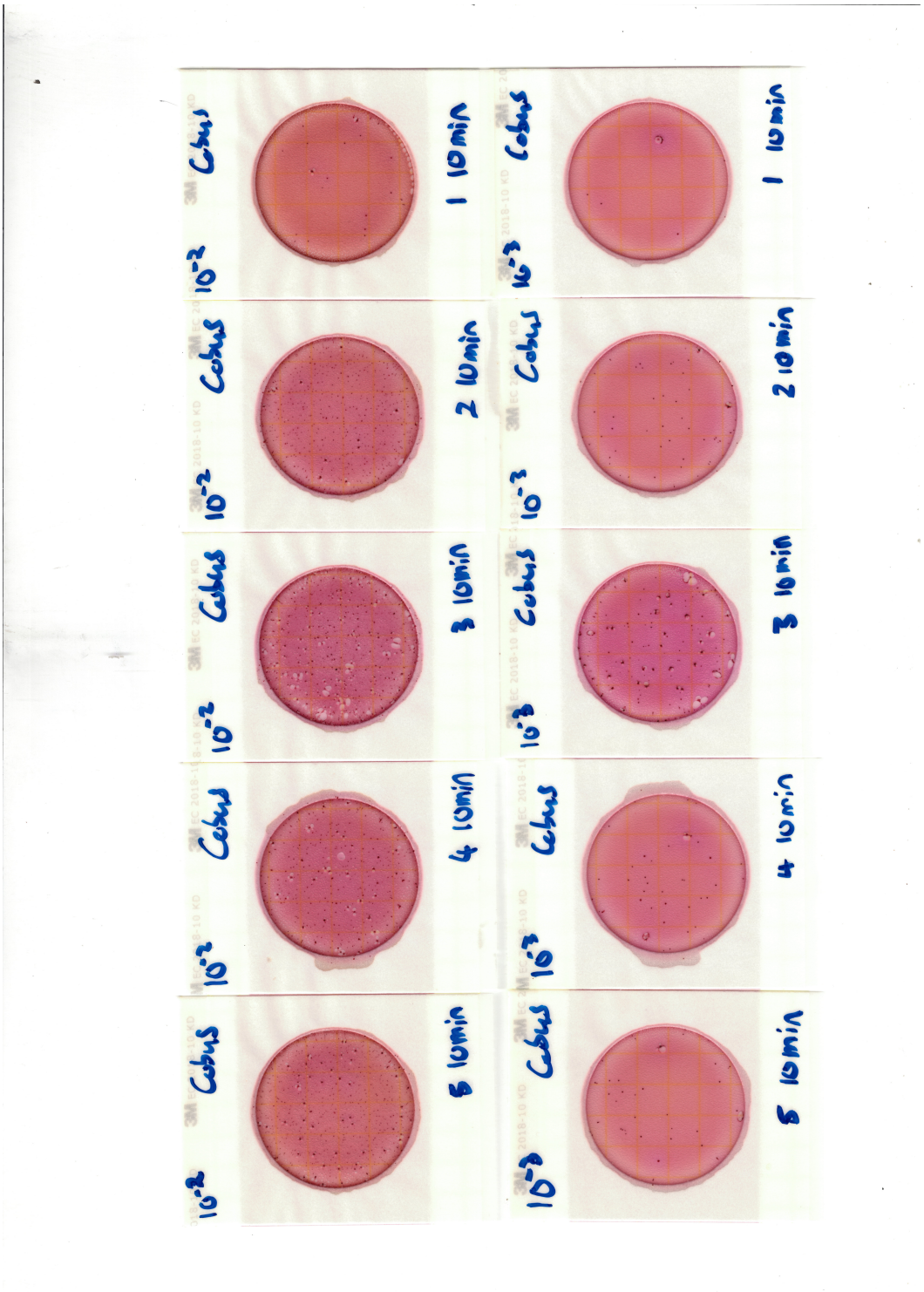

Figure C.19: E.Coli count for 10 min at 150 W for sterilisation Test 3 results.

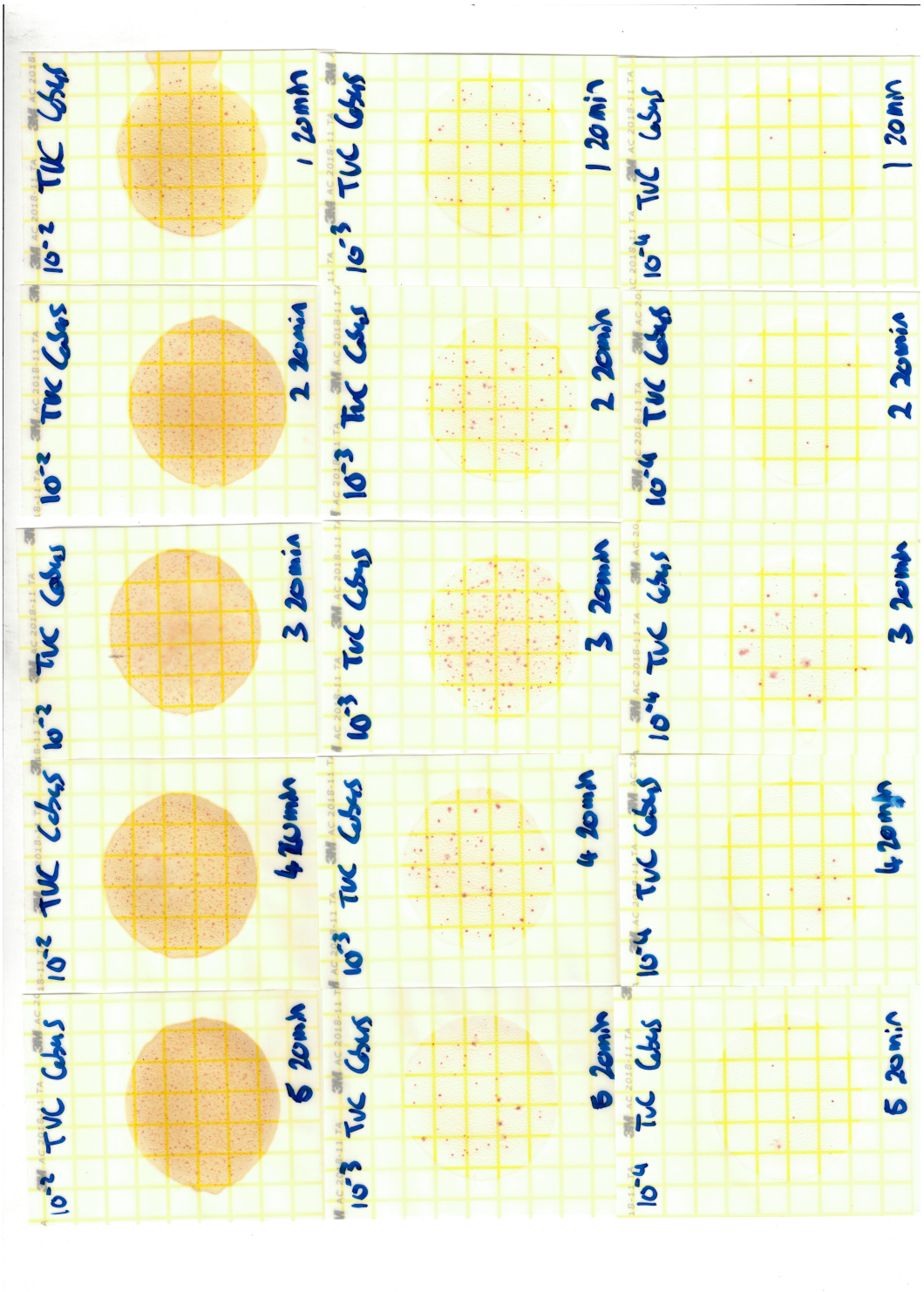

Figure C.20: Aerobic plate count for 20 min at 150 W for sterilisation Test 3 results.

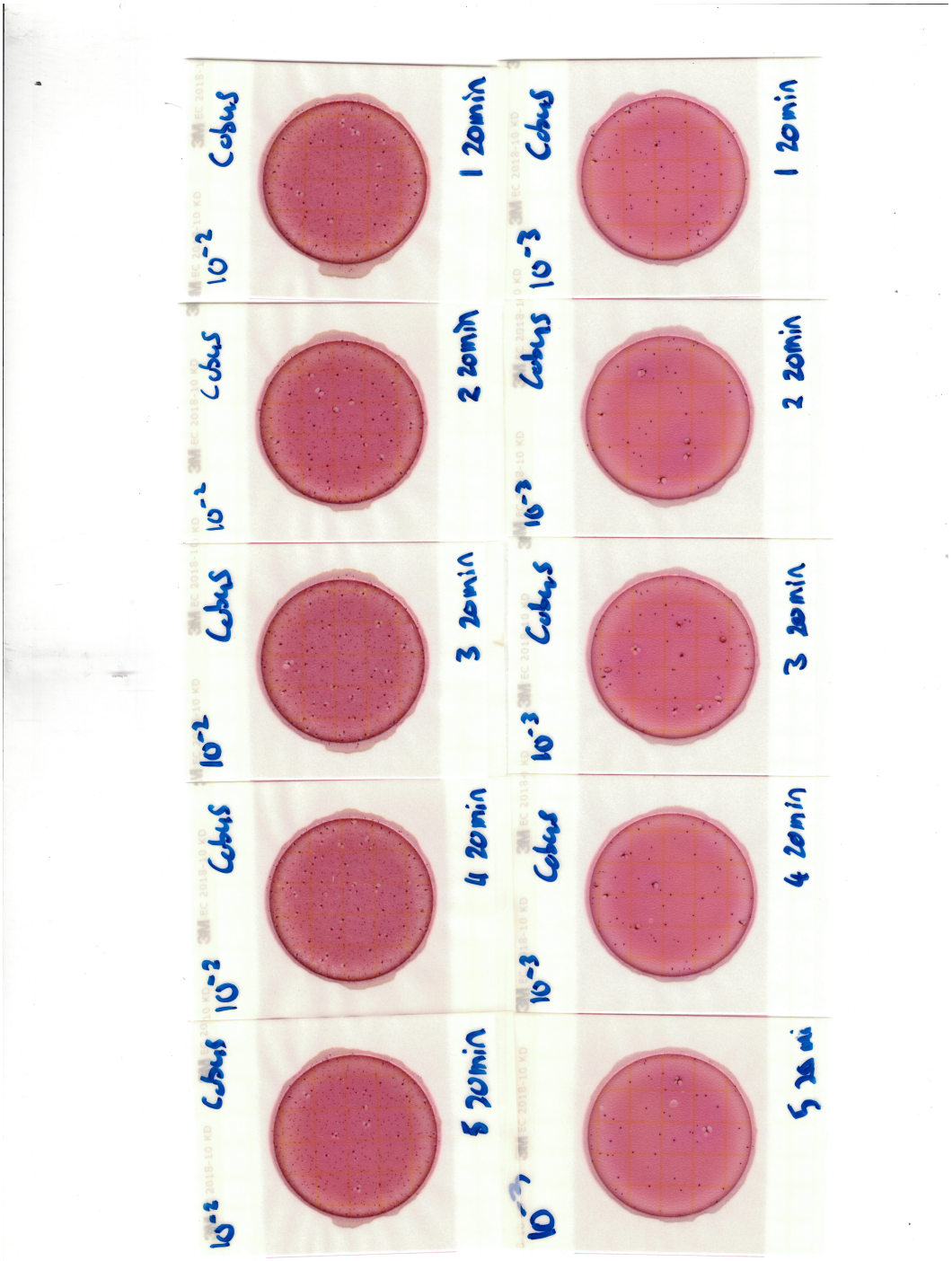

Figure C.21: E.Coli count for 20 min at 150 W for sterilisation Test 3 results.

List of References

[1] Prymak, J., Randall, M., Blais, P. and Long, B.: Why that 47 uf capacitor drops to 37 uf, 30 uf, or lower. In: *28th Symposium for Passive Electronics*. Newport Beach, CA, March 2008.
Available at: `https://www.researchgate.net/publication/229019152`

[2] Gallawa, J.C.: The magnetron tube used in microwave ovens, structure and operation. 2013. (17-05-2018).
Available at: `http://www.microtechfactoryservice.com/magnetron.html`

[3] K.Nuanyai, N.Puangngernmak and S.Chalermwisutkul: A Novel Low Cost Magnetron Power Control for Microwave Heating Applications. In: *Proc. IEEE The International Conference on Electrical Engineering/Electronics, Computer, Telecommunications and Information Technology (ECTI 2010)*, pp. 1123–1126. Chiang Mai, Thailand, May 2010.

[4] van der Merwe, J. and de Swardt, J.: Power Control of a Domestic Microwave Oven. In: *Proc. IEEE 2017 IEEE Africon*, pp. 595–599. Cape Town, South Africa, 2017.

[5] Open circuit (oc) and short circuit (sc) test on single phase transformer. . (25-10-2018).
Available at: `http://www.ee.iitb.ac.in/course/~emlab/assets/oc_sc.pdf`

[6] Oberholzer, A.E.: *Development of a Continuous Flow Sterilisation System Using Microwaves by*. Master's thesis, Stellenbosch University, 2016.

[7] J.D., F.G.P. and A., E.: *Feedback Control of Dynamic Systems*, chap. 5.1, Root Locus of a Basic Feedback System, pp. 239–244. 6th edn. Pearson, 2010.

[8] Alcamo, I.E.: *Fundamentals of Microbiology*, chap. 21, Physical Control of Microorganisms, pp. 649 –663. 5th edn. The Benjamin/Cummings Publishing Company, 1996.

[9] Fellows, P.: *Food Processing Technology*, chap. 1.4.5, Effect of heat on mirco-organisms. 2nd edn. Woodhead Publishing Limited and CRC Press LLC, Abington Hall, Abington, Cambridge CB1 6AH, England, 2000.

[10] Alcamo, I.E.: *Fundamentals of Microbiology*, chap. 4, Anatomy and Growth of Bacteria, pp. 104–105. 5th edn. The Benjamin/Cummings Publishing Company, 1996.

[11] Microwave oven owner's manual. Tech. Rep., Defy. Model DMO 349 Metallic.

[12] Gouws, P., Hartel, T. and vanWyk, R.: The influence of processing on the microbial risk associated with Rooibos (Aspalathus linearis) tea. *Journal of the Science of Food and Agriculture*, vol. 94, no. 15, pp. 3069–3306, 2014.

[13] Dababneh, B.F.: An innovative microwave process for microbial decontamination of spices and herbs. *African Journal of Microbiology Research*, vol. 7(8), pp. 636–645, feb 2013.

[14] Shamis, Y., Croft, R., Taube, A., Crawford, R.J. and Ivanova, E.P.: Review of the Specific Effects of Microwave Radiation on Bacterial Cells. *Applied Microbiology and Biotechnology*, vol. 96, pp. 319–325, 2012.

[15] Joubert, E. and de Beer, D.: Rooibos (Aspalathus linearis) beyond the farm gate: From herbal tea to potential phytopharmaceutical. *South African Journal of Botany*, vol. 77, pp. 869–886, 2011.

[16] Brink, D.: private interview, 10-2017. Carmien Tea PTY LTD.

[17] Tang, D.J., Mikhaylenko, G. and Simunovic, D.J.: Microwave sterilization technology. Report, Biological Systems Engineering, Washington State University and Department of Food, Bioprocessing and Nutrition Sciences, North Carolina State University, 2008.

[18] Metaxas, A.: Fundamentals of microwave heating. Report, Puschner Mikrowellen Energietechnik, .
Available at: `http://www.pueschner.com/en/microwave-technology/microwave-heating`

[19] Heggannavar, M. and Kulkarni, H.: Power supply Design for Magnetron Power Source from Single Phase Supply. In: *Proc. IEEE 2015 International Conference on Energy Systems and Applications (ICESA 2015)*, pp. 546–551. Pune, India, October 2015.

[20] Fu, B., Chen, M.Q., Huang, Y.W. and Luo, H.: A Combined effects of additives and power levels on microwave drying performance of lignite thin layer. *Drying Technology*, vol. 35, no. 2, pp. 227–239–645, 2017.

[21] Alcamo, I.E.: *Fundamentals of Microbiology*, chap. 4, Anatomy and Growth of Bacteria, pp. 106 –107. 5th edn. The Benjamin/Cummings Publishing Company, 1996.

[22] Griffiths, D.J.: *Introduction to electrodynamics*, chap. 4, Electric Fields in Matter. 3rd edn. Prentice-Hall In., UpperSaddle River, New Jersey, 1999.

[23] Metaxas, A.C. and Meredith, R.J.: *Industrial Microwave Heating*, chap. 2, Dielectric Loss. The Institution of Engineering and Technology, London, United Kingdom, 1988.

[24] Guru, B. and Hiziroglu, H.: *Electromagnetic Field Theory Fundamentals*, chap. 7, Time-varying electromagnetic fields. 2nd edn. Cambridge University Press, Cambridge, United Kingdom, 2004.

[25] Osepchuk, J.M.: Microwave Power Applications. *IEEE Transaction on Microwave Theory and Techniques*, vol. 50, pp. 975–985, March 2002.

[26] Bengtsson, N.E. and Ohlsson, T.: Microwave heating in the food industry. In: *Proceedings of the IEEE*, vol. 62. GÃ¶teborg 16, Sweden, January 1974.

[27] Celandroni, F., Longo, I., Tosoratti, N., Giannessi, F., Ghelardi, E., Salvetti, S. and Baggiani, A.: Effect of microwave radiation on Bacillus subtillis spores. *Applied Microbiology*, vol. 97, pp. 1220–1227, 2004.

[28] Shazman, A., Mizrahi, S., Cogan, U. and Shimon, E.: Examining for possible non-thermal effects during heating in a microwave oven. *Food Chemistry*, vol. 103, pp. 444–453, 2007.

[29] Apollonio, F., Liberti, M., Paffi, A., Merla, C., Marracino, P., Denzi, A. and Marino, C.: Feasibility for microwaves energy to affect biological systems via nonthermal mechanisms: A systematic approach. *IEEE Transaction on Microwave Theory and Techniques*, vol. 61, no. 5, pp. 2031–2045, may 2013.

[30] Korkua, S.K., Chandhaket, S., Thinsurat, K. and Pornbandit, K.: Design of Automatic Phase-controlled Converter based on Temperature for Microwave Drying System. In: *Proc. IEEE 2nd IEEE International Symposium on Robotics and Manufacturing Automation (ROMA 2016)*. Ipoh, Malaysia, September.

[31] Metaxas, A.C. and Meredith, R.J.: *Industrial Microwave Heating*, chap. 9, The microwave heating circuit, breakdown phenomena and vacuum processing. The Institution of Engineering and Technology, London, United Kingdom, 1988.

[32] Metaxas, A.: magnetron theory of operation. Report, Communications and Power Industries, 150 Sohier Road, Beverly, Massachusetts 01915, .
Available at: `www.cpii.com/bmd`

[33] Verweel, J.: Magnetrons. Report, Philips, 1952.
Available at: `http://www.extra.research.philips.com/hera/people/aarts/\_Philips\%20Bound\%20Archive/PTechReview/PTechReview-14-1952\_53-044.pdf`

[34] Martin, D., Jianu, A. and Ighigeanu, D.: A Method for the 2.45-GHz Magnetron Output Power Control. *IEEE Transactions on Microwave Theory and Techniques*, vol. 49, no. 3, pp. 542–545, 2001.

[35] Triac tutorial. (17-10-2018).
Available at: `http://www.electronics-tutorial.ws/power/triac.html`

[36] Poole, I.: Triac theory and operation. (21-10-2018).
Available at: `http://www.radio-electronics.com/info/data/semicond/triac/theory-operation.php`

[37] Korkua, S.K., Chandhaket, S., Thinsurat, K. and Maneenopparat, K.: Development and evaluation of multi-stage phase-controlled converter for magnetron driver. In: *Proc. IEEE 2nd IEEE International Symposium on Robotics and Manufacturing Automation (ROMA 2016)*. Ipoh, Malaysia, September 2016.

[38] Cheng, W., Raghavan, G., Ngadi, M. and Wang, N.: Microwave power control strategies on the drying process I. Development and evaluation of new microwave drying system. *Journal of Food Engineering*, vol. 76, pp. 188–194, 2006.

[39] Kako, H., Chandhaket, S. and Thinsurat, K.: Development of Compact Inverter Power Supply for Microwave Oven. *IEEE Transactions on Consumer Electronics*, vol. 37, pp. 611–616, 1991.

[40] Sadati, S., Tahani, A., Jafari, M. and Dargahi, M.: Derating of Transformers under Non-sinusoidal Loads. In: *Proc. IEEE 11th International Conference on Optimization of Electrical and Electronic Equipment (OPTIM 2008)*, pp. 263–268. Brasov, Romania, May 2008.

[41] Gupta, A. and Singh, R.: Computation of transformer losses under effects of non-sinusoidal currents. *Advanced Computing: An Intrnational Journal*, vol. 2, no. 6, pp. 91–104, 2011.

[42] Smith, J., Speaks, J. and Rashid, M.: An overview of the modern light dimmer: Design, Operation and Application. In: *Proc. IEEE 37th Annual North American Power Symposium)*, pp. 299–303. december 2005.

[43] Fundamental characteristics of thyristors. Tech. Rep., Littlefuse, Inc, September 2013. AN1001.

[44] Rc snubber circuit design for triacs. Tech. Rep., STMicroelectronics, October 2007. AN437 Application note.

[45] Zeng, H., Jiang, T. and Zhang, J.: A primary side control Scheme for Triac dimmable LED driver based on indirect output current sensing. In: *Proc. IEEE Energy Conversion Congress and Exposition)*, pp. 3249–3256. september 2012.

[46] Open circuit and short circuit test on transformer. . (25-10-2018).
Available at: `http://www.electricaleasy.com/2014/04/open-and-short-circuit-test-on-transformer.html`

[47] Open circuit and short circuit test on transformer. . (25-10-2018).
Available at: `http://www.electronicshub.org/open-and-short-circuit-test-on-transformer/`

[48] Oberholzer, A.E.: *Development of a Continuous Flow Sterilisation System Using Microwaves by.* Master's thesis, Stellenbosch University, 2016.

[49] Iserhardt, M.R. and Russi, J.L.: A New Flicker Mitigation Technique for Zero-Crossing AC Power Control. In: *Proc. IEEE 2014 11th IEEE/IAS International Conference on Industry Applications*. december 2014.

[50] Moc8050 data sheet. Tech. Rep., Vishay Semiconductors, April 2004. Optocoupler, Photodarlington Output, High Gain.

[51] Pt100-temperature-sensor type tf101. Tech. Rep., ZIEHL industrtie-elektronik, April 2016.
Available at: `http://components101.com/sites/default/files/components_datasheet/PT100\%20Temperature\%20Sensor\%20Datasheet.pdf`

[52] 3 and 4 wire pt100 measurements. (30-10-2018).
Available at: `http://www.status.co.uk/files/Products/310.pdf`

[53] Ina126 data sheet. Tech. Rep., Texas Instruments, December 2015. INAx126 MicroPower Instrumentation Amplifier Single and Dual Versions.

[54] L293d data sheet. Tech. Rep., STMicroelectroics, July 2003. Push-Pull Four Channel Driver With Diodes.

[55] Stepper function. (30-10-2018).
Available at: `http://www.arduino.cc/en/Reference/Stepper`

[56] Metaxas, A.C. and Meredith, R.J.: *Industrial Microwave Heating*, chap. 6, Multimode oven applicators. The Institution of Engineering and Technology, London, United Kingdom, 1988.

[57] Pozar, D.M.: *Microwave Engineering*, chap. 2.3, The Terminated Lossless Transmission Line. 4th edn. John Wiley and Sons, Inc, 222 Rosewood Drive, Danvers, MA 01923, 2012.

[58] J.D., F.G.P. and A., E.: *Feedback Control of Dynamic Systems*, chap. 1, An Overview and Brief History of Feedback Control, pp. 19 –27. 6th edn. Pearson, 2010.

[59] J.D., F.G.P. and A., E.: *Feedback Control of Dynamic Systems*, chap. 4.3.4, Ziegler-Nicols Tuning of the PID Controller, pp. 210 –211. 6th edn. Pearson, 2010.

[60] J.D., F.G.P. and A., E.: *Feedback Control of Dynamic Systems*, chap. 6.8, Time Delay, p. 399. 6th edn. Pearson, 2010.

[61] Toochinda, D.V.: Digital pid controllers, 2011.
Available at: `http://www.controlsystemslab.com/doc/b4/pid.pdf`

[62] B.V., S. and R.Y., D.U.: Analysis and implementation of discrete time pid controllers using fpga. *International Journal of Electrical and Computer Engineering*, vol. 2, no. 1, pp. 71–82, 2010.

[63] J.D., F.G.P. and A., E.: *Feedback Control of Dynamic Systems*, chap. 4.3.4, Ziegler-Nicols Tuning of the PID Controller, pp. 212–216. 6th edn. Pearson, 2010.

[64] Marler, B.: Foodborne illness, salmonella. (20-10-2018).
Available at: `http://foodborneillness.com/salmonella_food_poisoning`

[65] Alcamo, I.E.: *Fundamentals of Microbiology*, chap. 8, Foodborne and Waterborne Bacterial Diseases, pp. 228–240. 5th edn. The Benjamin/Cummings Publishing Company, 1996.

[66] Barbara M Lund, T.C.B.-P. and Gould, G.W.: *The microbiological safety and quality of food*, chap. 36, pp. 966–967. 1st edn. Gaithersburg, Md. : Aspen Publishers, 1999.

[67] Britz, P.T.: Summary of microbiological methods for product development. Food Science 478 Notes.

[68] INC., M.-B.L.: Aerobic plate count. 2017. (16-10-2017).
Available at: `http://mb-labs.com/resources/aerobic-plate-count/`

[69] Alcamo, I.E.: *Fundamentals of Microbiology*, chap. 8, Foodborne and Waterborne Bacterial Diseases, pp. 243 –246. 5th edn. The Benjamin/Cummings Publishing Company, 1996.

[70] E. coli/coliform count interpretation guide. Application note, 3M Petrifilm, 2014.
Available at: `https://multimedia.3m.com/mws/media/2362460/petrifilm-ecoli-coliform-interpretation-guide.pdf`

[71] Jarvis, B.: On the compositing of samples for qualitative microbiological testing. *The Society for Applied Microbiology, Letters in Applied Microbiology*, vol. 45, pp. 592–598, 2007.